UNIVERSITÀ DEGLI STUDI DI PADOVA

慶應義塾大学
Keio University
Tokyo, Japan

University of Padova & KEIO University

Master's Degree in Mechatronic Engineering

Department of Technology and Management of Industrial Systems
&
Faculty of Science and Technology - Department of System Integrated Design Engineering

---

Master Thesis in Mechatronics Engineering

Application of DOB & RTOB in Sensorless Control of an Upper Limb Exoskeleton

Supervisor: Oboe Roberto

Supervisor: Toshiyuki Murakami

Filippo Toffano
フィリッポ トッファーノ
2054713-IMC

Accademic Year: 2023-24

" Engineering is a great profession. There is the fascination of watching a figment of the imagination emerge through the aid of science to a plan on paper. Then it moves to realisation in stone or metal or energy. Then it brings homes to men or women. Then it elevates the standard of living and adds to the comforts of life. This is the engineer's high privilege."

HERBERT CLARK HOOVER
31st President of the United States

First of all, I want to congratulate myself for the courageous choices I've made and for learning from my mistakes. I've grown by facing my errors, addressing problems and difficulties head-on, and not being afraid of them. During my Japanese adventure, I worked a lot on myself and managed to defeat some of my enemies, including my old and best friend, anxiety.
I must also thank my family, starting with my parents, Fiorenza and Sandro, for all their support and trust in me over these six years, especially my time in Japan. A special thanks goes to my sister Alessia for supporting me in difficult times and helping me confront my fears.
Equally important, my girlfriend Sara, who stood by me, cheering me on in good and bad moments, and especially for enduring me every single day.
I'm also incredibly grateful to have two personal psychologists, Mattia and Andrea; with you, every day began with laughter and good advice. Thanks also to my other friends (maybe more accurately, colleagues) Caterina, Federico, Alberto, and Emanuele, for listening to my daily ideas and for sharing so many days at university.
Roberta-San, thank you for all the fun days of adventure around Japan; we supported each other to achieve great things and overcome our insecurities.
Finally, I want to thank all my close friends for sharing a lot of moments with me, always with a big smile, and for encouraging me in every choice I made, both good and bad.

- Filippo

ACKNOWLEDGEMENTS

KEIO UNIVERSITY

The present thesis was conducted, from September 2023 to March 2024, at Keio University of Tokyo, in the Department of System Integrated Design Engineering - Faculty of Science and Technology under the supervision of Professor Toshiyuki Murakami.

Keio University is a prestigious, and also private, university which was founded in 1858 by Yukichi Fukuzawa. Being a scholar-oriented university, it has a great reputation among the entire globe. Its history dates back to the Edo $(1603-1868)$ period when the founder started a school named *Keio Gijuku* whose objective was to broaden western education in Japan. He affirmed "*It is said that Heaven does not create one man above or below another man. Any existing distinction between the wise and the stupid, between the rich and the poor, comes down to a matter of education.*" to underline equality, freedom and human rights, underscoring the importance of imparting education to cultivate a better and innovative world.

The University is actively involved in research and development in a wide variety of areas. It encourages and supports research and cross-discipline interaction to infuse innovative and critical thinking within the environment. The Engineering School is committed to promoting and supporting international activities. It works hard to attract foreign guests with its exchange programs. Also, Keio created partnerships with top universities all over the world to enable students to travel abroad for studies, research, and cultural activities. In fact, thanks to the *Ulisse* program between the University of Padua and Keio University, I had the opportunity to spend six months in Japan to work on a project and improve myself and my research skills. After that, I also learned about a new beautiful country and culture, and I met many new friends and colleagues who have enriched me greatly. In particular, I would like to express my gratitude to my lab mates Hirotaka, Ryoya, Kazuto, Katsuto, Jin, Kasun, and Murakami-Sensei for their support during my time in the laboratory. I had a wonderful experience, both within and beyond the university setting. From the initial day, they helped me, and together, we addressed numerous challenges, working side by side in the lab every day and resolving various issues in our research.

I am thankful for the chance to remain in Japan and be part of Murakami's Laboratory. I look forward to approaching the job world with the knowledge and experience I have gained here, and to continuing to improve myself and my skills.

Keio University: https://www.keio.ac.jp/en/
Murakami Professor: https://www.st.keio.ac.jp/en/tprofile/sd/murakami_toshiyuki.html
Murakami Laboratory: https://www.murakami.sd.keio.ac.jp/index.html

Group photo of the research team and students from the Murakami Laboratory.

Keio University - Main Building Hiyoshi Campus.

CONTENTS

LIST OF FIGURES

LIST OF TABLES

ABSTRACT

This thesis presents a study conducted on the design and implementation of a sensorless control approach for an exoskeleton system intended for human rehabilitation. The primary objective is to propose an accessible and simplified rehabilitation method that supports static and dynamic exercises in the x and y spatial directions.
We would also construct a lightweight and portable system. Achieving this requires meticulous research into the selection of components, such as actuators, and materials for the system's structure. In addition, the sensorless control approach is proposed to minimize issues related to error feedback and ensuring a high level of safety for users; this requires studying the phenomena acting on the system and deriving a mathematical model to represent them, as accurate as possible.

The thesis is organized into the following chapters.

Chapter 1 introduces the role of robots in daily life and in various work areas, such as industrial and medical fields. Then, it present different exoskeleton structures and rehabilitation approaches. Finally, it define the main project objectives.

Chapter 2 offers an overview of different exoskeleton systems available, with a focus on those for rehabilitation. In addition, this chapter defines the system by deriving its kinematics and dynamics through mathematical equations.

Chapter 3 illustrate the system components. It presents a detailed overview of the chosen actuators and structure, highlighting the motor type, its characteristics, and the associated advantages and disadvantages.

Chapter 4 is focused on the control design. First, it presents the exercises to be performed. Then, after an overview of the available control approaches, it exposes the proposed sensorless controls, covering the theoretical background of the algorithms and their implementation. Additionally, it provides the necessary discretization process.

Chapter 5 study the friction phenomena in mechanical components and presents the estimation methods used. This chapter discusses frictional forces, how they change, how they arise, how they can be represented, and their impact on the system's performance.

Chapter 6 presents the experimental results collected to validate the effectiveness of the implemented controls.

Chapter 7 summarizes the goals achieved in the project and provides ideas for further improvement and development. Beyond presenting these ideas, it describes a possible solution for each proposed improvement.

1 INTRODUCTION

In the last century's second half, robotics was limited to the industrial sector. However, today, robots have become more widespread and are playing a crucial and fundamental role in each industrial and economic sector as well as in society. Human-Robot Interaction (HRI) is increasing and spreading quickly with the goal of enhancing human life through advanced communication and processing technologies. For example, Artificial Intelligence (AI) is paving the way for continuous and unpredictable changes as it is being applied to every daily task to reduce people's workload and stress.

Thus, robots (autonomous or collaborative) and advanced technologies are now present in various industries, such as construction, transport (public bus, small airport bus, etc...), material handling, assembly, packing, welding, etc... They are becoming increasingly integrated into our daily lives. Some of these examples are shown in Figure 1.1.

(a) Collaborative Robot for Assembly Tasks.

(b) Optimizing Material Handling using AGV[1].

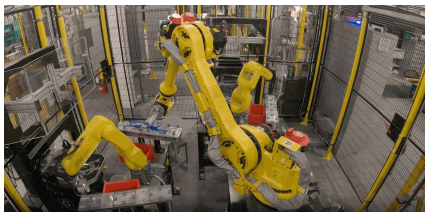

(c) Robotic Assembly-Welding Cell.

(d) Automated Transport.

Figure 1.1: Examples of different applications of robots and advanced technologies in industry.

However, while it may seem that technological evolution is replacing human operators' jobs, in reality, it is merely transforming and adapting their work to these new machines. Today, we are witnessing

1 Automated Guided Vehicles

a profound change in the job market, and young people entering the workforce have the potential to lead healthier lives compared to their parents or grandparents.

Industrial robotics isn't the only category that has seen significant advancements. Medical robotics has also made remarkable progress in recent years, to avoid many deaths that occur worldwide due to medical errors. To address this issue, the medical field aims to make procedures and related tasks safer. The goal is to further develop and integrate sophisticated surgical robots to assist doctors, providing high precision and accuracy in delicate movements within the human body (both internally and externally). By adopting this approach, the possibility of errors is significantly reduced, and patient confidence, especially in high-risk surgical operations, is greatly increased. Also, the advantages that come with their use can be less invasive procedures, faster recovery time, shorter hospitalization, customized therapies and long-term cost savings. On the other hand, the economic investment necessary to buy of develope these robotic machines remains the primary challenge, as it could prove to be a substantial and challenging expense for some medical centres, with a potentially extended payback period. Moreover, such equipment might quickly become outdated as innovation progresses swiftly. Obviously, it is necessary to find a trade-off between the pros and cons of medical robotics, always considering that it has the potential to change people's lives in certain cases.
Some examples of applications in the medical area, such as robot-assisted surgery and radiotherapy (fig.1.2b), laboratory analysis, social support (fig.1.2a), etc. . . are reported in Figure 1.2.

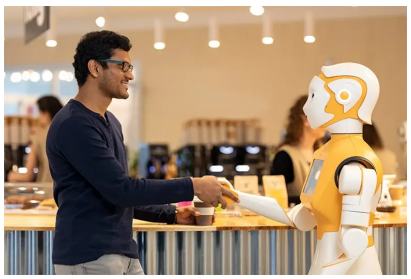

(a) Social Robot.

(b) Surgical Robot.

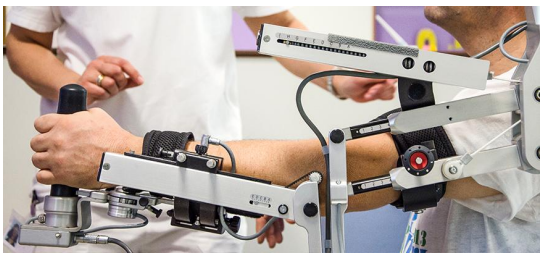

(c) Rehabilitative Robotics.

Figure 1.2: Examples of different applications of robots in medicine.

Another particular application of medical robot that represent at all the HRI is *Rehabilitative Exoskeletons* robot that help people after accidents on injuries[2] (also if the patient is in critical conditions) with movements to strengthen or rebuild muscles in a specific part of the body (leg, arm, shoulder, etc.. . .) [21].
Some rehabilitative exoskeletons examples are shown in Figure 1.3.

(a) Arm Rehabilitation [1].

(b) Legs Rehabilitation [8].

Figure 1.3: Examples of Rehabilitative Exoskeleton.

This type of exoskeleton is used for human rehabilitation, which is a targeted therapy aimed at recovering normal bodily functions through personalized programs that involve power-assisted exercises. It assists the patient to perform the assigned exercise, compensating with the amount of force that the user cannot apply. The exoskeleton acts as a guide, teaching users how to perform normal movements and improving muscle effort. The given help reduce recovery time, increase the patient's confidence in the rehabilitation process, and maximize the effectiveness of the exercises. Additionally, the system

2 Derived from surgical operations, illnesses, or neurological events (e.g. ischemic stroke or partial paralysis)

can be adjusted to respond to the patient's pain and progress, increasing or decreasing the interaction force as needed. This adaptability is crucial for a comfortable and effective rehabilitation experience.
Nowadays, recovery time has become a crucial factor related to a person's job. For example, an important athlete needs to return to the field as soon as possible after an arm or leg injury to avoid losing overall physical condition and to help the team continue or return to win. Similarly, a worker is in a same situation because they need to perform their tasks, and without them, the company could lose money or need to hire a new person and train him for the job. Also, without a worker, the productivity can decrease, and the consequences for the company can be different, such as losing a contract or a customer or delays in order deliveries. Naturally, the recovery program is defined by the expert physiotherapist that define precise exercises and minimum period, according with the patient's history and the kind of injury, to restore a good level (not total) of autonomy of movement.

A rehabilitative exoskeleton can be classified into different categories, depending on its characteristics. Regarding the structural ones, it is possible to identify the following categories [23]:

1. **Hard** $\longrightarrow$ the links are made of stiff and undeformable materials (steel, aluminum, etc...) that support the entire weight of the patient's injured limb;

2. **Soft** $\longrightarrow$ the structure is made with soft materials (sponge, rubber, technical fabrics, etc.) that deform when external force is applied;

3. **Semi-Hard** $\longrightarrow$ the structure is made with a mix of stiff and soft materials. The latter can deform due to external forces applied by the patient;

while regarding its portability level, it can be categorized into other three categories [23]:

1. **Wearable** $\longrightarrow$ the structure has no external connection, and the main support is the patient's back;

2. **Mobile** $\longrightarrow$ there is an external support structure with wheels that can be moved freely;

3. **Semi-Mobile** $\longrightarrow$ there is a similar structure to the mobile one, but the movements are limited.

Finally, it can also be divided according to the rehabilitation mode implemented [23]. In details, it can work in:

1. **Assistive Mode** $\longrightarrow$ used when the patient has lost all muscle strength or is inhibited to perform basic movements;

2. **Corrective Mode** $\longrightarrow$ used for patients with good muscle health. It provides the necessary force to assist the patient's muscles in performing a movement, supporting semi-autonomous individual movements. This is also called power-assist mode;

3. **Resistive Mode** $\longrightarrow$ used for patients with good to high muscle health. It provides resistance during movement to increase muscle effort. In this way, the patient regains muscle autonomy by reacting to external forces exerted by the exoskeleton.

To define a final exoskeleton product, combining different categories according to the medical application is necessary. Additionally, a single exoskeleton can implement all rehabilitation modes, which can be adjusted based on the patient's health progress.

After realizing the potential of medical exoskeletons and understanding how they are becoming fundamental in post-surgery or post-sickness, it is necessary to maintain a high level of technological advancement and propose new approaches or upgrades with the goals of improving rehabilitation methods and, consequently, the patient's quality of life. At the same time, we need to safeguard and reduce the costs, one of the main and high obstacles in this sector. Additionally, enhancing Human-Robot Interaction (HRI) is essential to create something comfortable and user-friendly.

Starting from these ideas, this thesis project was born with the aim of developing an upper-limb exoskeleton prototype with the following characteristics:

- **Compactness and Lightweight:** the exoskeleton must have a compact and lightweight structure to be portable and wearable. The user should be able to utilize it at home with ease, potentially without the help of a physiotherapist[3];

- **Customization:** the exoskeleton must be adaptable to the patient's arm characteristics. It is necessary to regulate the link lengths to position the actuators correctly, ensuring comfortable movements;

- **Energy and Control Autonomy:** the exoskeleton should be independent of external power supply to avoid potential issues caused by external wires (such as twisting or interlocking). It has to be power supplied by a battery with sufficient autonomy to allow the user to perform exercises without interruption. Additionally, this ensures that the user can carry out rehabilitation exercises in any available and appropriate location, depending on the exercise type. The control system should also allow for remote control to adjust parameters and upload exercises;

3 This is possible depending on the patient's condition; in the case of severe conditions, it is applicable after the initial rehabilitation period with physical assistance.

- **Safety and Adaptability:** the exoskeleton can operate in different modes based on the control settings: power-assisted, corrective, and resistive. By adjusting the gains, it is possible to achieve the desired response, always ensuring safe and controlled operation;

- **Sensorless:** this is the main challenge of the project. It stems from the difficulty of positioning force sensors in a way that ensures accurate measurement of interaction forces. Additionally, sensors can introduce errors and malfunctions that may compromise the exoskeleton's performance, leading to dangerous situations. By minimizing the use of sensors and adopting estimation techniques, we can achieve excellent performance and safety. Although this increases computational complexity, modern microcontrollers, even low-range ones, are powerful enough to manage this without issues.

These features combined allow for the creation of a cost-effective and robust product, accessible not only to medical centers but also to private users. However, initial external support from a physiotherapist is still necessary. The low cost is achievable by reducing the sensors' number and by designing a compact, lightweight, and simple structure with only two Degrees of Freedom (DoF), corresponding to two actuators: one for the shoulder and one for the elbow. Robustness is ensured by the control techniques employed, which guarantee a correct and safe response in all situations.

This thesis will be a journey through the realization steps of this project. We will begin with an overview of different types of exoskeletons and their main and common characteristics in various applications. Next, we will focus on the upper-limb exoskeleton and define its mathematical model, considering it as a two-link manipulator. We will then proceed with the selection of components, such as actuators and the frame, highlighting the reasons for these choices based on characteristics and cost. The next step will involve control design, starting with an overview of available control methods and culminating in the final control implemented and tested. This control system has been defined for a specific set of static and dynamic rehabilitation exercises. Finally, to validate the control system's effectiveness, experimental tests were conducted, and the collected data were analyzed. Based on this analysis, areas for improvement were identified to further enhance the performance. In conclusion, possible future upgrades in autonomy, structure, and control are proposed.
In Figure 1.4, the prototype of the upper limb exoskeleton constructed is shown.

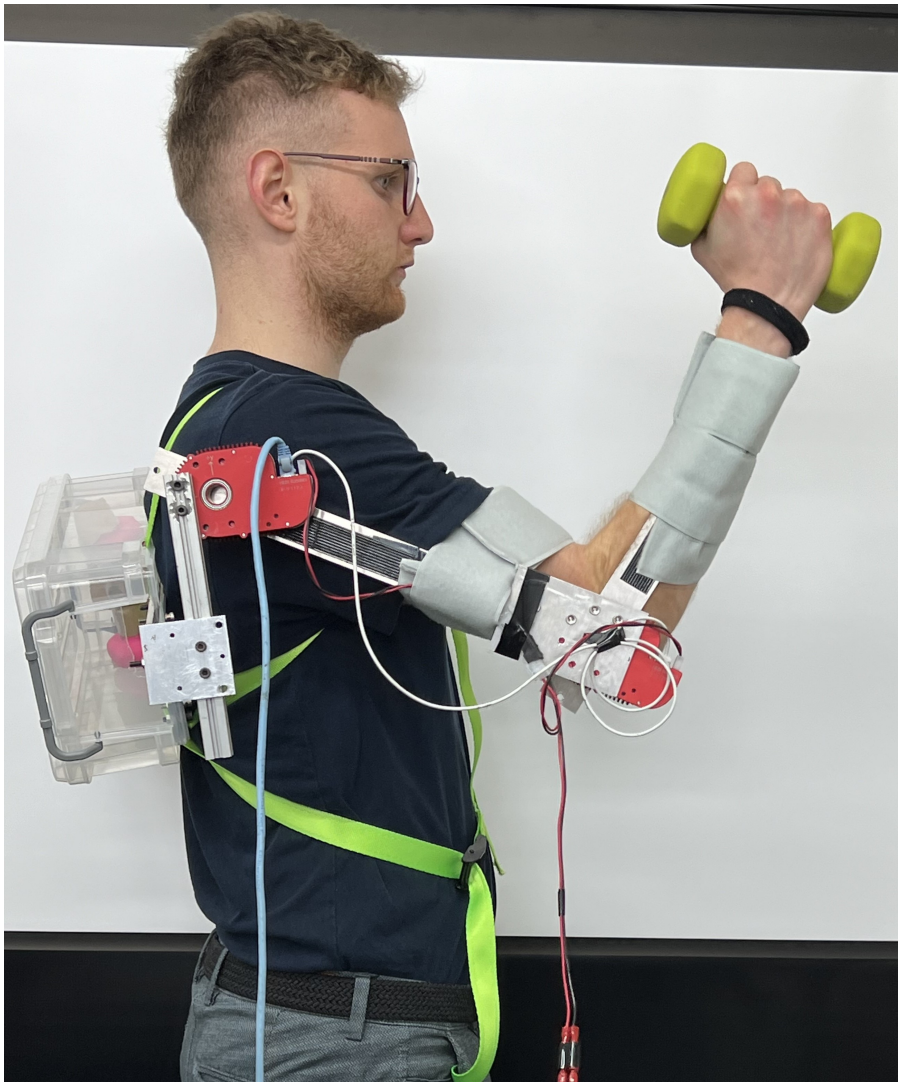

Figure 1.4: Constructed Upper-Limb Exoskeleton Prototype.

2

EXOSKELETONS

Exoskeletons, in general, are wearable robotic devices designed to assist and facilitate human movement. They can also be defined as automatically operated machines intended to improve movement in individuals with impaired physical functioning. Their main goal is enhancing a person's physical abilities, such as strength, agility, and power, in various tasks during their professional life or after a trauma or an accident.

These systems are typically divided in two big group: active or passive. The first one is composed of rigid or/and flexible structures, sensors, actuators[4], battery and control systems while the second one is characterized on the use of joints, passive actuators (composed by springs, dampers or counterweights) without any electronic control and power supply; it support the user's movements taking advantage of physics and gravity. The main differences can be seen in Figure 2.1.

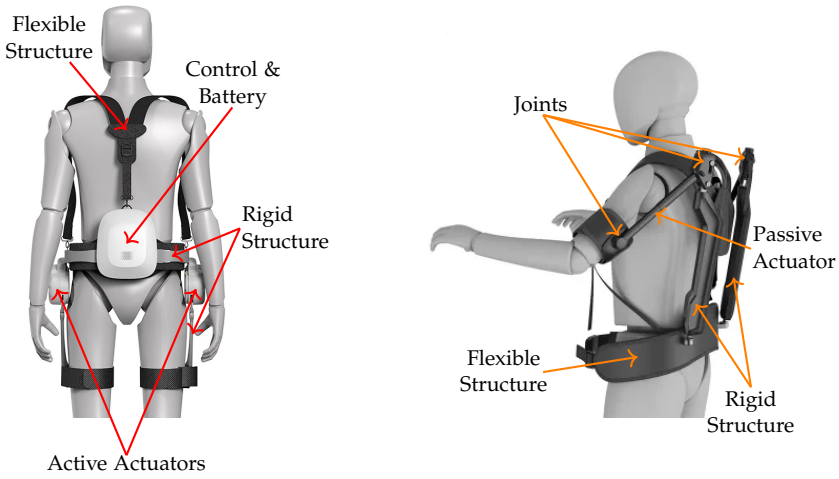

Figure 2.1: Comparison Active - Passive Exoskeletons.

They are used in a wide range of applications, including medical rehabilitation, health care, material handling in construction, industrial work and military operations. Some examples are reported in Figure 2.2.
Another case is in military applications where they enhance soldiers' endurance and load-carrying capacity, improving their overall performance in the field (Figure 2.2c).
In industrial environments, it is possible to summarize that the exoskeletons reduce the physical strain on workers that do repetitive

4 The actuators correspond to the system's joints.

(a) Worker with assistive full body exoskeleton.

(b) Worker with assistive upper body exoskeleton.

(c) Military Exoskeleton.

Figure 2.2: Examples of Different Types of Industrial-Militar Exoskeletons.

tasks or moving heavy lift and increasing productivity; also they improve strength and force supporting the user's movements and posture. They also ensure a better health and safety for human operators, reducing the risk of injuries, such as back problems, bone wear, and muscle fatigue. Another significant sector where exoskeletons are extensively used is the medical field. Rehabilitation exoskeletons assist patients (they may be old people or athletes) in regaining mobility and muscle strength after injuries or surgeries through personalized exercise programs that control and apply the correct amount of force, avoiding additional complications. They are also used to restore a patient's previous range of motion and independence more quickly than rehabilitation methods that rely solely on human support from a physiotherapist. They exist for all parts of the body and some example are reported in Figure 2.3.

In addition, thanks to the control technology behind it is possible to collect and analyzed data to adapt (online or offline) the exoskeleton to the user's needs or request. Using these data, the company can also monitor some important user parameters (force applied, fatigue, tiredness etc.. . .) through the sensors present on the system and do an estimation the user's health status.

From this point of view, it is easy to understand that the exoskeletons will applicable more and more day by day to facilitate the daily life, the working conditions and reach a good level of health for people, preventing the problems associated with arduous work and not only. On the other hand, it is important to highlight that this technology is very expensive and requires a significant investment. Addition-

(a) Lower Exetremities.

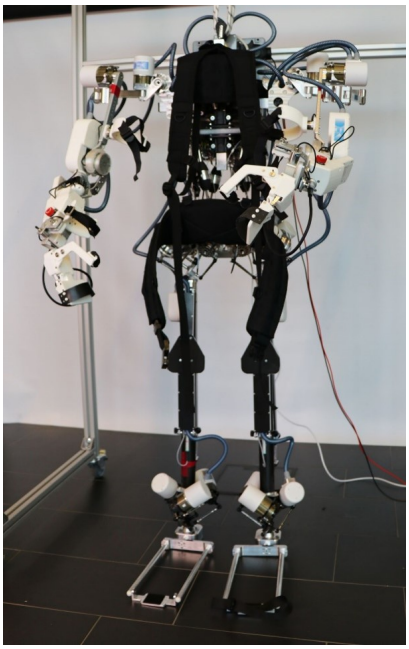

(b) Full Body Exoskeleton.

(c) Upper Extremities.

Figure 2.3: Examples of Different Types of Rehabilitative Exoskeletons.

ally, users[5] need to undergo specific training to learn how to use the system, which demands both time and money. Other factors to consider include maintenance, updates, limitations in movements and continuous data analysis to optimize performance for each operator.

In this chapter, we have provided an overview of various types of exoskeletons and their applications. Subsequently, we will focus on the specific Upper Limb Exoskeleton, discussing its general functions and uses. We will then define the kinematic and dynamic models.

5 By *users*, we refer to individuals who directly operate the exoskeleton system on their own bodies (in industrial or military sectors) as well as those who assist patients during rehabilitation, such as physiotherapists, rehabilitation specialists, or, in general, rehabilitation support staff.

2.1 EXOSKELETONS FOR UPPER LIMB REHABILITATION

A specific category of exoskeleton, which will be covered in this thesis, is designed to assist patient in upper limb rehabilitation. The main target is to improve upper limb motion functions, such as shoulder and elbow movements, and to help patients regain independence in daily activities. Without their usage, some normal and simple movements can be impossible for injured individuals, significantly limiting their life quality and requiring them to seek assistance frequently. Starting from this point of view, they are engineered to assist and guide movements during rehabilitation process, providing the correct support during training and accelerating the recovery process. The level of assistance is tailored to the patient's arm health status, allowing the physiotherapist to adapt the exercises for maximum efficiency and effectiveness. Also, the exercises are defined according to the part of the arm to be improved. They give a lot of benefits but the main problem is the cost of the system due to the high technology behind it. Also, the system most of the system, depending on its structure, require a lot of space and also it is very heavy. For these reasons, researchers are currently trying to reduce these difficulties and simplify the system, such as by converting them into wearable and very light devices. This transformation allows for home use and remote care by physical therapists, eliminating the need for patients to visit the clinic periodically. Some consequences of there are cost and complexity reducing.

Indeed, there are many different types of upper limb exoskeletons, which vary based on several factors, such as the ones mentioned in the introduction of this thesis. The mains are:

- **Structure**: material composition (rigid, flexible,aluminum, carbon fiber, polymers, etc...), modularity and design (wearable or fixed to external supports).
- **Degrees of Freedom (DoF)**: this determines the adaptability and the range of exercises possible. We can find 1 DoF or Multi-DoF (up to 5 DoF or more) exoskeletons;
- **Actuators**: electric, pneumatic, hydraulic, etc...and this affect the typology of possible movements and also the structure;
- **Interface and Control System**: methods for user interaction and control to set the appropriate exercise and the correct set-up of the system (level of help, stiffness, etc...);
- **Sensors**: the are useful for monitoring system and patient/user conditions. The most common are position, torque, and electromyographic (EMG) signals;
- **Power Supply**: battery-powered or plug-in systems.

Some examples are reported in Figure 2.4.

All of the reported examples aim to mimic the natural daily move-

(a) Multi-DoF and Heavy with External Rigid Support [12].

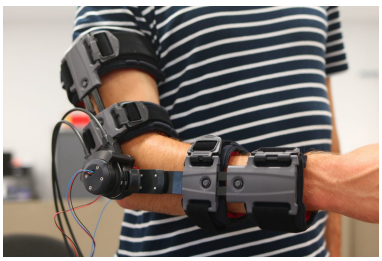

(b) 1DoF and Wearable Exoskeleton for Elbow Rehabilitation with Light Structure [22].

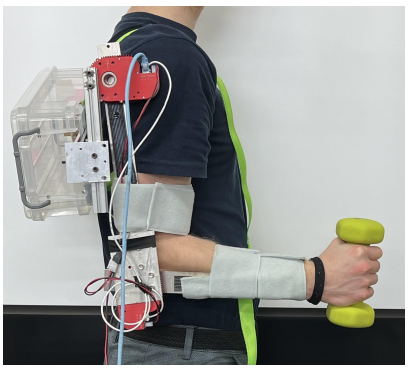

(c) 2DoF, Wearable, Lightweight Prototype Exoskeleton.

Figure 2.4: Examples of Different Types of Upper-Limb Exoskeletons.

ments of the human arm (whether at home, while participating in sports, or exercising at the gym). To identify the optimal design, it is essential to mix robotics, mechanics, electronics, and control systems. Additionally, having an external specialist in rehabilitation exercises is crucial for proper setup and control, ensuring that the movements and force assistance are accurate and effective. Furthermore, considerations must include ergonomics, user comfort, safety, and ease of use.

It is clear that this represents largely a mechatronic application, encompassing all the disciplines necessary to define and optimize an effective exoskeleton.

Actually, if we take the word *Mechatronic* and break it down, we can see that it's composed of *mechanics and electronics*. We can see that this discipline combines two significant elements that were often kept separate in the past. But it's not just that; it is more. Mechatronics is a combination of mechanics, electronics, control applications, and computer software in the development of new things, such as robots, automatic systems, etc... [7]. The goal of mechatronics is to implement a system with most control processes using software, running

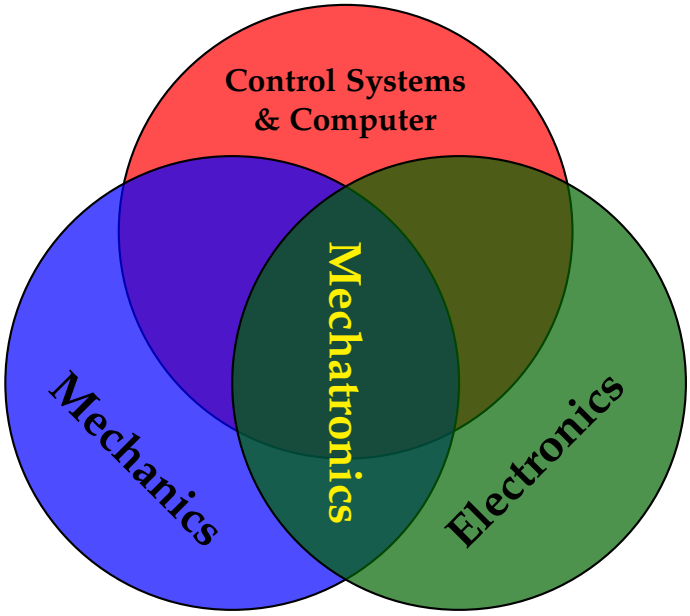

Figure 2.5: Mechatronics Disciplines.

in microcontrollers with appropriate code written in `C, C++, Python` languages. Another ambition is to use the estimation of a significant portion of the system's state variables (with appropriate techniques such as Kalman Filter, estimators, etc...) to have a few sensors and decrease problems caused by them. This control needs to exhibit robustness, with practically negligible errors, to ensure stability, reliability, and safety in the system's operation.
In conclusion, the Mechatronic discipline include all the goal that we also would like to include in this exoskeleton project.

2.2 KINEMATIC AND DYNAMIC MODELS

An exoskeleton system can be modeled as a rigid structure comprising two links connected by rotational joints. In simpler terms, it can be viewed as a two-link manipulator, where the rotational joints serve as actuators, and the two links form the rigid elements of the structure. This representation is illustrated in Figure 2.7, which shows the joint coordinates θ_1 and θ_2, representing the shoulder and elbow positions of the user's arm, respectively. Additionally, the end-effector is positioned at the point (x, y), which corresponds to the linear coordinates and aligns with the user's wrist.

In the system, we move the rigid structure using the actuators, but we can work in two different approaches: joint space or workspace coordinates, also called *forward kinematics* and *inverse kinematics*, respectively.

In the first approach, we control the system directly by positioning the actuators θ_1 and θ_2 to achieve the desired final angular positions

of the joints. In the second one, the desired position is (x, y) of the end-effector. To achieve this, we need to determine the actuator positions θ_1 and θ_2, and this calculation is a bit more complex than the first one.

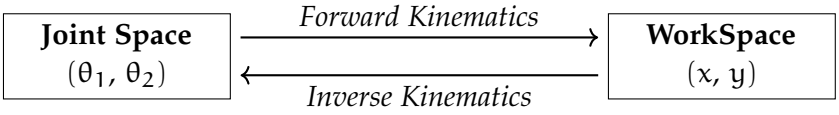

Figure 2.6: Kinematics Approaches.

Based on this information, it is possible to derive the kinematic equations and the dynamic equations to define the physical behavior of the system and to understand how to control the system through the exercises to be performed.
In the following rows, we will explore both approaches and determine the appropriate equations needed to define the desired system behavior.

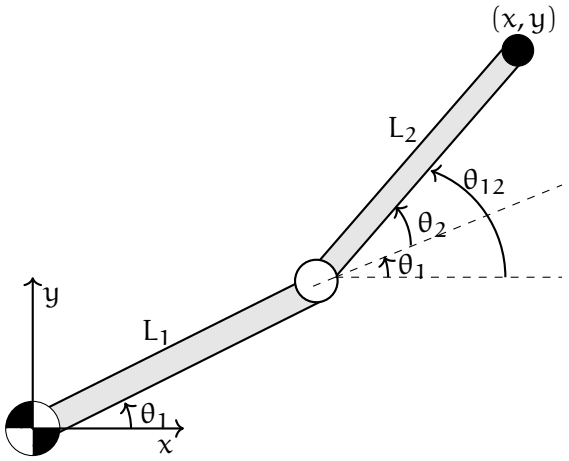

Figure 2.7: Upper Limb Exoskeleton Model as a Two Link Manipulator.

2.2.1 *Kinematics Analysis*

Before starting with the equations, it is helpful to define the nomenclature that will be used in the following subsections. For a faster and more efficient writing, we will use the following notation:

- $\theta_1 + \theta_2 \longrightarrow \theta_{12}$, which is necessary to calculate the correct position of link 2 and highlight its dependence on the position of link 1.

- $\cos(\theta_i) \longrightarrow c_i$
- $\sin(\theta_i) \longrightarrow s_i$
- $\cos(\theta_{ij}) \longrightarrow c_{ij}$
- $\sin(\theta_{ij}) \longrightarrow s_{ij}$

◦ ***Forward Kinematics***

Working in workspace coordinates, we would define the end-effector position as a function of the joint angles. The equations are defined as follows:

$$\begin{cases} x = L_1 \cos(\theta_1) + L_2 \cos(\theta_{12}) \\ y = L_1 \sin(\theta_1) + L_2 \sin(\theta_{12}) \end{cases} \tag{1}$$

Now, we have to derivate the eq. 1 to obtain first end-effector velocity and then acceleration. It is obtained:

$$\begin{cases} \dot{x} = -L_1 \sin(\theta_1)\dot{\theta}_1 - L_2 \sin(\theta_{12})\dot{\theta}_{12} \\ \dot{y} = L_1 \cos(\theta_1)\dot{\theta}_1 + L_2 \cos(\theta_{12})\dot{\theta}_{12} \end{cases} \tag{2}$$

and it is also possible to decompose the velocity components of $\dot{\theta}_{12} = \dot{\theta}_1 + \dot{\theta}_2$ and rewrite them in matrix form as follows:

$$\underbrace{\begin{bmatrix} \dot{x} \\ \dot{y} \end{bmatrix}}_{\dot{x} \in \mathbb{R}^{2\times 1}} = \underbrace{\begin{bmatrix} -L_1 \sin(\theta_1) - L_2 \sin(\theta_{12}) & -L_2 \sin(\theta_{12}) \\ L_1 \cos(\theta_1) + L_2 \cos(\theta_{12}) & L_2 \cos(\theta_{12}) \end{bmatrix}}_{J_{aco} \in \mathbb{R}^{2\times 2} = \text{Jacobian Matrix}} \underbrace{\begin{bmatrix} \dot{\theta}_1 \\ \dot{\theta}_2 \end{bmatrix}}_{\dot{\theta} \in \mathbb{R}^{2\times 1}} \tag{3}$$

The found *Jacobian matrix* $\boldsymbol{J_{aco}} \in \mathbb{R}^{2\times 2}$, which collects the partial derivatives, is crucial for simple mapping the joint velocities to the end-effector (or workspace) velocities. It will be very useful in the dynamic analysis, as we will see later.

Similarly, the process for deriving the acceleration involves additional steps to obtain the final results. Below are the steps to clearly illustrate the procedure.

Starting with the (3), we need to compute again the time derivative. We apply the product rule

$$\frac{d}{dt}\begin{bmatrix} \dot{x} \\ \dot{y} \end{bmatrix} = \frac{d}{dt}\left\{ \mathbf{J_{aco}} \cdot \begin{bmatrix} \dot{\theta}_1 \\ \dot{\theta}_2 \end{bmatrix} \right\}$$

and we obtain:

$$\begin{bmatrix} \ddot{x} \\ \ddot{y} \end{bmatrix} = \frac{d\mathbf{J_{aco}}}{dt}\begin{bmatrix} \dot{\theta}_1 \\ \dot{\theta}_2 \end{bmatrix} + \mathbf{J_{aco}}\begin{bmatrix} \ddot{\theta}_1 \\ \ddot{\theta}_2 \end{bmatrix} \tag{4}$$

where the time derivative of the Jacobian matrix $\mathbf{J_{aco}}$ is:

$$\frac{d\mathbf{J_{aco}}}{dt} = \begin{bmatrix} -L_1 c_1 \dot{\theta}_1 - L_2 c_{12}(\dot{\theta}_1 + \dot{\theta}_2) & -L_2 c_{12}(\dot{\theta}_1 + \dot{\theta}_2) \\ -L_1 s_1 \dot{\theta}_1 - L_2 s_{12}(\dot{\theta}_1 + \dot{\theta}_2) & -L_2 s_{12}(\dot{\theta}_1 + \dot{\theta}_2) \end{bmatrix}$$

Combining these expressions, we obtain the acceleration equations:

$$\begin{bmatrix} \ddot{x} \\ \ddot{y} \end{bmatrix} = \begin{bmatrix} -L_1 c_1 \dot{\theta}_1 - L_2 c_{12}(\dot{\theta}_1 + \dot{\theta}_2) & -L_2 c_{12}(\dot{\theta}_1 + \dot{\theta}_2) \\ -L_1 s_1 \dot{\theta}_1 - L_2 s_{12}(\dot{\theta}_1 + \dot{\theta}_2) & -L_2 s_{12}(\dot{\theta}_1 + \dot{\theta}_2) \end{bmatrix} \begin{bmatrix} \dot{\theta}_1 \\ \dot{\theta}_2 \end{bmatrix} + \\ + \begin{bmatrix} -L_1 s_1 - L_2 s_{12} & -L_2 s_{12} \\ L_1 c_1 + L_2 c_{12} & L_2 c_{12} \end{bmatrix} \begin{bmatrix} \ddot{\theta}_1 \\ \ddot{\theta}_2 \end{bmatrix} \iff$$

$$\dot{x} = \mathbf{J_{aco}}\ \ddot{\theta} + \dot{\mathbf{J}}_{\mathbf{aco}}\ \dot{\theta} \tag{5}$$

- ***Inverse Kinematics***

Inverse kinematics is essential for defining the reference position in control systems to achieve a desired end-effector position or hand position for human arm. In simple terms, it involves determining the joint angles θ_1 and θ_2 that provide the correct exoskeleton configuration. This is crucial because while the actuators in the system can rotate 360°, certain configurations may be infeasible due to the natural limits of the human anatomy.

Starting with the position case, we need to compute the vector connecting the origin of the system to the end-effector's position, as illustrated in Figure 2.8.

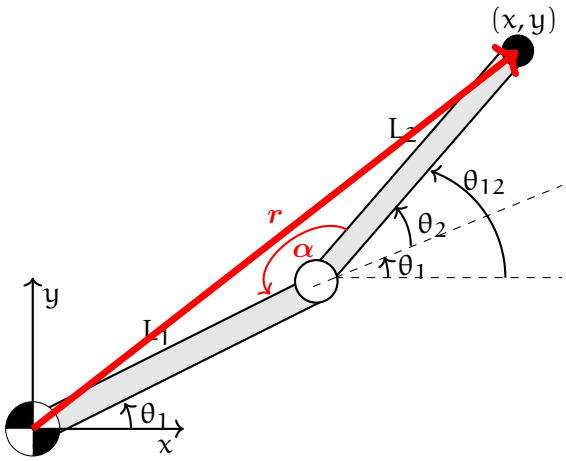

Figure 2.8: Upper Limb Exoskeleton Model as a Two Link Manipulator - Inverse Kinematics (part 1).

To define the vector $\boldsymbol{r}$, we use first the *Pythagorean Theorem* and then the *Law of Cosines*. It is obtained by the following equations:

$$r^2 = x^2 + y^2 = L_1^2 + L_2^2 + 2L_1 L_2 \cos(\alpha)$$

and we can calculate the angle α as follows:

$$\cos(\alpha) = \frac{L_1^2 + L_2^2 - r^2}{2L_1 L_2} \tag{6}$$

We are searching for the angles θ_2 and it corrispond to $\theta_2 = \pi - \alpha$. Therefore

$$\begin{aligned}\cos(\theta_2) &= \cos(\pi - \alpha) = \\ &= \cos(\pi)\cos(\alpha) + \sin(\pi)\sin(\alpha) = \\ &= -\cos(\alpha)\end{aligned} \tag{7}$$

The final equation is

$$\cos(\theta_2) = \frac{r^2 - L_1^2 - L_2^2}{2L_1L_2}$$

and returns two possible solutions:

$$\theta_2 = \begin{cases} \pi - \cos^{-1}\left(\dfrac{L_1^2 + L_2^2 - r^2}{2L_1^2L_2^2}\right) \\ \\ \cos^{-1}\left(\dfrac{r^2 - L_1^2 - L_2^2}{2L_1^2L_2^2}\right) \end{cases} \tag{8}$$

Found this angle, we are left to calculate $\mathtt{theta}_1$. To do this, we have to apply the *Law of Tangents* and we need the angles β and γ as shown in Figure 2.9.

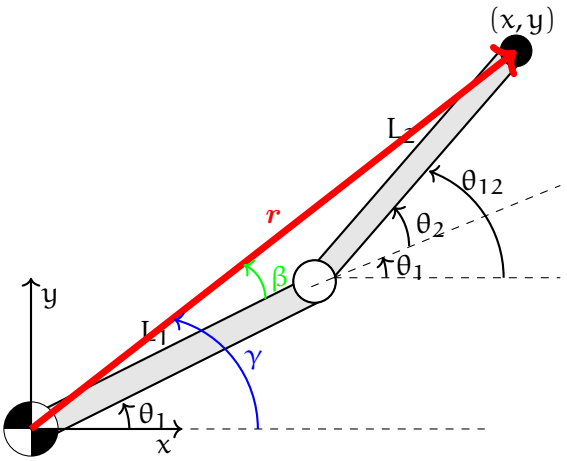

Figure 2.9: Upper Limb Exoskeleton Model as a Two Link Manipulator - Inverse Kinematics (part 2).

It is possible to write:

$$\tan(\theta_1 + \beta) = \frac{y}{x} \quad \Longrightarrow \quad \theta_1 = \underbrace{\tan^{-1}\left(\frac{y}{x}\right)}_{\gamma} - \beta = \gamma - \beta \tag{9}$$

and we also define as:

$$\beta = \tan^{-1}\left(\frac{L_2\sin(\theta_2)}{L_1 + L_2\cos(\theta_2)}\right) \tag{10}$$

Adding (10) to (9), we obtain the final equation for θ_1:

$$\theta_1 = \tan^{-1}\left(\frac{y}{x}\right) - \tan^{-1}\left(\frac{L_2 \sin(\theta_2)}{L_1 + L_2\cos(\theta_2)}\right) \tag{11}$$

By combining (11) and (8), we can achieve two possible system configurations to obtain the desired end-effector position. Specifically, we have:

- High Elbow Configuration $\longrightarrow \theta_2 < 0$

$$\begin{bmatrix}\theta_1\\ \theta_2\end{bmatrix} = \begin{bmatrix}\tan^{-1}\left(\frac{y}{x}\right) - \tan^{-1}\left(\frac{L_2 \sin(\theta_2)}{L_1 + L_2\cos(\theta_2)}\right)\\ \\ \pi - \cos^{-1}\left(\frac{L_1^2 + L_2^2 - r^2}{2L_1^2L_2^2}\right)\end{bmatrix} \tag{12}$$

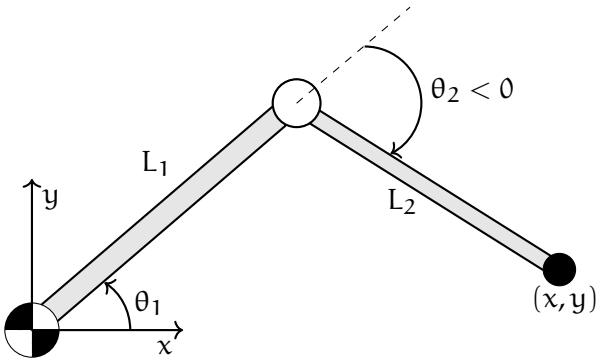

Figure 2.10: Exoskeleton in High Elbow Configuration ($\theta_2 < 0$).

- Low Elbow Configuration $\longrightarrow \theta_2 > 0$

$$\begin{bmatrix}\theta_1\\ \theta_2\end{bmatrix} = \begin{bmatrix}\tan^{-1}\left(\frac{y}{x}\right) - \tan^{-1}\left(\frac{L_2 \sin(\theta_2)}{L_1 + L_2\cos(\theta_2)}\right)\\ \\ \cos^{-1}\left(\frac{r^2 - L_1^2 - L_2^2}{2L_1^2L_2^2}\right)\end{bmatrix} \tag{13}$$

For obvious reasons related to the natural limits of the human body, we can only choose the low elbow configuration as shown in Figure 2.11 and represented by (13).

Regarding velocity and acceleration, the end-effector's terms can be mapped to the joint space leveraging the *Jacobian matrix* $\mathbf{J_{aco}}$. This is much easier than the position case. In fact, starting from (3), we can simply write:

$$\begin{bmatrix}\dot\theta_1\\ \dot\theta_2\end{bmatrix} = \mathbf{J_{aco}}^{-1}\begin{bmatrix}\dot x\\ \dot y\end{bmatrix} = \frac{1}{L_1 s_2}\begin{bmatrix} c_{12} & s_{12}\\ \\ -\left(\frac{L_1 c_1}{L_2} + c_{12}\right) & \frac{L_1 s_1}{L_2} + s_{12}\end{bmatrix}\begin{bmatrix}\dot x\\ \dot y\end{bmatrix} \tag{14}$$

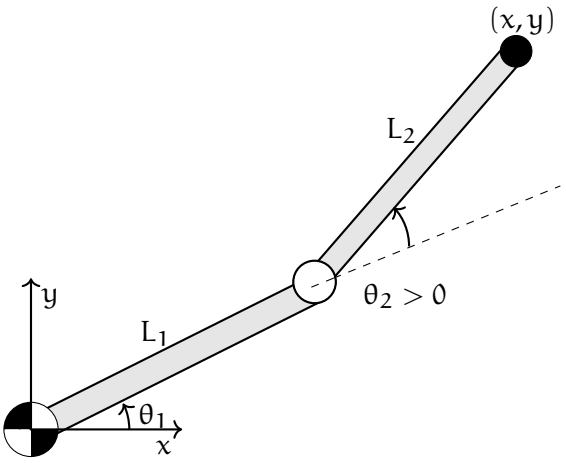

Figure 2.11: Exoskeleton in Low Elbow Configuration ($\theta_2 > 0$).

It is necessary to highlight that the $\mathbf{J_{aco}}$ matrix is not always invertible. This situation occurs when the exoskeleton achieves a singular configuration. The possibilities of singular configurations are:

- $\theta_2 = 0$
- $\theta_2 = \pm\pi$

In our study, singular configurations are not considered since these positions are neither feasible nor useful for rehabilitation exercises.

The acceleration problem is very similar. The (5) can be inverted as:

$$\begin{bmatrix} \ddot{\theta}_1 \\ \ddot{\theta}_2 \end{bmatrix} = \mathbf{J_{aco}}^{-1} \left(\begin{bmatrix} \ddot{x} \\ \ddot{y} \end{bmatrix} - \dot{\mathbf{J}}_{\mathbf{aco}} \begin{bmatrix} \dot{\theta}_1 \\ \dot{\theta}_2 \end{bmatrix} \right) = \mathbf{J_{aco}}^{-1} \left(\begin{bmatrix} \ddot{x} \\ \ddot{y} \end{bmatrix} - \dot{\mathbf{J}}_{\mathbf{aco}} \mathbf{J_{aco}}^{-1} \begin{bmatrix} \dot{x} \\ \dot{y} \end{bmatrix} \right) \tag{15}$$

The (15) can be simplified under the assumption that the *Jacobian matrix* $\mathbf{J}_{aco}$ variations are negligible compared to the joints velocities and accelerations of the joints. This approximation holds only when the manipulator moves very slowly, allowing the Jacobian matrix $\mathbf{J}_{aco}$ to be considered approximately constant.

An example of this situation is when the exoskeleton trajectory for the assisted exercises is designed to be smooth (the jerk value is very low) and without sudden changes in velocity and acceleration.

Hence, the simplified equation (15) is:

$$\begin{bmatrix} \ddot{\theta}_1 \\ \ddot{\theta}_2 \end{bmatrix} = \mathbf{J_{aco}}^{-1} \left(\begin{bmatrix} \ddot{x} \\ \ddot{y} \end{bmatrix} - \cancel{\dot{\mathbf{J}}_{\mathbf{aco}} \mathbf{J_{aco}}^{-1} \begin{bmatrix} \dot{x} \\ \dot{y} \end{bmatrix}} \right) \approx 0 = \mathbf{J_{aco}}^{-1} \begin{bmatrix} \ddot{x} \\ \ddot{y} \end{bmatrix}$$

Now, we have all the necessary kinematic equations to define the system's movements and positions in the two reference systems.

2.2.2 *Dynamic Analysis*

The dynamic analysis of the exoskeleton system is essential for studying the inertial, velocity, and gravity components that influence the system's behavior. By defining the dynamic model, we can design the control system based on the derived information. Additionally, this analysis helps us better understand the system's behavior in the presence of external disturbances, such as friction and force/torque disturbances.

An effective approach is using *Lagrange's Formulation*, which leverages an energy-based approach by defining the kinetic and potential energy of the system. This provides information to calculate the amount of torque τ that each actuator (or joint) must apply to move the system. The formulation is defined as follows:

$$\mathcal{L}(\theta, \dot{\theta}) = \mathcal{K}(\theta, \dot{\theta}) - \mathcal{P}(\theta) \tag{16}$$

where $\mathcal{K}(\theta, \dot{\theta})$ represents the kinetic energy and $\mathcal{P}(\theta)$ represents the potential energy. Then, staring by (16), we proceed to define the torque τ as reported in the following equation:

$$\tau = \frac{d}{dt}\left(\frac{\partial \mathcal{L}}{\partial \dot{\theta}}\right) - \frac{\partial \mathcal{L}}{\partial \theta} \tag{17}$$

To define $K(\theta, \dot{\theta})$ and $P(\theta)$ energies, we can use a simplified representation of the exoskeleton by concentrating the mass of the links at their ends. Also we need to add the mass of the actuator 2 to the link 1. Specifically, we can consider the mass of the motor as a part of the link and define

$$m_1 = m_{L_1} + m_{M_2}$$

The mass of actuator 1 M_1 is fixed to the frame and is not considered because it does not produce any effect.
This is a common approach in robotics that simplifies the dynamic study. The system can then be schematized as shown in Figure 2.12.

We need to determine the coordinates of joints 1 and 2. The first ones are given by:

$$\begin{cases} x_1 = L_1 \cos(\theta_1) \\ y_1 = L_1 \sin(\theta_1) \end{cases} \implies \begin{cases} \dot{x}_1 = -L_1 \sin(\theta_1)\dot{\theta}_1 \\ \dot{y}_1 = L_1 \cos(\theta_1)\dot{\theta}_1 \end{cases}$$

while the second ones are the just found in (1) and (3).
Therefore, $\mathcal{K}(\theta, \dot{\theta})$ and $\mathcal{P}(\theta)$ can be defined as follows:

- Link 1

$$\mathcal{K}_1 = \frac{1}{2} m_1 v_1^2 = \frac{1}{2} m_1 \left(\dot{x}_1^2 + \dot{y}_1^2\right)^2 =$$

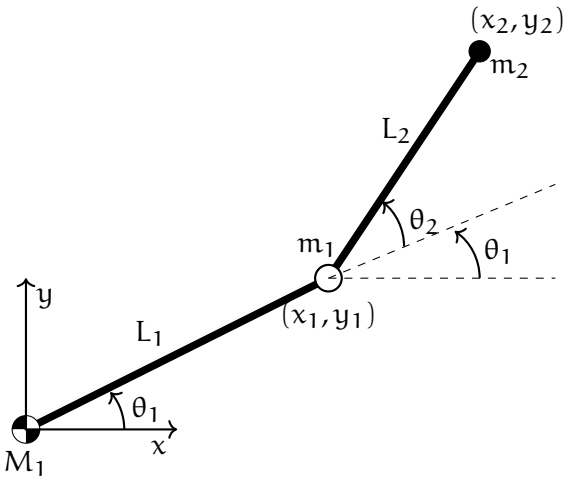

Figure 2.12: Upper Limb Exoskeleton - Simplify Model.

$$= \frac{1}{2} m_1 \left[L_1^2 \sin^2(\theta_1)\dot{\theta}_1^2 + L_1^2 \cos^2(\theta_1)\dot{\theta}_1^2 \right] = \frac{1}{2} m_1 L_1^2 \dot{\theta}_1^2$$

$$\mathcal{P}_1 = m_1 g y_1 = m_1 g L_1 \cos(\theta_1)$$

- Link 2

$$\begin{aligned} \mathcal{K}_2 &= \frac{1}{2} m_2 v_2^2 = \frac{1}{2} m_2 \left(\dot{x}_2^2 + \dot{y}_2^2 \right)^2 = \\ &= \frac{1}{2} m_2 \left[\left(L_1^2 + L_2^2 + 2 L_1 L_2 \cos(\theta_2) \right) \dot{\theta}_1^2 \right. \\ &\quad \left. + \; L_2 \dot{\theta}_2^2 + 2 \left(L_2^2 + L_1 L_2 \cos(\theta_2) \right) \dot{\theta}_1^2 \dot{\theta}_2^2 \right] \end{aligned}$$

$$\mathcal{P}_2 = m_2 g y_2 = m_2 g \left(L_1 \cos(\theta_1) + L_2 \cos(\theta_1 + \theta_2) \right)$$

Applying now, first the (16) and later the (17), we obtain:

$$\begin{aligned} \tau_1 &= [m_1 L_1^2 + m_2 (L_1^2 + 2 L_1 L_2 \cos(\theta_2) + L_2^2)]\ddot{\theta}_1 + \\ &+ \; m_2 (L_1 L_2 \cos(\theta_2) + l_2^2)\ddot{\theta}_2 + \\ &- m_2 l_1 l_2 \sin(\theta_2)(2\dot{\theta_1}\dot{\theta_2} + \dot{\theta}_2^2) + \\ &+ \; (m_1 + m_2) l_1 g \cos(\theta_1) + m_2 g l_2 \cos(\theta_1 + \theta_2) + f_1 \dot{\theta}_1 + \tau_{s,1} \end{aligned}$$

$$\begin{aligned} \tau_2 &= m_2 [l_1 l_2 \cos(\theta_2) + l_2^2]\ddot{\theta}_1 + m_2 l_2^2 \ddot{\theta}_2 + m_2 l_1 l_2 \theta_1^2 \sin(\theta)_2 + \\ &+ \; m_2 g l_2 \cos(\theta_1 + \theta_2) + f_2 \dot{\theta}_2 + \tau_{s,2} \end{aligned} \tag{18}$$

In (18), the friction components are included as the last term of each equation, representing the viscous friction of the actuators. The coefficients f_1 and f_2 are the viscous friction coefficients.
Also we can rewrite the (18) in the form

$$\tau - \tau_d = M(\theta)\,\ddot{\theta} + C(\theta, \dot{\theta})\,\dot{\theta} + G(\theta) + F\,\dot{\theta}$$

identifying the following matrix:

$$M = \begin{bmatrix} M_{11} & M_{12} \\ M_{21} & M_{22} \end{bmatrix} = \text{Inertial Matrix}$$

$$M_{11} = m_1 L_1^2 + m_2(L_1^2 + 2L_1 L_2 c_2 + L_2^2)$$

$$M_{12} = M_{21} = m_2(L_1 L_2 c_2 + L_2^2)$$

$$M_{22} = m_2 L_2^2$$

$$C = \begin{bmatrix} -m_2 L_1 L_2 s_2 \dot{\theta}_2 & -m_2 L_1 L_2 s_2(\dot{\theta}_1 + \dot{\theta}_2) \\ m_2 L_1 L_2 s_2 \dot{\theta}_2 & 0 \end{bmatrix} = \text{Velocity Terms}$$

$$G = \begin{bmatrix} (m_1 + m_2) L_1 c_1 + m_2 L_2 c_{12} \\ m_2 L_2 c_{12} \end{bmatrix} \cdot g = \text{Gravity Terms}$$

$$F = \begin{bmatrix} f_1 & 0 \\ 0 & f_2 \end{bmatrix} = \text{Viscous Friction Terms}$$

$$\tau_s = \begin{bmatrix} \tau_{s,1} \\ \tau_{s,2} \end{bmatrix} = \text{Static Friction Terms}$$

$$\tau_d = \begin{bmatrix} \tau_{d,1} \\ \tau_{d,2} \end{bmatrix} = \text{External Disturbance}$$

Completed the kinematic and dynamic analysis of the exoskeleton system as a two link manipulator, we have all the information to proceed to the control design.
Before that, in the next chapter of this thesis we will see the choice of components and their characteristics.

3

ELECTRO-MECHANICAL DESIGN

In this chapter, we will present the components of the 2DoF prototype exoskeleton. In particular, we will discuss the Hebi Robotics Actuator®, that is the main and fundamental components. In the next pages, we will highlight its specifications (voltage, output torque, sensors, dimensions, etc...) and also we will discuss why it is a good choice. In addition, we will talk about the structure which was chosen to be lightweight, wearable and completely autonomous by any external support.

3.1 HEBI ROBOTICS ACTUATOR®

The Hebi Robotics Actuator® X-Series (Figure 3.1) is a *serial-elastic actuator* (*SEA*) and an actuator (or motor), gear train, spring, sensors, and control electronics into a compact package. The composition of this motor can be better understood by referring to Figure 3.2, which shows its schematic.

Figure 3.1: Hebi Robotics X5-Series Actuator® [9].

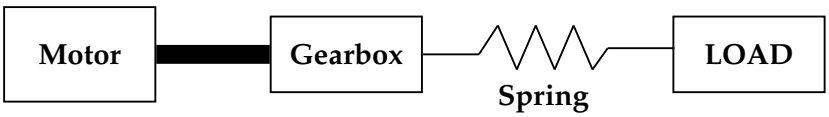

Figure 3.2: SEA Equivalent Scheme.

HEBI motors are versatile, ethernet-connected that serve as the foundation for constructing robots for different research application or automated systems.
Equipped with actuators for motion generation and interfaces for various sensors and inputs/outputs, these modules operate indepen-

dently using embedded firmware. This architecture enables seamless communication and control over a standard Ethernet network.

SEA actuator was presented in 1995 from G.A. Pratt and M.M. Wiliamson [17]. It provides a different perspective because it approaches the interface between motor and load differently than the traditional stiff approach[6]. In addition to its lightness, it can offer a lot of benefits in terms of mechanics and control, in particular in force/torque control applications. It furnishes lower reflected inertia, greater shock tolerance to impact load, lower mechanical output impedance, and capacity for storage energy, and using force control we can obtain more accuracy. Also, inside the box, there is a gear reduction to achieve high torque delivered in the output. It comport some issues such as friction, backlash, torque ripple, noise and reflected inertia[7] that comports more force in the gear teeth. Thanks to the presence of the spring that works as a low-pass filter, many of these disadvantages introduced can be avoided. While the spring offers certain advantages, its flexibility poses challenges in control system design. Specifically, it increases the complexity of control algorithms, narrows the control loop bandwidth, and often results in higher overall system costs when compared to a rigid motor with a gear train.
This type of actuator represents a novel approach to coupling loads with motors without a stiff connection, gaining increasing popularity in industrial applications. While the presence of a spring between motor and load might initially seem challenging for control system design, appropriate strategies and component selection (such as sensors) can yield precise position control performance.

The main components of a SEA actuator, as it is possibile to see in Figure 3.3, are:

1. Actuator: DC brushless motor;
2. Gear train: gear reduction to use a small motor and achieve output high torque at the same time;
3. Spring: it work as a low-pass filter to the vibration and allows a more precise and safer control in the interaction between human and robot.
4. Sensors: position (encoder), gyroscope, voltage, current, output torque, etc. . . ;

Also, the *X serie* Hebi Robotics® actuator is equipped with an Ethernet connector for computer communication and an LED indicating motor status.

6 The traditional approach is to make as stiff as possible the motor-load interface.
7 To transform the inertia from the motor side to the output side, or vice-versa, it is necessary to introduce the factor N^2, where N is the gear ratio (1 : N).

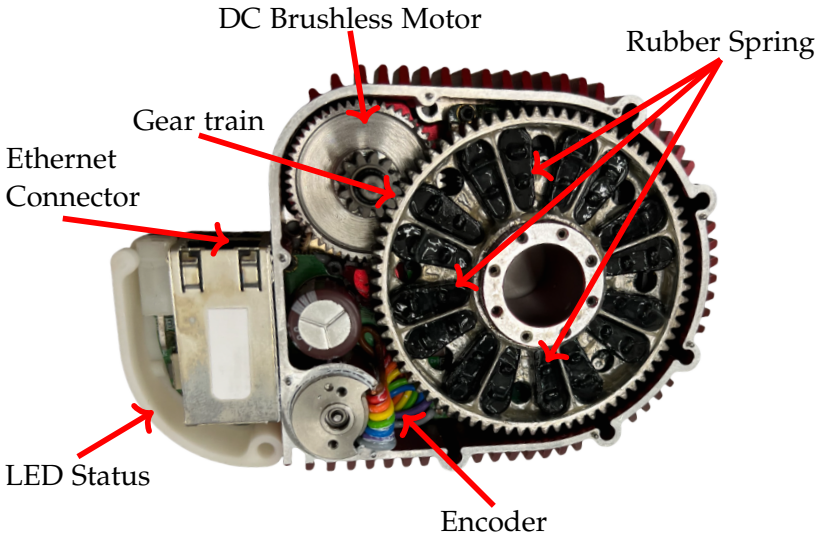

Figure 3.3: Hebi Robotics Actuator® - Main Components.

3.1.1 X5 – 9 *Specifications*

Hebi Robotics® offers a variety of actuators primarily differentiated by gear ratio (1:N) and output torque. Based on a thorough evaluation of output torque and actuator weight, critical parameters for exoskeleton applications, the X5-9 model was selected. Its specifications are detailed in Table 1.

On the motor, it is possible to find mounted the following sensors:

- Position: absolute encoder multi-turn = ±4 turns;
- Angular Velocity;
- 3-axis Gyroscope;
- DC Bus Voltage;
- Motor Current;
- Output Torque;
- Temperature.

As outlined in the project objectives, our exoskeleton application employs a sensorless approach, relying solely on position feedback. Output torque will be estimated using a method detailed in subsequent Chapter 4.

The encoder is strategically positioned on the load side of the system to accurately capture system position. Given the spring's elasticity, mounting the encoder on the motor side would introduce significant errors due to spring deflection. This error, compounded by external disturbances like human arm torque, cannot be reliably compensated. Consequently, a *no-colocated control* strategy, where the controlled variable differs from the measured variable, is essential. To do that, it is essential that the encoder has a very high resolution as we can find in the Hebi Robotics X5 – 9 actuator.

Rather than relying on the motor-mounted torque sensor provided by Hebi Robotics, which has a declared accuracy of 10 – 15%, we

Parameter	Variables	Value
Power Supply	Vcc	$24 - 48\,[V]$
Peak Current	I_{pk}	$1.6\,[A]$
Continuous Current	I_{cnt}	$0.5\,[A]$
Actuator Weight	M_m	$0.360\,[Kg]$
Max Speed	Ω_{out}	$14\,[rpm]$
Max Speed	Ω_{out}	$1.465\,rad/s$
Peak Torque	τ_{pk}	$13\,[Nm]$
Continuous Torque	τ_{cnt}	$8\,[Nm]$
Torque Constant	k_t	$7.1\,[Nm/A]$
Motor Resistance	R_m	$10\,[\Omega]$
Gear Ratio	N	1742.222
Spring Stiffness	K_S	$130\,[Nm/rad]$
Encoder Angular Resolution	θ_{res}	$0.005\,[°]$
Torque Sensor Resolution	τ_{res}	$0.001\,[Nm]$
Backlash	b	$\pm 0.25\,[°]$

Table 1: Electrical and Mechanical Parameters [9].

will implement a torque estimation method. This decision is driven by the insufficient accuracy of the sensor for our application, which requires precise torque control to ensure both optimal performance and patient safety during exercises.

To fully understand the motor's capabilities, its speed-torque performance curve, illustrated in Figure 3.4, is essential. This curve also depicts output power. The graph distinguishes between continuous and intermittent operating regions, highlighted in gray and red respectively. For our exoskeleton application, the continuous region is of primary interest, indicating a sustained torque output of 8 Nm up to a maximum speed of 14 rpm. This operating range aligns well with the slow, controlled movements required for exoskeleton applications. The curves were generated using a 36V power supply. However, their

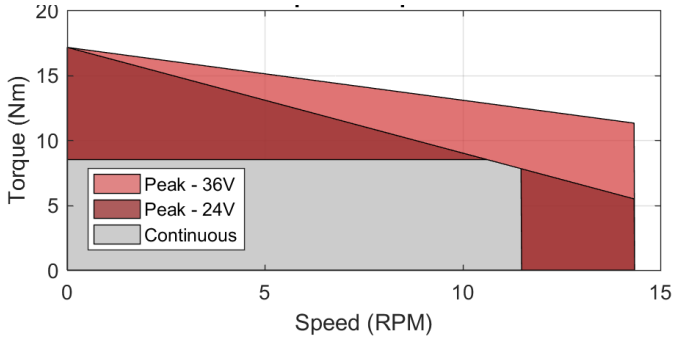

(a) Speed-Torque Curve

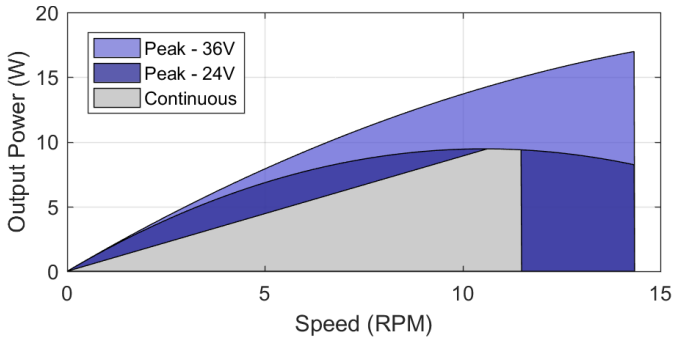

(b) Speed-Power Curve

Figure 3.4: Performance Curve X5 – 9 [9].

applicability extends to configurations with different voltages, such as our specific case of 24 V.

3.1.1.1 *How to Control the Hebi Robotics Actuator®*

Hebi Robotics provides four distinct control strategies. Three of these strategies combine position, velocity, and effort controls in a cascaded, parallel, or hybrid configuration. The remaining strategy is a Pulse Width Modulation (PWM) control. We will utilize this final strategy as it affords us the flexibility to define our custom controller.
This strategy necessitates communicating to the motor the percentage of supply voltage to apply to the DC bus in order to achieve the desired output torque. To develop the control code, we can leverage one of the available APIs, including C++, ROS, Python, or MatTLab®. We will employ MatLab® due to its simplicity in data acquisition, graph generation, result analysis, and the ease with which control gains can be adjusted.

Other Information

Additional information, such as dimensions and MATLAB code, can be found in Appendix C.

3.2 SUPPORT STRUCTURE

The exoskeleton must be both lightweight for portability and rigid to ensure accurate exercise execution, preventing unintended movements by the user. To achieve this, aluminum was selected for the rigid structure due to its availability, low weight, high strength, ductility, non-magnetic properties, and affordability. The structure must be sufficiently stiff to support heavy loads while accommodating the arm's range of motion.
In our design, the structure connects the two motors, forming the system's two links, and also serves as the primary support for the user's back. A detailed illustration of the structure is provided in Figure 3.5.

(a) Right View.

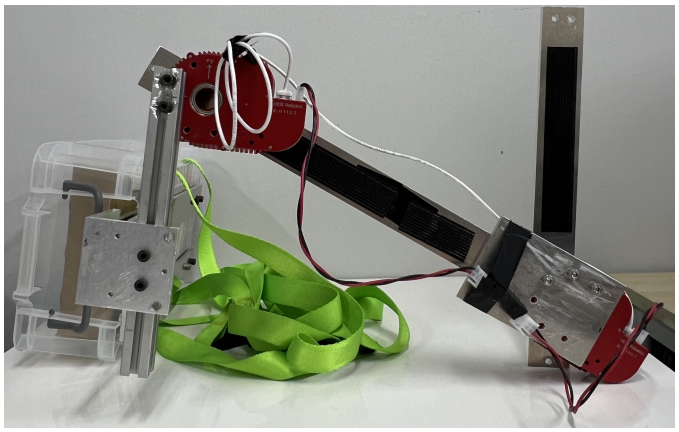

(b) Left View.

Figure 3.5: Prototype Structure - Right View.

3.3 FINAL PROTOTYPE

Following a comprehensive analysis of potential components and their respective advantages and drawbacks, the final exoskeleton prototype was designed. This structure will accommodate our custom

control system, enabling subsequent performance testing.
To realize this prototype, the following components are required:

- Two Hebi actuators, one for each joint - shoulder and elbow;
- One back pack to include rigid back structure, counterweight and future update;
- Two alluminium bars to connect the two motors;
- Two shoulder pads to wear the system;
- Power supply (24V battery or external generator);
- Ethernet cables for the computer$\longleftrightarrow$motors communication;
- Strips to fix the arm to the bars.

All of them are highlighted in Figure 3.6 and comment in Table 2.
The training weight can be used during the exercises to increase the load on the arm and improve the muscle strength. It can be added after the initial hand-free rehabilitation phase or based on the user's arm condition.

n.	Component-Part	Comments
/	link 1	$l_1 \in [0.26, 0.33]m$
		$m_{l_1} = 0.156\,Kg$
/	link 2	$l_2 \in [0.24, 0.30]m$
		$m_{l_2} = 0.140\,Kg$
1	Shoulder Actuator $1 - M_1$	Serial Number: $X - 01122$
2	Elbow Actuator $2 - M_2$	Serial Number: $X - 01157$
3	BackPack Support	//
4	Cables	—— Ethernet Cable[8]
5	Cables	—— Power Supply
6	Training Weight	//
7	Strips	To ensure the arm
8	Rigid Aluminum Framework	Adjustable height-lenght

Table 2: Exoskeleton Prototype Parts.

8 Also the white cable that connect M_1 to M_2 and vice versa is an Ethernet cable.

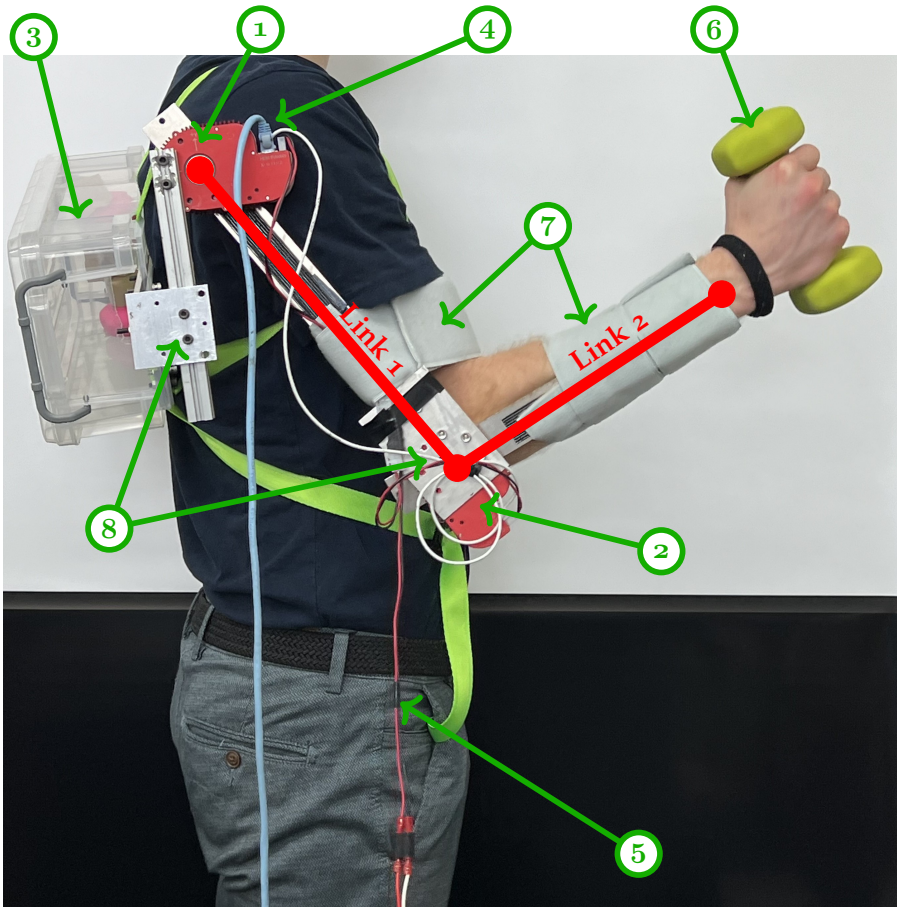

Figure 3.6: Final Exoskeleton Prototype.

The prototype has a total weight of 2.8 Kg [9], optimizing portability and structural integrity and finding also a good trade-off between the same properties.
The modular design, featuring adjustable links length via multiple holes on the connection part (visible on Figure 3.5a), enables customization for various users, requiring corresponding adjustments to system parameters. Also, the structure permits, how it is visible in Figure 3.6 to adjust the shoulder actuator.

Once we've defined the components, the next step is to design the control system for the exercise movements and human-robot interaction. This will be the subject of the next chapter.

9 This total weight excludes the battery for autonomous energy; the exoskeleton's actuators are powered by an external power supply generator. Adding a 24V lithium battery would increase the weight by approximately 3 to 5 kg.

4

CONTROL DESIGN

This chapter discusses the design of the system's control and is organized as follows. We begin by presenting the exercises used in the performance system tests[10]. Then, before detailing the final control strategy implemented in the exoskeleton system, we provide an overview of the available options and explain why they are not appropriate for the application under consideration.

4.1 REHABILITATION EXERCISES

The rehabilitation exercises with exoskeleton are based on the principles of maximizing muscle effort and reducing patient recovery time. These exercises are customized to the patient's injury type, condition, history and employment and may not be suitable for all patients. Specifically, the exercises we studied focus on athletes.The exercises include:

- **Static (or Isometric) Exercises** (Figure 4.1): these exercises involve muscle contraction without any articular motion, generating force without changing muscle length. They are used in the initial phase of rehabilitation, especially in cases of surgery and with post-operative weakness, to strengthen muscles. During these exercises, the patient pushes against a vertical or horizontal surface for about $15 - 20s$, followed by a $20 - 30s$ pause. This has to be repeated for $10 - 15$ minutes o more, depending on the patient response. The exoskeleton assists by keeping the arm in a fixed position to target the injured muscle or muscle group; it has to work as a stiff system that inhibit any possible arm movement.

- **Dynamic (or Active) Exercises** (Figure 4.2): in these exercises, muscles contract and lengthen due to articular movement in the space. They are introduced after static exercises, once the patient has regained some strength, and are crucial for restoring muscle flexibility and strength. Here, the arm has to follow a specific trajectory at a constant speed and apply the correct amount of force. The exoskeleton supports the patient's movements by maintaining the arm on the correct path and applying additional force if needed, while also preventing sudden movements.

10 This work was conducted by another member of Murakami's laboratory. He studied how these types of exercises can maximize muscle response during rehabilitation and reduce recovery time.

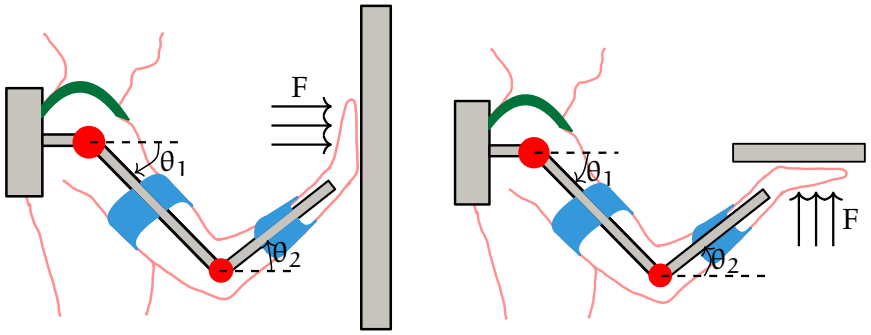

(a) Vertical Surface. (b) Horizontal Surface.

Figure 4.1: Static Exercises - θ_1, θ_2 fixed.

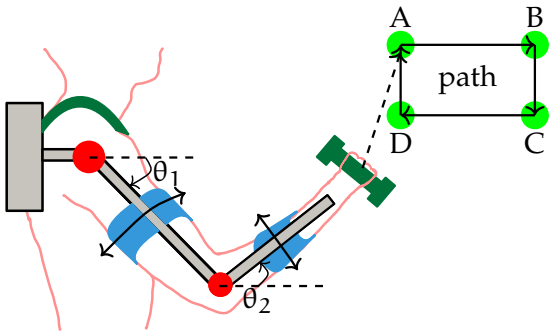

Figure 4.2: Dynamic Exercises - Example of Trajectory Path.

Each rehabilitation plan is personalized according to the patient's arm condition and the type of injury[11]. The duration of each phase and the type of exercises depend on muscle improvement and patient feedback, such as feelings of comfort, discomfort, or pain. The assistance provided by the exoskeleton can significantly accelerate recovery time, allowing athletes to return to their sport quickly and support their team.

To define the trajectory path for dynamic exercises (an example is the Figure 4.2) or the fixed position θ_1, θ_2 (as in Figures 4.1a or 4.1b), a preliminary force measurement using a $4-axis$ force sensor is required. The patient needs to push a bar attached to the sensor in four directions: x, y, $-x$, and $-y$. From the data collected, we define a hexagonal distribution in the (x, y) space to identify which muscles need improvement and determine the necessary direction (or directions) for targeted exercises.

11 In particular, which muscle or muscle groupe is injured.

Another important diagnostic exam to perform during or after rehabilitation is the *electromyography (EMG)* test. This test measures the electrical activity produced by a muscle[12]. By analyzing the voltage peaks recorded during activity, it is possible to assess muscle activity and improvements in strength.

4.2 OVERVIEW OF CONTROL STRATEGIES - SINGLE LOOP

4.2.1 *Position Control - Single Loop*

The concept of *Position control* (or motion control) originated in the 20th century with the introduction of the first automation in CNC machines, where precision in working on materials like metal remains crucial to this day. Initially, it was an analogue process, but with the advent of computers and microcontrollers, it transitioned into a digital form and started being applied to robots and new technologies that require precision and accuracy.
Today, in robotics applications, *Position control* is essential for guiding movements to perform various tasks, with accuracy and repeatable, such as working on materials (cutting, painting, etc.), fixing components within a structure, or welding two pieces together; in each example, the robot must follow a specific trajectory in space. The basic concept of position control is to use the sensor's output to adjust each joint's position to align with the desired output by closing the loop in the controller.
The structure is straightforward and can be illustrated in Figure 4.3, where the *Encoder* serves as the position sensor, the *Mechatronic system* is the component where control is applied, *Position control* can be achieved using P, PD, PI, or PID controllers, x_{ref} is the position reference, e_p is the position error, u_p is the control output, x is the position of system and x_{meas} is the position measurement [7].

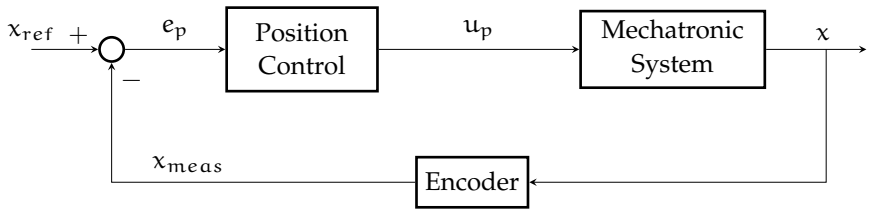

Figure 4.3: Position Control - Block Diagram.

4.2.2 *Force Control - Single Loop*

The human senses are hearing, sight, smell, taste, touch and, nowadays we are trying to implement them in robots with particular equip-

12 Or a muscle group, depending on how many electrodes are used.

ment or with sensorless technique. The sense of touch is one of the most important senses in humans because it provides feedback on the surrounding environment, allowing us to touch and move safely without accidents. Since the 1970s, researchers have been working on implementing touch sense in robots and to achieve this, another type of control, known as force control, became important. Many studies have been done in the past years but only in recent industries started to implement in applications [15]. It emerged also as a response to the need for robots to handle objects without causing damage, collaborate with or, for example, assist in rehabilitation by applying the correct force or help to lift heavy loads reducing the muscle force applied by the worker. Its definition depends on applications and it can be a specific control used to manage the interaction between a robot and the environment, ensuring safety, especially when there is an operator within the robot's work area.
The idea behind Force Control and the block diagram is very similar and analogous to the one used in the position control scheme shown in Figure 4.3. We can find the scheme illustrated in Figure 4.4 where the components are analogous to the previous ones., *Force sensor* serves to measure the force applied by the end-effector, the *Mechatronic system* is the component where control is applied, *Force Control* is often defined a P controller, F_{ref} is the force reference, e_F is the force error, u_F is the control output, F is the force generated and F_{meas} is the force measurement.

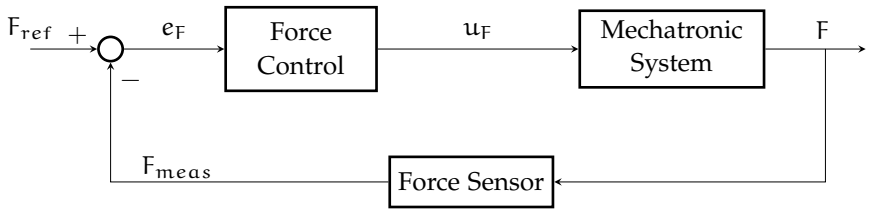

Figure 4.4: Force Control - Block Diagram.

In short, it is essential that the system can detect environmental changes or collisions, such as bumping into an object (such as a wall) or a person, and immediately cease exerting force. To achieve these goals, many industries construct systems with integrated force kits, where it is present (most of the time) a force sensor. Such it is more time along this thesis, sensors are a good solution but not the best in terms of errors and cost. To remedy this, it is helpful to implement the appropriate control system, for example using sensorless solutions with observers or estimators. For example, one possible solution is to implement the *Disturbance Observer (DOB), Reaction Force Observer (RFOB)* or *Reaction Torque Observer (RTOB)* to realize a robust and reliable sensorless Force Control.

For more information about them, it is possible to refer to Appendix [A]-[B].

4.3 OVERVIEW OF CONTROL STRATEGIES - MIXED CONTROL

In the previous Section 4.2, we discussed position and force control, which can be considered pure control when applied separately.
If we implement, for example, a pure position control:

- the position command is to move the robot's joints (or robot's actuators) and, consequently, its arm to a specific position, according to the task to do;
- the robot attempts to reach its target, regardless of any external forces or obstacles.

It is easy to note that, in this case, the robot can apply very high force to reach the position desired, without control over the applied one and the only limit is physical constraints. Damages or problems are very probable. On the other hand, pure force control, similar to pure position control, will try to maintain the force which has been designated on the environment in the controlled system. This comports some limitations, for example, we cannot have good performance in free motion (without external force) or if we would achieve a precise location. Following that, it is possible to say that, today, in all robotic applications (from industrial to medical) is necessary to combine *Position & Force Control* to attain great performance of the system, in terms of precision, security, repeatability and reliability. Additionally, the controlled task may require the pursuit of a specific path (position control) and the application of a necessary force (force control).
Some advantages of the position-force (or motion-force) combined control can be:

- high precision in every task;
- adaptability in case of the environment (ex. obstacles), external conditions or load variations;
- Avoiding excessive forces applied to the environment, an object or to an human operator or patient;
- handling delicate objects with care;
- higher safety;
- lower risk of damage or injury, applying (or adapting) the correct force in each situation;
- in medical applications, no risk of compromising the patient's health or worsening the injury situation.

Nowadays, there are different types of *motion & force control*, which differ in their control structure. It is possible to implement solutions in various ways, such as *hybrid*, *parallel*, *compliance* control. A fast explanation of each type is proposed in the following subsections.

4.3.1 *Hybrid Position-Force Control*

When operating a robot, it may be necessary to control both its position and force simultaneously, especially when the robot is moving in multiple axes (in free space) and presents fast dynamics in both force and position. A good control solution was proposed in 1981 by M. Raibert and J.J. Craig and a formulation was realized by M.T. Mason in the same year. They defined a *Hybrid Motion-Force Control*.
The main concept behind this approach is to generate two distinct and complementary subspaces, i.e. two independent controllers with feedback. In addition, the control part of the system use the selection matrix S technique, subspaces are controlled to direct control input either towards position or force, allowing for cooperation between the controllers. The selection matrix S is represented by a diagonal matrix

$$S = \begin{bmatrix} s_1 & 0 & 0 & \dots & 0 \\ 0 & s_2 & 0 & \dots & 0 \\ 0 & 0 & s_3 & \dots & 0 \\ \vdots & \vdots & \vdots & \ddots & \vdots \\ 0 & 0 & 0 & \dots & s_n \end{bmatrix} \in \mathbb{R}^{n \times n}$$

where n is the number of DoF of the system where the control is applied.
Thus, the two controls are placed in parallel but applied to a different subspace. To decide, which one is referred to the specific control it is necessary to know the robot application. The main rule is to put:

- *motion control* in the unconstrained direction by the environment;
- *force control* in the constrained direction by the environment;

For a better understanding, please refer to the control schema depicted in Figure 4.5 where P_{ref} is the desired position or path, F_{ref} is the desired force, S is the selection matrix, P_{meas} is the encoder measurement, $\hat{F}_{estim}$ is the estimation of the environment force[13] and u_{PF} is the control command generated by the hybrid control.

From the block diagram of Figure 4.5 is possible to derive the control law in *Laplace* domain as below:

$$\begin{aligned} U_{PF} &= S \cdot C_P(s)\,[P_{ref}(s) - P_{meas}(s)] + \\ &\quad + (I_{n\times n} - S) \cdot C_F(s)\left[F_{ref}(s) - \hat{F}_{estim}(s)\right] = \\ &= S \cdot C_P(s) E_P(s) + (I_{n\times n} - S) \cdot C_F(s) E_F(s) \end{aligned}$$

in which C_P is the motion control, C_F is the force control, S is the selection matrix, I is the identity matrix, E_P is the position error,

13 It can be estimated differently, as using RTOB.

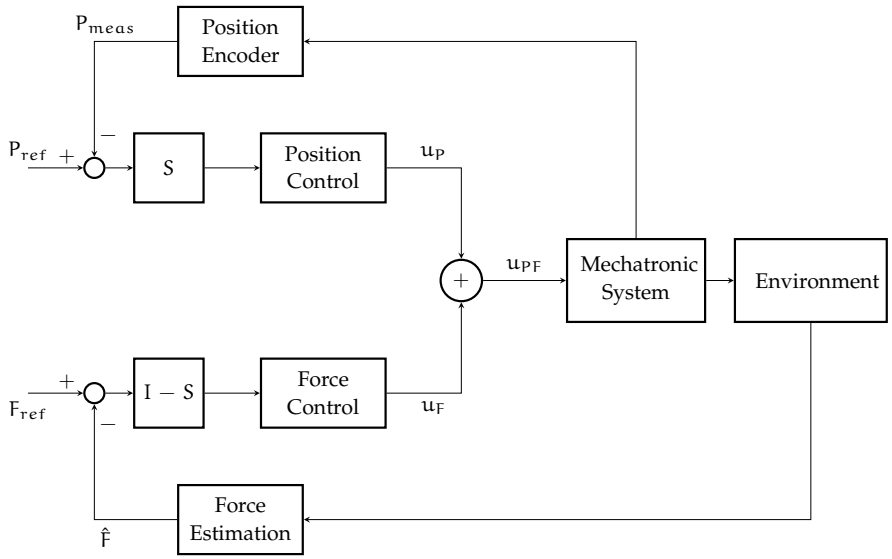

Figure 4.5: Hybrid Control - Block Diagram.

E_F is the force error and U_{PF} is the control output. In the case of a multi-degree of freedom system, $P_{ref}, Pmeas, F_{ref}, \hat{F}, E_P, E_F$ variables are vector with dimension n, which is equal to the number of DoF of the system.

To successfully apply this approach, it is crucial to have a clear knowledge of the environment model and define the subspaces. This is especially important in dynamic environments as the robot's response could be incorrect or cause damage. To accomplish a specific task where it is necessary to control position and force in a different direction and at different times, the system has to change the selection matrix properly. This action needs to be done online and this involves structure modifications and, maybe, in some operations, it is not the best solution. Also, it is essential to execute the selection matrix S change at the right time, which requires a system with high precision in synchronization for a fast and accurate response.
In conclusion, the hybrid control approach is useful in applications where the environment is well-known (and without change[14]) and the path to follow is predetermined. Considering exoskeleton applications, this type of control is not suitable due to the necessity for online adjustments, which may demand high computational resources and code complexity. Additionally, the simultaneous control of applied force in both directions is crucial, a capability that hybrid control lacks.

14 in operations where there is a static environment as in painting, welding, smearing, etc...

4.3.2 *Parallel Position-Force Control*

In the previous Section 4.3.1, we learned that in some situations, a robot needs to move along a path and also respond with the appropriate force when it comes into contact with the environment during task execution. Also sometimes, it is impossible to know the environment model with accuracy[15] or maybe the environment can change dynamically. Using the control approaches discussed above, we can't obtain a good response. In particular, we can define position control as stiff because it tries to follow the trajectory seeing the external force as a disturbance and rejecting them to achieve the position command. Large interaction force is the consequence and may result in instability, saturation, problems, damages or failure [4].

It is convenient to move to a *Parallel Position-Force Control*. In this control approach, position and force outputs are controlled and applied in the same direction (or all directions) at the same time. This control strategy was first proposed by S. Chiaverini and L. Sciavicco in 1988 and new ideas were released in $1992 - 1996$ [7]. Their idea was to have a full-dimensional task force controller operating with a position controller at the same time. The meaning of the idea is to construct a controller where the force action is the dominance above the position action [5]. By implementing this control idea in various applications, it becomes possible to reach the intended position without causing any damage. This is because the controller will restrict the applied force in case of obstacles or anything that may obstruct the robot's path or movement. Also, we cannot have instability, saturation or failure phenomena, reducing the problems that may occur. In a few words, we can say that the main aim of parallel control is to enable the resulting system to adjust its motion to environmental constraints.
The structure is the same as the hybrid control (Figure 4.5) but without any selection matrix S, as reported in Figure 4.6 and the control law can be defined in the *Laplace* domain with the transfer function in eq.19.

$$\begin{aligned} U_{PF} &= C_P(s)\left[P_{ref}(s) - P_{mes}(s)\right] + C_F(s)\left[F_{ref}(s) - \hat{F}_{estim}(s)\right] = \\ &= C_P(s)E_P(s) + C_F(s)E_F(s) \end{aligned} \tag{19}$$

In (19) it is possible to identify C_P as the motion control, C_F as the force control, e_P as the position error, e_F as the force error and u_{PF} as the control output. In the case of a multi-degree of freedom system, $P_{ref}, P_{meas}, F_{ref}, \hat{F}, e_P, e_F$ variables are vector with dimension n, which is equal to the number of DoF of the system.

15 most of the time, the environmental model is a mathematical model, and it may have significant deviations that cannot represent reality well.

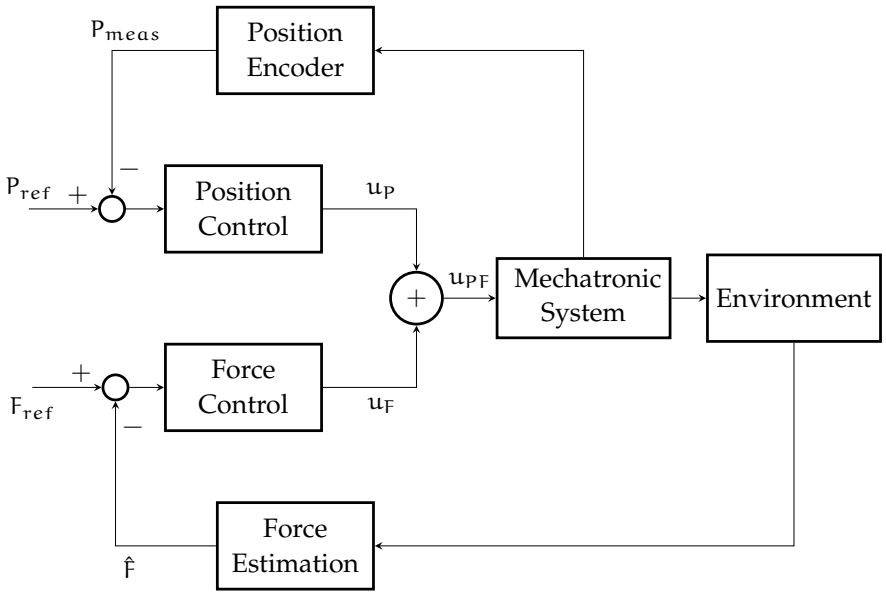

Figure 4.6: Parallel Control - Block Diagram.

In conclusion, the parallel approach offers robustness against the uncertainties affecting the environment knowledge. Also, it can give the system a very high level of safety in some task execution, maybe where it is possible to find one or more operators or when it has to work on the human body, like a rehabilitation exoskeleton.

4.3.3 *Compliant Position-Force Control*

Controls discussed in the previous sections, are not the only solutions. A *Compliant Control* (or *Compliance Control* [16]) is another solution that can regulate the transfer of energy between the robot and the environment, ensuring safe interaction. This control approach is used in a lot in manipulator applications and also in rehabilitation robotics, namely it is very useful in cases where there is a human-robot interaction. Two important control types are found in this approach: *impedance* and *admittance* control. We will discuss them later in this section.

The target of compliant control is to generate a compliant motion. To better understand, we can take the historical definition of compliant motion given by J. De Schutter in 1987: 'Any robot motion during which the end effector trajectory is modified, or even generated, based on online sensor information' [6]. Today, it can be translated as compliant control, to define the robot's behavior, model the position-force[17] relation, or the mechanical impedance. The latter is the inverse of stiffness and it denotes the capacity to display displacement when subjected to a force. In simpler terms, it refers to the ease

16 When there is a static position-force relation, this type of definition is used.
17 The forces referred to are those of the environment.

with which a mechanical element can move or deform under an external applied force. A system with low compliance is stiffer and less susceptible to deformations, whereas a system with high compliance can more easily adapt to applied loads. By developing this technique, and managing the impedance of the system controlled, we can control the transfer of power in the interaction between the robot and the environment. So compliant control can be defined as an interaction control.
In reality, it is possible to represent a system with an equivalent system composed of mass M, spring K and damper D, as in Figure 4.7 [18] where M correspond to the system mass (or inertia), K to the stiffness and D to the damping. K and M are energy-storing elements, whereas D is an energy-dissipating device.

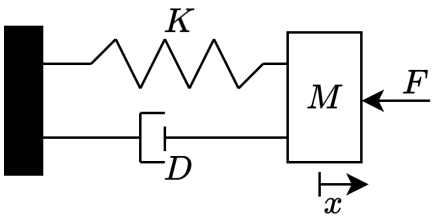

Figure 4.7: Equivalent System Mass-Spring-Damper.

The real value cannot be changed but, in the control part, we can define a virtual system to achieve the desired behaviour with desired parameters: M_d, K_d, and D_d. Varying these parameters allows us to design the desired system response when interacting with the external world. The definition of parameters is application-dependent or adaptive in case of a task change during robot operation.
Exoskeleton applications, particularly in rehabilitation, require adaptable control due to the dynamic nature of the human body[19]. Compliance control offers a promising solution as it allows for easy adjustment to changing user demands while minimizing computational complexity and overall costs.

We can now present the two types of compliant control, defining each and highlighting their key differences.

4.3.4 *Impedance Control*

This idea of compliance control was formulated by N. Hogan in 1985 and he regulated the robot-environment interaction defining a virtual system dynamics [7], as a mass-spring-damper system (Figure 4.7).
First of all, it is good to define mechanical impedance. It refers to the relationship between the amount of force produced and the amount

18 x is the *Lagrangian coordinate*
19 The human body response change according to the muscle effort.

of motion required to produce that force and it is possible to draw an analogy between this concept and electrical impedance, which is defined as the ratio of output voltage to input current. In other words, impedance refers to the amount of resistance experienced by a moving object when a force is applied. It can be written as follows:

$$Z(s) = \frac{F(s)}{X(s)} \tag{20}$$

Impedance control is constructed with a nested structure of two loops: an outer position loop and an inner force loop, as reported in Figure 4.8, where P_{ref} is the rest position[20] reference, e_p is the error position, F_{ref} is the force reference to define the rest position[21], e_F is the force error, u_{impd} is the impedance control command, $\hat{F}$ is the estimated force and P_{meas} is the position measurement. The scheme is defined generically for a system working with workspace coordinates and force control, but it will remain the same for a system with joint space coordinates[22].

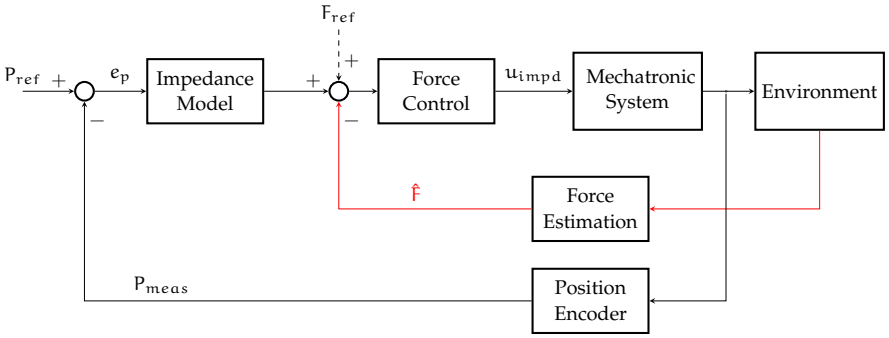

Figure 4.8: Impedance Control - Block Diagram.

The *Impedance Model* can be defined as:

- first order desired impedance: $Z(s) = sD_d + K_d$
- second order desired impedance: $Z(s) = s^2M_d + sD_d + K_d$

where M_d is the desired inertia, D_d is the desired damping and K_d is the desired stiffness of the virtual system. By adjusting these parameters, we can regulate the robot's impedance, which is the force of resistance to external motion from the environment.

The definition of the control law of impedance control is as follows:

$$U_{impd}(s) = C_F \cdot \left[Z(s) \cdot E_p(s) - \hat{F} + F_{ref}\right] \tag{21}$$

20 The rest position refers to the position where the robot remains stationary in the absence of any external (environmental) forces acting upon it.

21 It is connected with a dashed line because most of the time is set to 0, $F_{ref} = 0$

22 it is necessary to change the *force control* with torque control and the *force estimator* with torque estimator.

and in case of $F_{ref} = 0$, the eq.21 became

$$U_{impd}(s) = C_F \cdot \left[Z(s) \cdot E_p(s) - \hat{F} \right] \tag{22}$$

In both equations (eq.21 - eq.22), C_F is the force/torque control and often it is a simple proportional P control.

Through the use of impedance control, position and force can be controlled simultaneously. It is important to note that the approach differs from the controls discussed in the previous sections, as its structure is a series control and not a parallel one. Also, it is possible to obtain:

- a pure force control by selecting $Z(s) = 0$;
- a pure position control by selecting $Z(s) = \infty$.

Applying the control approach discussed in this section, we can obtain a very accurate system. However, it is hard to have a high impedance because requires an elevated gain in the impedance model and it can cause instability. To avoid this problem, it is necessary to find a trade-off between accuracy and high impedance.

The information doesn't cite upside and used to write this section has been taken from [2].

4.3.5 *Admittance Control*

The admittance control idea was developed in 1985 by D. Whitney. The construction of this control started from the previous discussion and the objective is the same, namely regulate the interaction of robot-environment, but from a different point of view.
Here, we have to consider the mechanical admittance, which is the inverse of impedance defined in Section 4.3.4. When a mechanism applies a force to the environment, the environment's response depends on its properties and the applied force. Out of this, it is easy to understand that also the control scheme is inverse, namely the admittance control uses an inner position loop and an outer force loop, as reported in Figure 4.9, where the elements present are the same as Figure 4.8.

The *Admittance Model* is also the inverse *Impedance Model* and its definition is:

- first order: $Z(s) = \dfrac{1}{sD_d + K_d}$
- second order: $Z(s) = \dfrac{1}{s^2 M_d + sD_d + K_d}$

where M_d, D_d, K_d are respectively the desired inertia, the desired damping and the desired stiffness of the virtual system.
Continuing, also here position and force can be controlled at the same time but if we set:

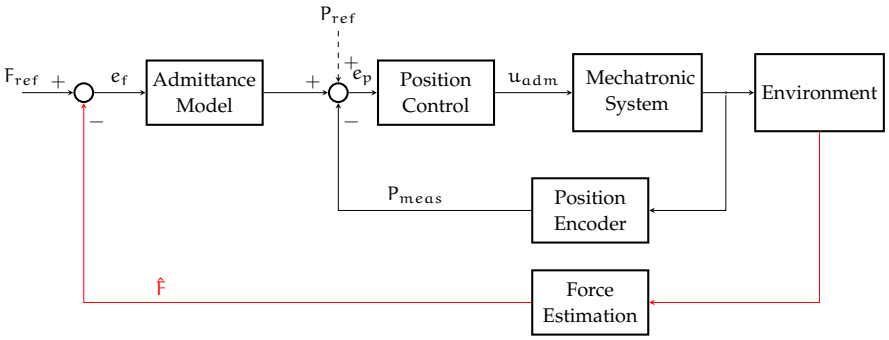

Figure 4.9: Admittance Control - Block Diagram.

- $Z(s) = 0 \longrightarrow$ we obtain a pure position control;
- $Z(s) = \infty \longrightarrow$ we have a pure force control.

In this control approach, the force loop regulates the force-position relation and it calculates a position value from the information of force. The best solution, probably, isn't a force estimation but by using a force sensor it may be possible to achieve better performance.

In this scenario, unlike the previous one, it is feasible to achieve a high impedance. However, obtaining a low desired impedance can be challenging, as it requires a high gain value in the admittance model. This, in turn, can lead to instability.

In conclusion, we can define that *Admittance* and *Impedance* are complementary control strategies.

4.4 PROPOSED CONTROL

After analyzing the different control approaches and identifying the advantages and the issues associated with each type, we can now construct our control strategy for the exoskeleton. We decided to use distinct approaches for each kind of exercise presented in Section 4.1. First of all, with the chosen actuators and their equipment, we follow an *no-collocated* control approach in every case; the general control scheme in reported in Figure 4.10.

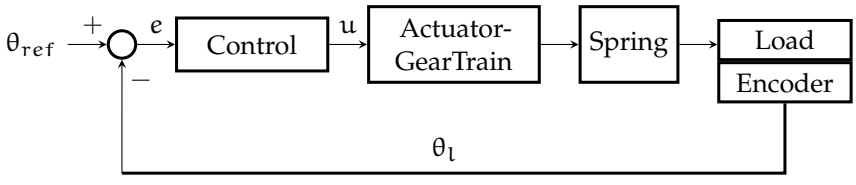

Figure 4.10: No-collocated Control Scheme for Upper Limb Exoskeleton.

Specifically, we will use for:

1. **Static Exercise** $\longrightarrow$ Position Control + DOB

2. **Dynamic Exercise** $\longrightarrow$ Impedance Control + DOB + RTOB

where DOB = DIsturbance Observer and RTOB = Reaction Torque Observer.
These choices are based on the fact that static exercises require a stiff structure to maintain a fixed position, while dynamic exercises need to adjust their response, becoming more or less stiff based on the patient's muscle condition. For example, if the preliminary and *EMG* test results show low muscle force, the exoskeleton needs to be stiffer to provide more assistance to the user. In the opposite case, if the patient exhibits greater strength, the exoskeleton can be less stiff, allowing the patient to perform more of the exercise independently and enabling semi-autonomous movement.

4.4.1 *Position Control + DOB for Static Exercises*

The first control strategy we implement is the Position Control with a Disturbance Observer (DOB), as shown in the block diagram in Figure 4.11.

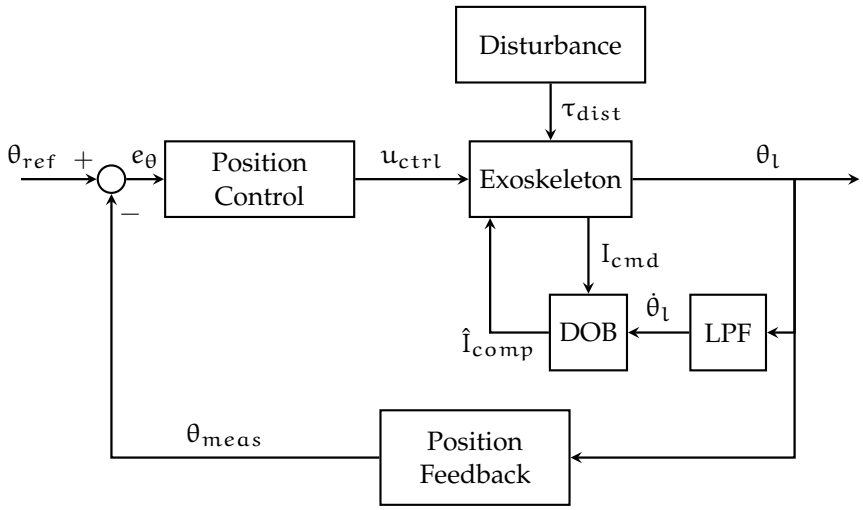

Figure 4.11: Block Diagram of Position Control with DOB.

The Position Control block is designed as a PD controller and can be represented by the following equation:

$$C_p(s) = K_p + K_d \cdot s$$

To adjust the response of the system and achieve the desired behavior, we must correctly tune the K_p and K_d gains. This control component is responsible for bringing the exoskeleton system to the calculated position for the static exercise, starting from any resting position. The movement needs to be slow and smooth for the patient's comfort and safe. To achieve this, it is recommended to define a trajectory beforehand, limiting the maximum actuator velocity and accel-

eration. We used the *Trajectory Function* provided by Hebi Robotics®, which will be presented later in its own section.

Then, the control must maintain the position for the duration of the rehabilitation. Alone, this control is insufficient to ensure the stiff response desired. Therefore, we add the DOB, which ensures a rigid structure of the exoskeleton. In particular, it compensates for possible external disturbances arising from incorrect movements by the patient or environmental factors. It also ensures a prompt response in these situations to prevent the patient from making incorrect and dangerous movements, maximizing exercise effectiveness with correct execution (see Figure 4.1).

Disturbances acting on the system can include arm inertia, gravity, friction, incorrect patient movements, etc... Together, these can be considered as an equivalent torque τ_{dist} acting on the two actuators. These phenomena can be considered matched disturbances, meaning they can be modeled, estimated, and canceled by adding compensation to the input control variable of the actuator, or the corresponding compensation current I_{comp}.

The DOB block can be schematized as shown in Figure 4.12, and

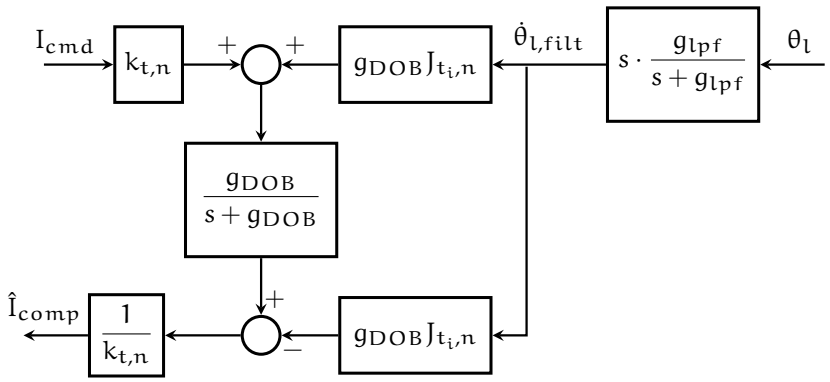

Figure 4.12: Disturbance Observer DOB - Scheme Applied.

the current compensation I_{comp} can be defined by the following equation:

$$\hat{I}_{comp} = \frac{1}{k_{t,n}} \left[\left(k_{t,n} I_{cmd} + g_{DOB} J_{t_i,n} \dot{\theta}_{l_i} \right) \frac{g_{DOB}}{s + g_{DOB}} - g_{DOB} J_{t_i,n} \dot{\theta}_{l_i} \right]$$

In Figure 4.12, according to the sensorless approach, it is necessary to derive the motor velocity from the position measurement. We decided to use a filtered derivative calculation, which will be presented in a specific section at the end of this chapter.

The DOB approach is applicable for SISO[23] systems. In our case, we have a MIMO[24] system, so we implement two DOB blocks, one for each actuator. Consequently, we need to tune each control correctly;

23 SISO = Single Input Single Output
24 MIMO = Multiple Input Multiple Output

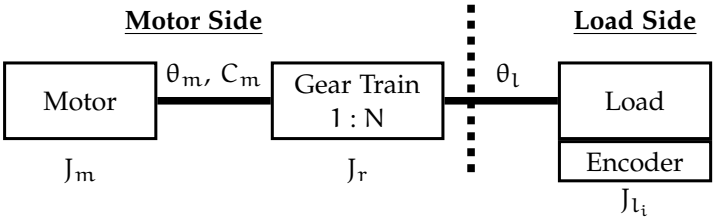

Figure 4.13: Equivalent System Representation.

the base is the same, but the parameter values (inertia and DOB gains) change according to the exoskeleton parts.

Parameters Definition

In Figure 4.12 we can identify the following parameters:

- $k_{t,n}$ = motor torque constant;
- $g_{DOB,i}$ = DOB LPF gain[25]: this must be tuned differently between the two actuators because the first motor feels the entire inertia of the system (first and second link), while the second one feels only the inertia related to the second link. Thus, the first one needs a larger bandwidth than the second one.
- g_{LPF} = cut-off frequency of the LPF for velocity calculation;
- θ_i = position of the actuator i on the load side;
- $\dot{\theta}_{i,filt}$ = velocity filtered of the actuator i on the load side;
- $J_{t_i,n}$ = total equivalent inertia of the system felt by motor i.

In detail, starting from the representation in Figure 4.13, the inertia felt by each actuator is defined as follows:

$$J_{t_1,n} = (J_m + J_r) * N^2 + \underbrace{m_1 L_1^2 + m_2 \left(L_1^2 + 2L_1 L_2 c_2 + L_2^2\right)}_{J_{l_1}}$$

$$J_{t_2,n} = (J_m + J_r) * N^2 + \underbrace{m_2 L_2^2}_{J_{l_2}}$$

The final control scheme that we implement on th exoskeleton prototype, using MatLab® code, is visible in Figure 4.14.

25 $i = 1$ is the shoulder actuator and $i = 2$ is the elbow actuator

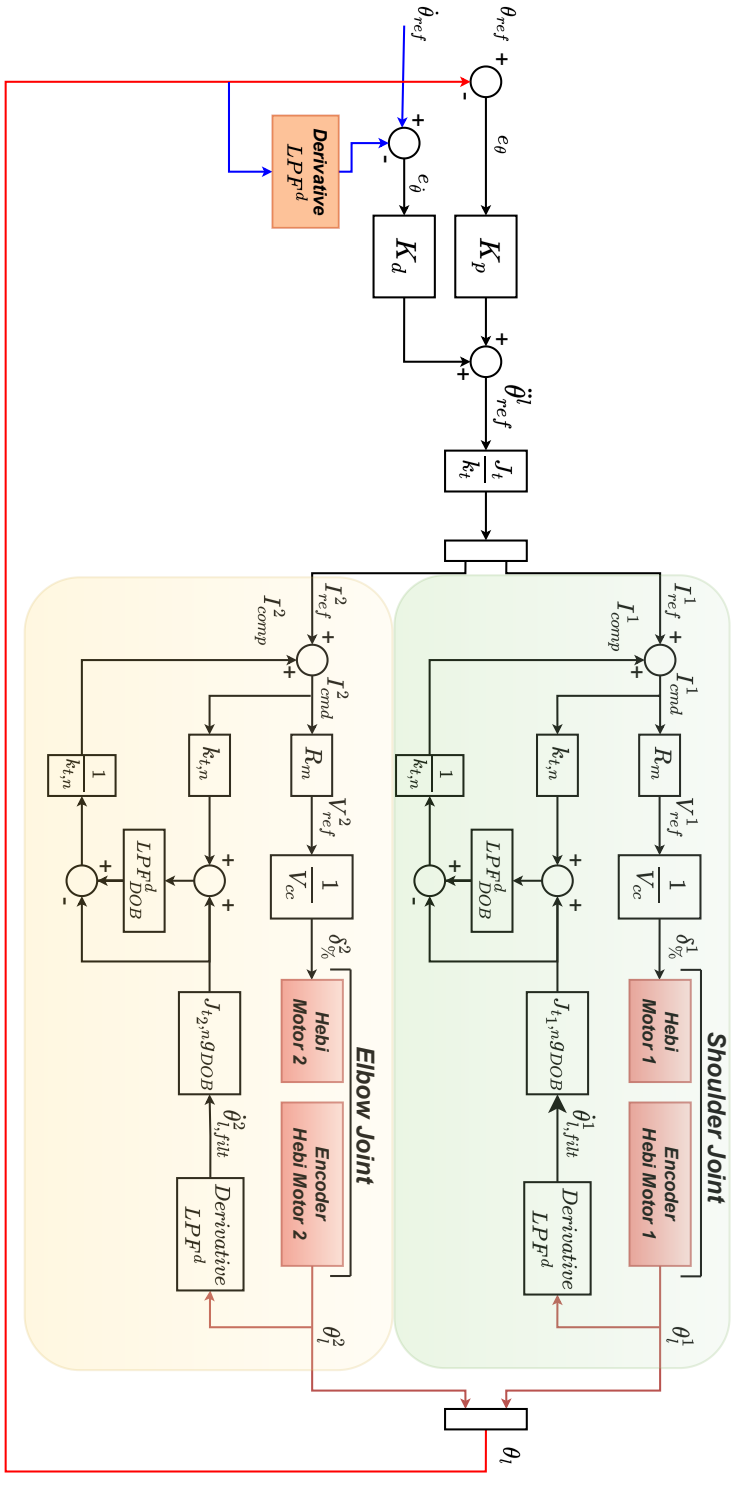

Figure 4.14: Final Control Scheme of Position Control with DOB - Static Exercise.

4.5 IMPEDANCE CONTROL + DOB + RTOB FOR DYNAMIC EXERCISES

The second control strategy we implement differs from the first one because here the main goal is to define the exoskeleton behavior according to the muscle recovery status. To achieve this, we propose an Impedance Control with Disturbance Observer (DOB) and Reaction Torque Observer (RTOB). The DOB estimates the current to cancel the disturbance present (as shown in the previous section), while the RTOB acts as a torque sensor, estimating the force applied by the patient to the exoskeleton to adjust (increasing or decreasing) the assistance provided. The block diagram that represents this control strategy is shown in Figure 4.15.

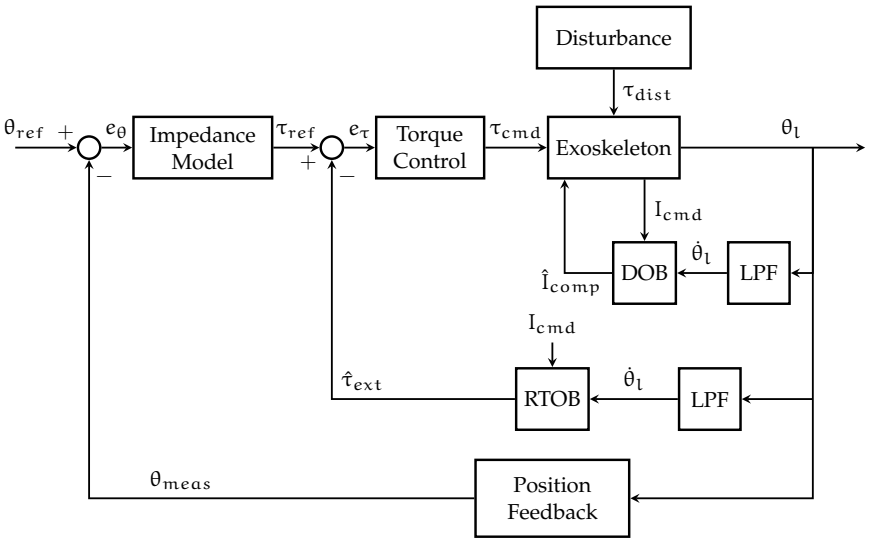

Figure 4.15: Block Diagram of Impedance Control with DOB & RTOB.

The DOB (Disturbance Observer) part works in the same way as presented in the previous section, and therefore, requires no further discussion. In this proposed control system, the focus will be on Impedance Model and the RTOB (Reaction Torque Observer).

Impedance Model

Impedance model is crucial in this system because its definition define the exoskeleton behavior via the reference torque for the torque control of the each joint. Its parameters can be adjusted to modify reference τ_{ref}, which is defined as:

$$\tau_{ref} = K\left(\theta_{ref} - \theta_{meas}\right) + D\left(\dot{\theta}_{ref} - \dot{\theta}_{meas}\right)$$

This equation models the response as a spring-damper system, where K represents stiffness and D represents damping. By varying the values of K and D, the overall stiffness and damping of the system

can be adjusted according to the results of preliminary examinations. For example:

- A high value of K results in a very rigid system, which is useful when the patient applies a low force;
- Conversely, a low value of K results in a less rigid system, providing lower assistance since the patient has sufficient strength to perform the exercise independently.

Torque Control

The *Torque Control* component is a straightforward proportional control with a gain K_τ to fine-tune the response. Additional components are not necessary for this part of the control system, as satisfactory results have been achieved with this simple control definition.

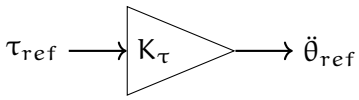

Figure 4.16: Torque Control Block.

RTOB - Reaction Torque Observer

This part of the control system is the most challenging and crucial for achieving a successful sensorless application. It requires accurate estimation of certain parameters that influence the actuators, such as the total friction which the components are the DC motor and the gear train static and viscous friction.

The Reaction Torque Observer (RTOB) functions as a virtual torque sensor, estimating the external torque τ_{ext} acting on the exoskeleton. This includes the torque generated by the patient on the actuators. The RTOB adjusts the actuator response based on this estimation, ensuring that the exercise path is maintained to maximize the efficiency of dynamic exercises.

To estimate the external torque, the only available information is the command current and the position of the patient's arm. The RTOB has a structure similar to the Disturbance Observer (DOB), but it subtracts all the components that have already been compensated by the DOB. The scheme is reported in Figure 4.17.

Most of the components of Figure 4.17 are the same of Figure 4.12.

The τ_{comp} is defined as follows:

$$\tau_{comp} = \tau_{static} + \tau_{viscous} + \tau_{gravity}$$

where the definition of $\tau_{viscous}$ depends on the chosen mathematical model and the gravity components are contained in matrix $\boldsymbol{G}$ of dynamic analysis of Chapter 2. The torque is also produced by the

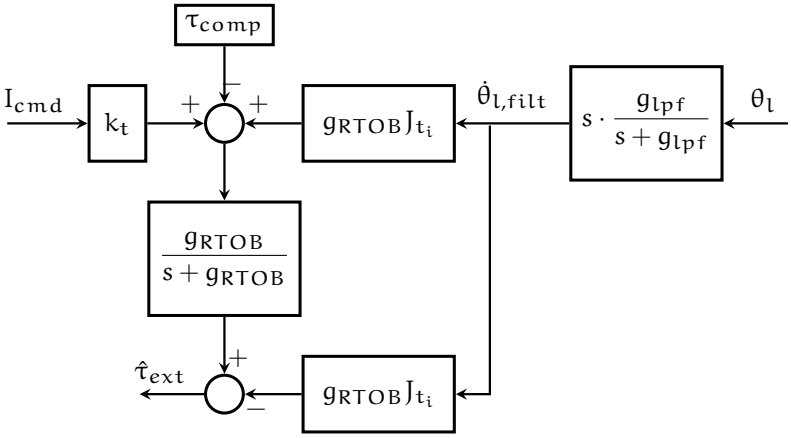

Figure 4.17: Reaction Torque Observe RTOB - Scheme Applied.

weight of the patient's arm; however, this component is considered part of the human-robot interaction torque and must be estimated by the RTOB.
For greater accuracy, it is essential to incorporate variations in inertia (ΔJ), torque constant (Δk_t), and other internal actuator parameters into the input. However, due to the high gear ratio N, these factors can be reasonably negligible. A precise model of friction within the system is critical and will be the focus of the next chapter, where we will delve into its underlying causes, components, and potential representations.

The final RTOB estimate equation is:

$$\hat{\tau}_{ext} = \left[k_t I_{cmd} + g_{RTOB} J_{t_i} \dot{\theta}_{l,filt} - \tau_{comp}\right] \frac{g_{RTOB}}{s + g_{RTOB}} - g_{RTOB} J_{t_i} \dot{\theta}_{l,filt}$$

For the same reasons of DOB, also for RTOB we have to define one for each joint and tune the parameters related to the exoskeleton part.

Precise and accurate estimation by RTOB can be achieved through careful parameter tuning. This eliminates the need for a torque sensor, which is susceptible to noise and damage. Additionally, the challenge of optimal sensor placement for accurate interaction force measurement is resolved.

Another, and last, important aspect in the dynamic exercise control is the path to follow. In the next section we will present a how do it.

The final control scheme that we implement on th exoskeleton prototype, using MatLab® code, is visible in Figure 4.18.

4.6 MOTION PLANNING

During the execution of dynamic exercises, the patient must follow a path composed of two or more points in x, y space. The movements are slow, and the patient must perform them with the correct timing

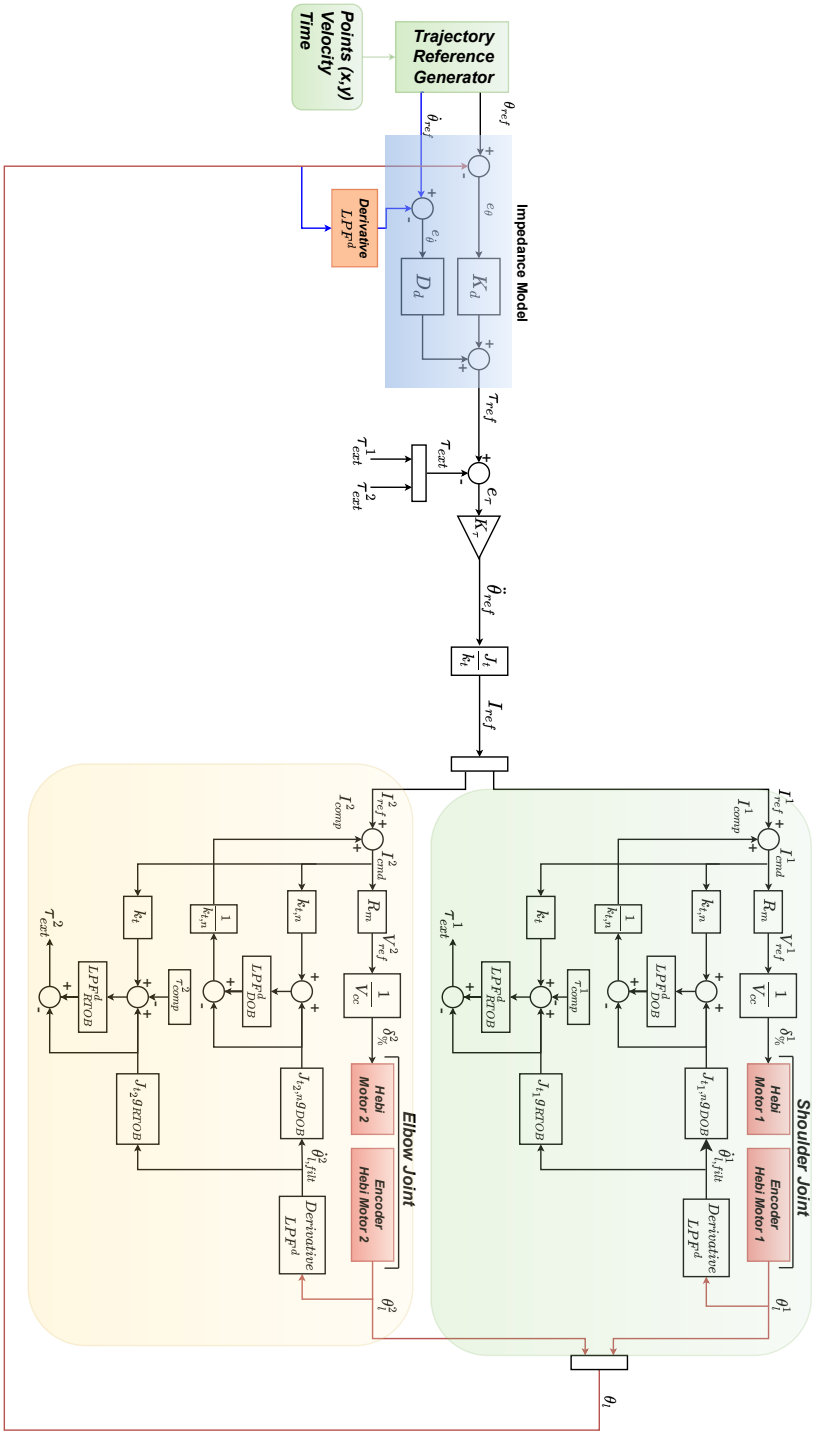

Figure 4.18: Final Control Scheme of Impedance Control with DOB & RTOB - Dynamic Exercise.

to maximize recovery. At the same time, the exoskeleton must also execute slow and smooth movements. For this reason, it is important to perform offline *motion planning* and calculate the necessary references, such as position and velocity.

By doing this, we can define the points along the path and the precise moments to pass through each one, while limiting velocity and acceleration.

To define the trajectory, various methods can be employed, such as using polynomial equations, sinusoidal functions, or trapezoidal representations, depending on the required continuity of position, velocity, etc. For simplicity and time efficiency, we decided to use the trajectory creation function provided by Hebi Robotics® company in their API.

This function takes as input the coordinates of the initial and final positions in (x, y) and the intermediate points. It is also possible to define the transit speed and time for each point. To interpolate all the information and obtain the references needed for exercise execution, the function uses a 5^{th}-order polynomial SPLINE method to minimize trajectory jerk and ensure smooth movements. This algorithm is an optimized version of the Richter algorithm; for more information, refer to [16].

An example of this algorithm results is shown in Figure 4.19.

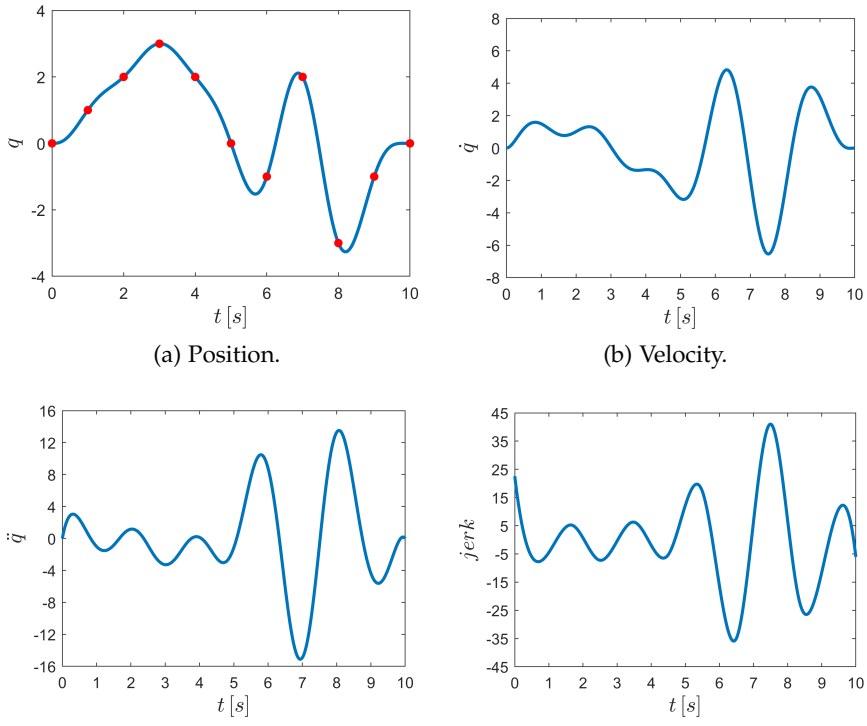

(a) Position.

(b) Velocity.

(c) Acceleration.

(d) Jerk.

Figure 4.19: Example of Spline Hebi Robotics® Algorithm.

4.7 VELOCITY CALCULATION AND DISCRETIZATION

The velocity definition in continuous time corresponds to the derivative of the position:

$$v(t) = \frac{dx(t)}{dt} \implies \dot{\theta}(t) = \frac{d\theta}{dt}$$

However, in digital systems, calculations are performed in discrete time, making them sensitive to noise entering the measurement chain (from the encoder sensor). The noise can cause significant errors in estimated velocity value, due to small fluctuations in the position measured by the encoder amplified during the calculation. For that, we use a filtered derivative approach, as shown in Figure 4.20.

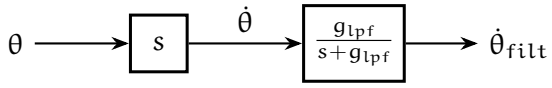

Figure 4.20: Velocity Calculation - Filtered Derivative.

The LPF introduces a delay in the availability of the velocity value, but at the same time, it reduces high-frequency noise, eliminates spurious peaks that can distort the estimation, and mitigates the Gibbs effect, which is the phenomenon of high-frequency oscillations at data discontinuity points.

By following this approach, it is possible to achieve a reliable and accurate velocity estimation for use in control calculations, such as in the Disturbance Observer (DOB) or PD position control. The only parameter that can be adjusted is g_{lpf}, which changes the cut-off frequency of the filter. To tune it, it is necessary to know the sampling rate of the encoder used in the system to estimate the introduced delay accurately.

In Hebi Robotics®, the encoder is resolute and operates with a variable sampling time that is user-configurable. The settable frequency is $f \in [100, 1000]\,\text{Hz}$. We decided to use the maximum value, corresponding to a $T_s = 1\,\text{ms}$, and then tuned the LPF with a cutoff frequency $f_{lpf} = 500\,\text{rad/s} \approx 80\,\text{Hz} = g_{lpf}$.

To estimate the delay introduced in the calculation, we can use the formula:

$$\tau = \frac{1}{2\pi \cdot g_{lpf}} \approx 2\,\text{ms} \implies \text{delay} = \frac{\tau}{2} \approx 1\,\text{ms}$$

This delay can be considered acceptable for the application.

After that, it is necessary to proceed with the discretization of calculation. In particular, the derivative block can be define as:

$$\dot{\theta}_l(k) = \frac{\theta(k) - \theta(k-1)}{T_s}$$

and the low-pass filter can be rewrite

$$\frac{g_{lpf}}{s+g_{lpf}} = \frac{\frac{g_{lpf}}{s}}{1+\frac{g_{lpf}}{s}}$$

and schematized as in Figure 4.21.

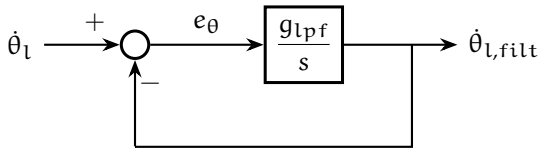

Figure 4.21: LPF - Discrete Time.

The Figure 4.21 can be write by mathematical equation as:

$$\begin{aligned}
\dot{\theta}_{l,filt}(k) &= g_{lpf} \cdot \sum_{i=0}^{k} e_\theta(i) \cdot T_s = \\
&= g_{lpf} \cdot [e_\theta(0) + e_\theta(1) + \cdots + e_\theta(k)]\, T_s = \\
&= g_{lpf} \cdot \underbrace{[e_\theta(0) + \cdots + e_\theta(k-1)]}_{\dot{\theta}_{l,filt}(k-1)} T_s + g_{lpf} \cdot e_\theta(k) T_s = \\
&= \dot{\theta}_{l,filt}(k-1) g_{lpf} + g_{lpf} \left[\dot{\theta}_l(k) - \dot{\theta}_{l,filt}(k)\right] T_s
\end{aligned}$$

and we find the filtered signal searched:

$$\dot{\theta}_{l,filt}(k) = \frac{1}{1+g_{lpf} \cdot T_s} \left[\dot{\theta}_{l,filt}(k-1) + g_{lpf} \cdot \dot{\theta}_l(k) T_s\right]$$

The approach to discretize the LPF in DOB and RTOB control schemes of Figure 4.12 is the same.

5

FRICTION ISSUES AND ESTIMATION METHOD

In this chapter, we will discuss about a phenomenon that we can find in every system where there are mechanical moving parts: friction. We will see how it affects the system and the control, how it arises, and how it can be estimated. We will also analyze some results from the estimation method applied to assess the friction in the Hebi Actuator. Accurate friction modeling is crucial for control, particularly in the RTOB, as the more precise the model, the more accurate the estimation of external (or interaction) torque will be.

5.1 FRICTION PHENOMENA

The phenomenon of friction is present everywhere, acting as a force that opposes the normal movement of a system. It is generated by the contact between two surfaces[26] and can be exploited in certain applications, such as when stopping a moving object. The effect of friction is particularly noticeable when an object is descending. In the other hand, it can be a problem when we want to move an object, as it requires more force to overcome the friction force. Its value may not be very large, but often considering it negligible can be a mistake. Its value can be influenced by factors such as surface roughness (irregularities or defects in the surface), the presence of lubricants, the nature of the materials, the normal force applied, temperature, pressure, humidity and the relative speed of the surfaces. In fact, depending on the application, the choice of components such as electric motors, gear trains, bearings, spheres, and frame supports, along with the materials they are made of, plays a fundamental role in determining the total amount of friction.
In energy analysis, friction is considered a dissipative component that converts part of the mechanical energy into heat. Depending on the application, this generated heat, along with heat from other components, must be managed with an appropriate cooling system to prevent overheating. If friction and other dissipative components are not minimized, the system's efficiency will decrease, as it is inversely proportional to the dissipative energy. Friction can also lead to other negative effects, such as component wear, which reduces their lifespan and increases noise due to vibrations. This, in turn, raises operational

26 Air can also be considered a surface. In fact, this is the case in aerodynamics, where friction is generated by the contact between a moving surface and the air, as seen in everyday examples like a car in motion.

and maintenance costs. Additionally, improper lubrication and premature component aging can result in potential failures.

Friction is a non-linear phenomenon, and finding a good mathematical model to represent it can be both an interesting and challenging task. The study of friction began centuries ago, and many models have been proposed over the years. One of the first significant contributions was made by Leonardo da Vinci in the 15th century, who defined the main principles of friction:

1. friction is proportional to the normal force applied to the surface;
2. friction is independent of the contact area between the two surfaces.

After, Eulero, Coulomb, Amontons, and many others had contributed to the friction study, defining some other theories, supported by experiments, about the nature and the influences of the friction.
Since then, numerous studies have been conducted (and continue to this day), all focusing on modeling friction through the definition of accurate coefficients. The study of friction a big challenge in research, driven by the discovery of new materials and the development of new technologies. One of the main today is to reduce friction to the point where it can be considered negligible, with material with low friction and good mechanical characteristics. However, it is not possible to eliminate it entirely.

There are different types of friction, such as static, dynamic, viscous, and Coulomb friction, etc... In this thesis work, we will estimate the static and viscous friction, which are the main components acting during the exoskeleton's motion. This estimation will be performed through a pre-test conducted on each actuator under no-load conditions, as described in the next section.

5.2 FRICTION MODELING METHOD

The importance of estimating friction in a system is fundamental for effective control. Without a good modelization system performance, reliability, and stability can be compromised. For example, in the case of position control, this can lead to positioning errors and unexpected behaviors. Therefore, it is crucial to accurately estimate friction, choose the best model that represents it, and implement a compensation strategy to achieve high control performance.

As discussed in Chapter 4, friction compensation is implemented in the feedforward path using the Disturbance Observer (DOB).

Additionally, the RTOB (Robust Torque Observer) should not consider friction in the estimation of external torque $\hat{\tau}_{ext}$ because friction is not an external force arising from human-exoskeleton interaction.

For this reason, friction must be accurately estimated and subtracted from the RTOB input, as shown in Figure 4.17.

At this point, the challenge lies in how to account for friction. Directly measuring this force (or equivalent torque) is not feasible because there is no suitable position to place a sensor. Additionally, friction is generated by contact between two surfaces, making change of scenery avoiding the contact. This completely alters the system and is not the correct approach to take. The only viable approach is to estimate it based on known variables. In the SEA Hebi Robotics®, we use current and velocity data to perform an interpolation and define the final mathematical model.
The actuators used in this project also include a gear train to amplify the output torque generated by the DC motor and a spring to couple with the load. The presence of these components generates friction due to the interaction between the different parts. Therefore, the total friction present can be defined as:

$$f = f_{motor} + f_{motor \leftrightarrow geartrain} + f_{geartrain \leftrightarrow spring}$$

Estimating the individual components is a difficult, and it may not be possible. However, we can estimate the total friction, assuming with reasonable confidence that the total friction is primarily felt by the motor, and that the motor current measurement in a no-load condition provides the necessary information for this estimation. Thus, we can write:

$$\begin{cases} \Omega_1 B_t = k_t \cdot I_1 - \tau_{static} \\ \Omega_2 B_t = k_t \cdot I_2 - \tau_{static} \end{cases} \implies B_t = \frac{k_t \Delta I}{\Delta \Omega} = \begin{array}{c}\text{viscous friction} \\ \text{coefficent}\end{array}$$

which corresponds to

$$\tau_{friction,i} = k_t \cdot I_{m,i} \quad \text{with} \quad i \in [1, \textit{n. step } V_m^{ref}]$$

where B_t is the total viscous friction coefficient, K_t is the motor torque constant, I_1 and I_2 are the motor currents at the load-side velocities Ω_1 and Ω_2, and τ_{static} is the static friction. To impose different motor velocities during the no-load test, we define different voltage levels to be applied to the motor's DC bus, which corresponds to using the PWM strategy provided by the Hebi API. The value of the duty cycle is defined as:

$$\delta_{\%} = \frac{V_m^{ref}}{V_{cc}}$$

This approach is consistent with the one described in Chapter 4, where the motor is controlled using the two defined strategies. This test should be repeated for each actuator and performed periodically to monitor friction variations caused by component wear and environmental factors.

With the collected data, we can now define a velocity-torque ($\Omega - \tau$) relationship and create a graph that represents the friction trend. To manipulate the data, we use MatLab® and its curve fitting tool. This tool allows to fit the collected data with a mathematical model and obtain the best fitting parameters. In simple terms, it constructs a model using a polynomial. It is important to note that the polynomial represents an approximation of the real friction trend, and choosing the correct degree is crucial to minimize errors in the interpolation. In this Hebi Motor® case study, we decided to try and present two different fittings:

1. a mathematical model using a 1^{st}-order polynomial;
2. a mathematical model using a 3^{rd}-order polynomial.

In Figure 5.1 is reported the scheme that summarize the friction estimation method described and applied for the exoskeleton prototype.

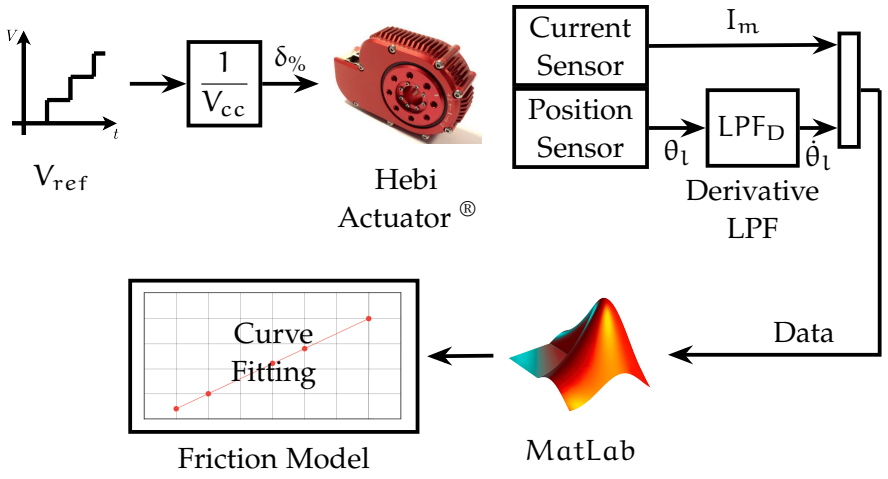

Figure 5.1: Motor Control Set-Up for Friction Estimation in Hebi Actuator® - Schematic Diagram.

In the the following last section oh this chapter, we will present the obtained graphs, highlight the main differences, and discuss the friction behavior. We will also emphasize the importance of having an accurate model to represent it.

5.3 FRICTION MODELING RESULTS

In the tests conducted on the Hebi Actuator®, multiple velocities Ω were used. Additionally, tests were performed for both positive Ω^+ and negative Ω^- velocities, as friction can vary depending on the motor's rotational direction. The applied velocities are shown in Figure 5.2. In particular, we tested the motor starting from $0\,rad/s$ to $1.25\,rad/s \approx 12\,rpm$ in increments of $0.25\,rad/s \approx 2.5\,rpm$, covering

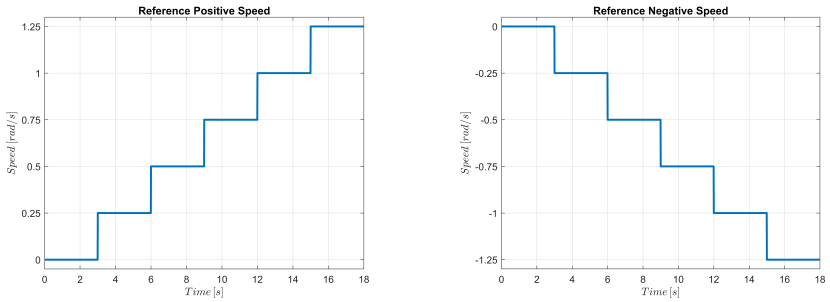

(a) Velocity Ω^{+}.

(b) Velocity Ω^{-}.

Figure 5.2: Velocity applied in the Friction Estimation Test.

almost the entire range of velocities that the motor can reach[27]. Since the rehabilitation exercise is performed at a speed lower than the maximum available, the collected data are sufficient to make an accurate estimation for the application..

The first model obtained from the data collected and using a 1^{st} order polynomial is reported in Figure 5.3 while the second one obtained using a 3^{rd} order polynomial is reported in Figure 5.4.

At this point, it is clear that there is a significant difference between the two models. The first model exhibits a substantial approximation of the friction trend, making it unsuitable for accurate results, particularly in the RTOB control part. The polynomial used in this model forces the friction behavior into a straight line, which does not accurately represent the actual friction, leading to potential errors.
On the other hand, the 3^{rd} order polynomial model provides a more accurate representation of the total actuator friction. The behavior is noticeably different, especially around $|\Omega| = 0.5\,rad/s$. In fact, at this point, the equivalent friction torque decreases to near $0\,Nm$, compared to the first model where $\tau_{ext} \simeq 1\,Nm$ at the same velocity. This difference is quite significant and highlights the importance of choosing a more accurate model. Wanting to explain this behavior, it can be attributed to the Stribeck effect (or Stribeck weakening). In every actuator, lubrication is present to improve component contact and movement, particularly between the motor and the gear train. Richard Stribeck designed a curve that represents the trend of the friction coefficient and identified three distinct zones:

1. Static friction and micro-sliding;
2. Mixed friction;
3. Hydrodynamic friction.

27 For more details on the Hebi Actuator®, refer to Table 1

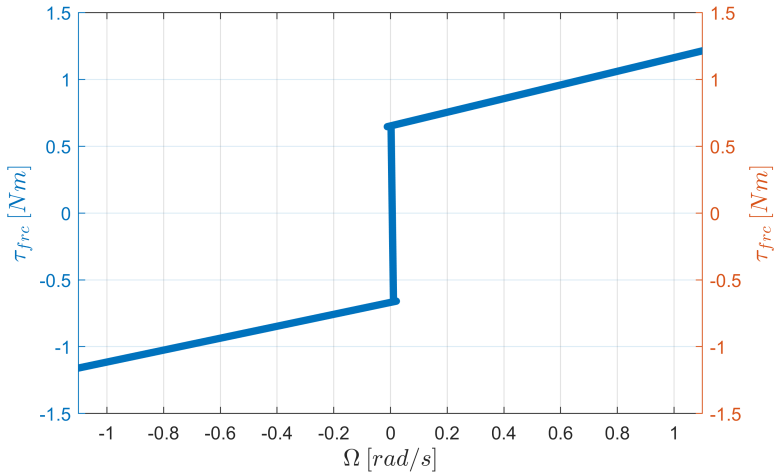

(a) Shoulder Actuator - X − 01122.

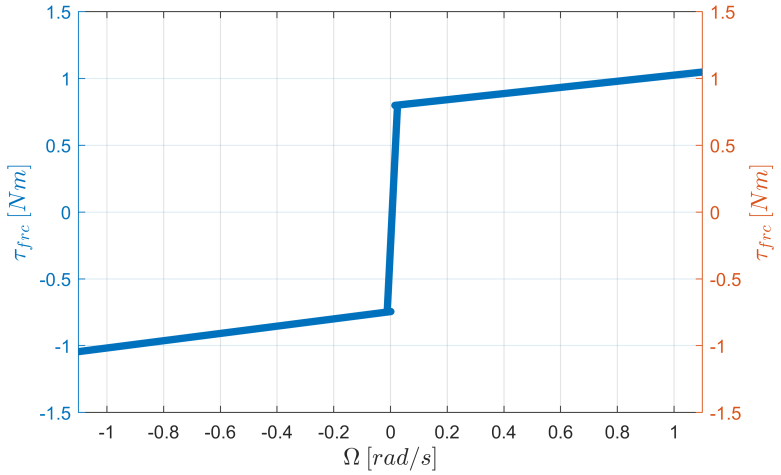

(b) Elbow Actuator - X − 01157.

Figure 5.3: 1^{st} order Polynomial Friction Model.

ACTUATOR	**Static Friction τ_{stat}**		**Viscous Friction**	
//	τ^{+}_{stat}	τ^{-}_{stat}	B^{+}_{t}	B^{-}_{t}
X − 01122	0.652	−0.669	0.511	0.446
X − 01157	0.794	−0.745	0.230	0.273

Table 3: Friction Coefficients - 1^{st} order Model.

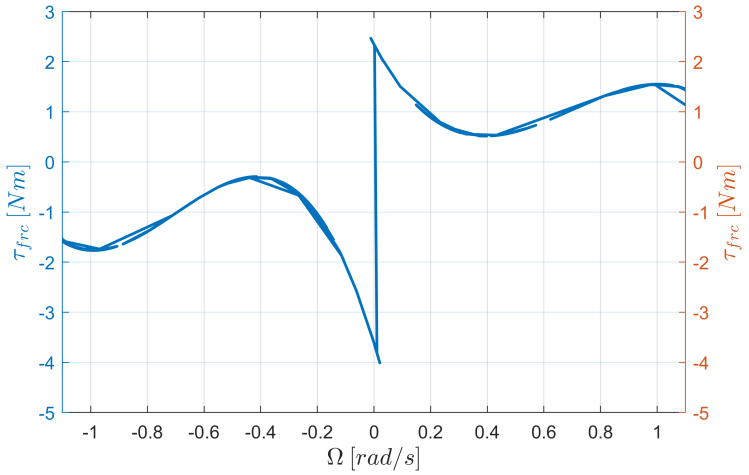

(a) Shoulder Actuator - X − 01122.

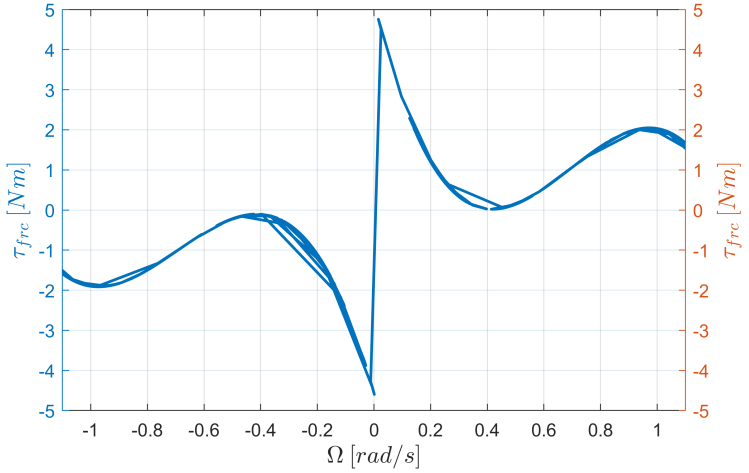

(b) Elbow Actuator - X − 01157.

Figure 5.4: 3rd order Polynomial Friction Model.

Coefficients		Actuator $X-01122$	Actuator $X-01157$
Ω^+	a^+	−9.119	−23.831
	b^+	19.067	49.6417
	c^+	−10.741	−28.975
	d^+	2.342	5.197
Ω^-	a^-	−15.258	−20.805
	b^-	−32.111	−43.281
	c^-	−18.697	−25.141
	d^-	−3.611	−4.567

Table 4: Friction Coefficients - 3rd order Model.

In the case being analyzed, we are in the second zone where the surfaces are moving, where the number and frequency of asperities[28] in contact decrease, leading to a temporary reduction in the system's friction torque [18].

At the extremities the value reached can be considered, more or less, the same. In fact, in both models and cases Ω^+ and Ω^- the final value at the maximum velocity is in the range $|\tau_{friction}| \in [1, 1.5]\,Nm$.

Another significant difference between the two models, which is important to highlight, is the value of static friction[29]. In fact, the static friction is much higher in the 3^{rd} order model than in the other model, as reported in Table 5. This difference can also be attributed

Actuator	τ_{static} [Nm] 1^{st} *order*		τ_{static} [Nm] 3^{rd} *order*	
//	Ω^+	Ω^-	Ω^+	Ω^-
$X-01122$	0.652	−0.669	2.342	−3.611
$X-01157$	0.794	−0.745	5.197	−4.567

Table 5: Friction Info - 3^{rd} order Model.

to the Stribeck effect. In this case, we are in the first zone of the curve, where the surfaces are in stationary contact, and their asperities interlock with each other. To overcome this and initiate motion, a force higher, than that required during motion, is needed to break or release the interlocked asperities.
Using a 1^{st} order model makes it impossible to accurately represent the peak value of static friction. Due to the interpolation, a rough approximation is introduced, leading to an equivalent (but unrealistic) static friction value. As a result, in cases of stationary conditions or low velocities ($\Omega \approx 0\,rad/s$), the RTOB (Reaction Torque Observer) estimation can be significantly distorted, causing incorrect system responses, which could be dangerous for the exoskeleton user.

The friction trends and corresponding values for each friction models analyzed of exoskeleton actuators used (Shouldert Actuator $X-01122$ and Elbow Actuator $X-01157$) are presented respectively in Figure 5.3-Table 3 and Figure 5.4-Table 4. The values reported in the tables may appear high because the friction effect is accounted for on the load side.

28 Irregularities on a surface. If the number is high, the surface can be defined as rough. A surface may appear perfect from a macroscopic view, but microscopic analysis may reveal many imperfections due to surface treatments, manufacturing processes, or normal operational shocks.

29 In Table 4, this corresponds to the coefficient $d^{+/-}$

The final aspect to address regarding static friction τ_{static} is its potential to exhibit two different values when transitioning from Ω^+ to Ω^-, or vice versa. This scenario can cause the microcontroller to encounter an ambiguous situation, leading to errors or even dangerous and unpredictable behaviors. To prevent these issues, it is advisable to incorporate an hysteresis cycle around $\Omega = 0\,\mathrm{rad/s}$.

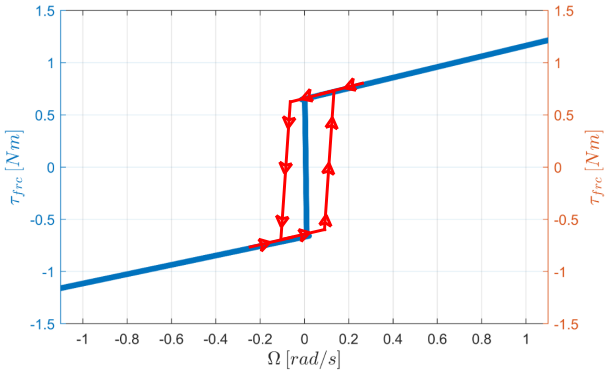

Figure 5.5: Static Friction Hysteresis 1^{st} order - Shoulder Actuator X − 01122.

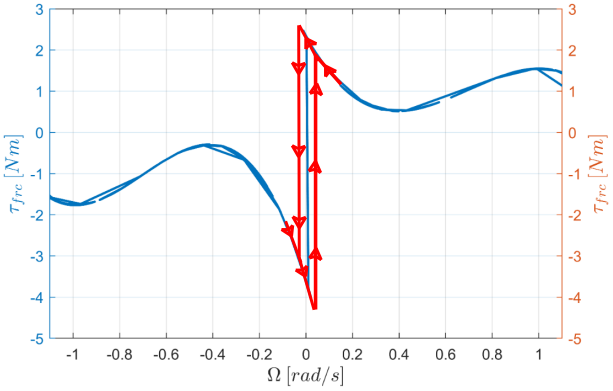

Figure 5.6: Static Friction Hysteresis 3^{rd} order - Shoulder Actuator X − 01122.

The modifications needed for each model are illustrated separately in Figure 5.5 and Figure 5.6, which correspond to the shoulder actuator X − 01122. The same principle applies to the elbow actuator X − 01157, but the corresponding figures are omitted to avoid redundancy.

By implementing this solution, not only is the issue of double values resolved but oscillations caused by changes in rotation direction or stopping the exoskeleton in a fix configuration are also mitigated, resulting in more stable and reliable control. This approach is thus essential at low speeds, where noise in velocity calculations can be problematic. If the low-pass filter is not correctly tuned, speed cal-

culation near zero may oscillate continuously, from positive to negative and vice versa, due to small movements detected by the high-resolution encoder on the Hebi Robotics Actuator®. This can lead to undesirable vibrations in the system's links, which may be abrupt and unsafe. The hysteresis cycle reduces unnecessary corrections by the control system, avoiding undesired behaviors like sudden configuration changes.

To achieve stable, oscillation-free control, it is essential to tune correctly the hysteresis cycle's width through experimental testing. The goal is to keep the hysteresis as small as possible without distorting the friction model and compromising the system's overall performance, in particular in the RTOB estimation.

5.4 SUMMARY OF FRICTION ANALYSIS

In this chapter, we analyzed the friction phenomena from its origin to its compensation through modeling, highlighting and commenting on the differences, behavior at certain points, and providing solutions to the emerging problems.

Thus, the final choices to be implemented in the control code of the exoskeleton prototype are reported in the following list:

- *Friction modeling*: we chose the 3^{rd} order polynomial model, defined as:

$$\tau^{+}_{friction} = a^{+}\dot{\theta}_l^3 + b^{+}\dot{\theta}_l^2 + c^{+}\dot{\theta}_l + d^{+} \quad \text{with } \dot{\theta}_l > 0\,rad/s$$
$$\tau^{-}_{friction} = a^{-}\dot{\theta}_l^3 + b^{-}\dot{\theta}_l^2 + c^{-}\dot{\theta}_l + d^{-} \quad \text{with } \dot{\theta}_l < 0\,rad/s$$

- *Hysteresis cycle*: we chose to use a small hysteresis cycle around $\dot{\theta}_l \approx 0\,rad/s$ to avoid the problems listed earlier and minimize distortion in the RTOB estimation.

- *Friction compensation*: we chose to use the Disturbance Observer (DOB) that can ensure high performance and accuracy.

At this point, we have all the necessary information to proceed with coding the defined control and conducting experimental tests. In parallel, we collect and analyze data to make appropriate adjustments and optimize performance, to achieve the desired results

6 SYSTEM EXPERIMENTAL VALIDATION

The final step of the project is experimental validation, essential for testing the previous design steps and verifying the desired operation. They were conducted on a healthy individual without any muscle injuries or issues due to the unavailability of a group of athletes with injured muscles. The primary goal was to verify the correct functioning of the proposed control methods, according to the thesis control topic, and not the effectiveness of the rehabilitation process or the specific exercises. In the following pages, we will present results related to the control system, such as position trends, position errors, and estimations.

The trajectories tested during the dynamic exercises represent possible movements a patient might perform, but they should not be considered ideal rehabilitation exercises. As mentioned earlier, the exercises were defined depending on the patient's situation and through pre-force tests and electromyography (EMG) analysis.

6.1 EXPERIMENTAL SETUP

The experimental setup is simple and does not require specific characteristics, in line with the goals outlined in the introduction (Chapter 1) of this thesis. It only needs a location[30] with sufficient space for free movement during dynamic exercises, as well as horizontal (e.g., a table) and vertical (e.g., a wall) rigid surfaces to perform the static exercises shown in Figure 4.1. For dynamic exercises, it should be possible to use a weight of $3-5Kg$ to improve more the muscle effort.

In this prototype setup, control was controlled via MatLab® from a computer, as this made data collection and analysis easier. Similarly, the power supply was provided by an external $24V$ generator. However, the ultimate goal remains to make the system fully portable and independent of external connections. This aspect will be discussed in the conclusion, where we will propose solutions to achieve that.

6.1.1 *Hebi Robotic Communication*

The HEBI Robotics® actuators are connected via Ethernet cable, and the data exchange process is illustrated in Figure 6.1. It is also possible to establish a direct connection, such as a private network, between the computer and the actuator without going through a router.

30 This could be a regular bedroom or living room.

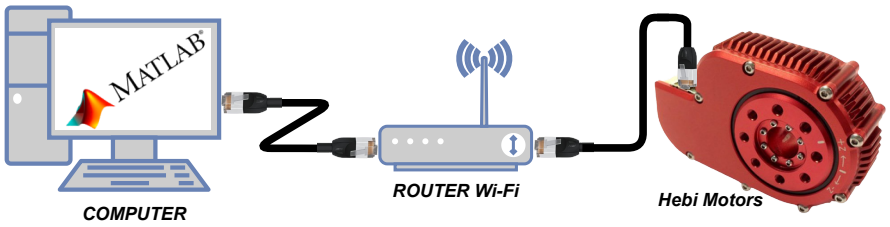

Figure 6.1: Computer $\Longleftrightarrow$ Hebi® actuators Connection.

Both solutions are equivalent, providing a data exchange speed of 100Mbps. The performance remains consistent in either case.

Each actuator is equipped with a real-time operating system (RTOS) that manages commands and feedback with a sampling time of $T_s = 0.1ms$ or a frequency of $f = 1kHz$. The company also declares that, under normal conditions, using a wired system as shown in Figure 6.1, the modules exhibit no packet loss during the data exchange process. Traffic congestion in the router is not a issue, and the latency[31], is very low (about $1 - 2$ ms) and negligible for this project.

In the MatLab® API[32], it is possible to tune the feedback frequency between 100 Hz and 1 kHz, using the appropriate command, to mitigate latency issues. In exoskeleton control, a feedback frequency of 600 Hz is sufficient and corresponds to the maximum reliable frequency using a Windows computer[33].

The wired network connection will play a fundamental role in remote exoskeleton control, particularly for potential tele-rehabilitation in advanced scenarios.

For other connection options or info about communication, such as using different network connections or changing IP address settings (static to dynamic or vice versa), refer to the HEBI Robotics® documentation consultable at [11].

6.2 STATIC EXERCISES - RESULTS

The Position Control with Disturbance Observer (DOB) for static exercises, presented in Chapter 4, was tested using a wall-pushing test. In this test reported, the subject has to maintain their arm in a fixed position helped by the exoskeleton, as shown in Figure 6.2. The position correspond to:

- shoulder $\longrightarrow \theta_1 = 0.341rad \approx 19.54°$
- elbow $\longrightarrow \theta_2 = 1.484rad \approx 85°$

31 The period of time between when a command is received and when the requested data is ready in output.

32 Application Programming Interface

33 For working with higher frequencies (up to 1kHz), it is recommended to use iOS or Linux systems.

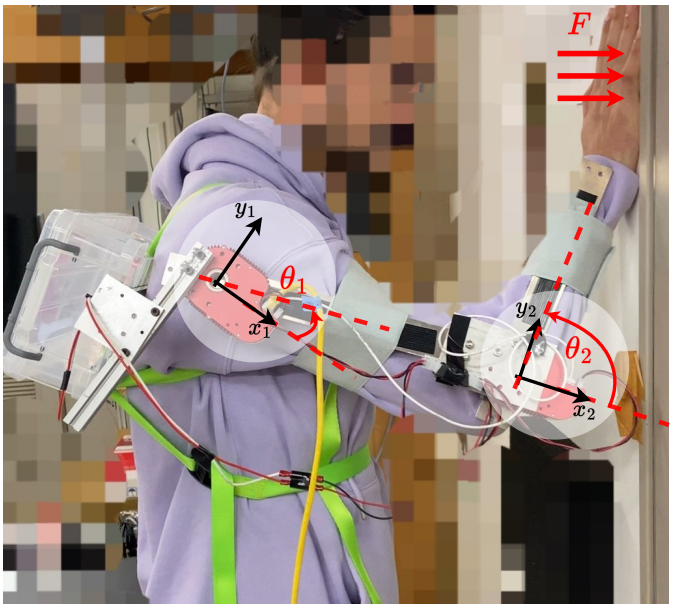

Figure 6.2: Static Exercises - Experimental.

That position is to train the muscle groups of the arm[34] and it was determined through pre-test force and EMG analysis.

During the exercise, it is expected that the patient, while pushing against the wall, might attempt movements that deviate the arm from the fix exercise position. The control system is expected to inhibit these deviations and maintain the correct fixed position by responding with an equivalent force to contrast the incorrect movements. The patient should feel the exoskeleton as very stiff, like a rigid structure that doesn't allow any movement.

The gain tuned to obtain the best performance of implemented control (Figure 4.14) are reported in Table 6.

Gain	**Value**	
//	Shoulder X − 01122	Elbow X − 01157
K_p	6	10
K_d	16	20
g_{LPF}	$80Hz \approx 500rad/s$	$80Hz \approx 500rad/s$
g_{DOB}	$18Hz \approx 113.1rad/s$	$10Hz \approx 62.83rad/s$

Table 6: Control Gains - Static Exercises.

Regarding the gains, it is important to note that we tuned the K_d gain higher than K_p in each joint to achieve smooth movement in the transient from the resting position to the exercise fix position. The cut-off frequency of the velocity calculation low-pass filter is set rela-

34 In general, when we say *arm*, we refer to the entire upper limb. However, in anatomy, the arm is the part from the shoulder to the elbow, while the part between the elbow and wrist is called the *forearm*.

tively low, as the actuator's velocity is low and cannot change rapidly. Additionally, the g_{DOB} (Disturbance Observer gain) in the shoulder control is higher because it has to move all the system and requires a faster response than the elbow control to effectively compensate for the external force applied by the patient.

In Figure 6.3, the complete control results of the exercise are displayed. It is important to highlight that the reference and real position values are opposite than the value wrote before, due to the way the actuator was mounted. Specifically, its inverted mounting configuration was the only option to position the exoskeleton actuators externally to respect the arm.

The exercise rules are:

- $T_{total} = 180s$
- $t_{push} = 20s$
- $t_{rest} = 10s$

and then the patient has to repeat this sequence for $8 - 10$ times.

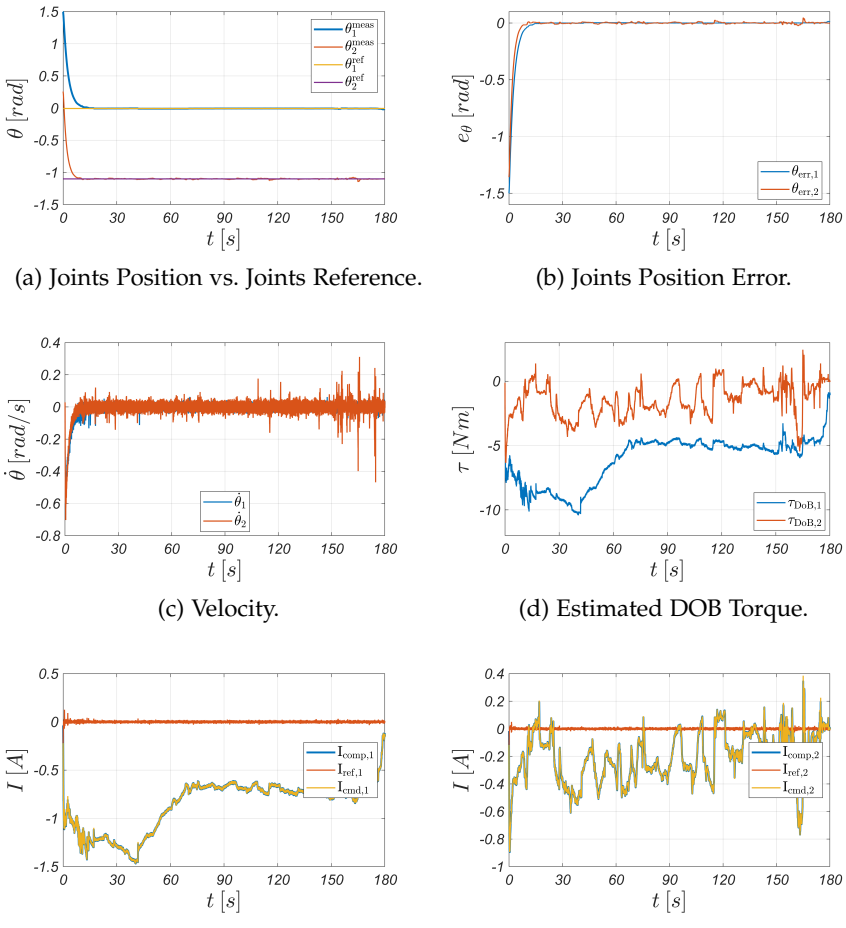

(a) Joints Position vs. Joints Reference.

(b) Joints Position Error.

(c) Velocity.

(d) Estimated DOB Torque.

(e) Currents Shoulder Actuator.

(f) Currents Elbow Actuator.

Figure 6.3: Results - Static Exercise.

First of all we can start with the transient analysis with the support of trends in Figure 6.4. The response is very smooth, and the

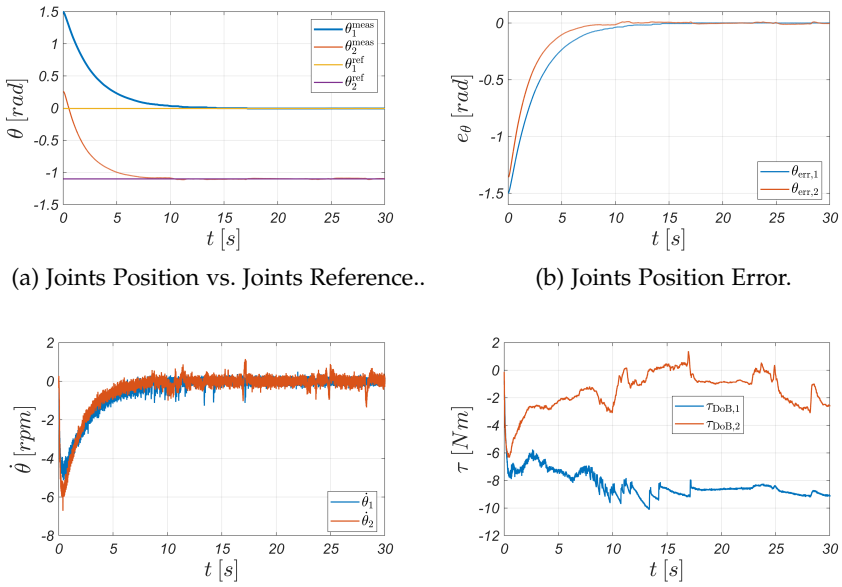

(a) Joints Position vs. Joints Reference..

(b) Joints Position Error.

(c) Velocity.

(d) DOB Torque Estimated.

Figure 6.4: Transient Results - Static Exercise.

exoskeleton brings the arm to the final position in $t = 17.2\,s$, without any overshoots of position and with peak speeds, respectively, of $\dot{\theta}_1 = -5.5\,rpm \simeq -0.576\,rad/s$ and $\dot{\theta}_2 = -4.72\,rpm \simeq -0.494\,rad/s$. The Disturbance Observer (DOB) (Figure 6.4d) estimates the force exerted by the arm due to gravity (and the other internal disturbance, such as friction, that are lower) and calculates the compensation current to I_{comp} contrast this disturbance and achieve the final position. Overall, the transient response is satisfactory, and the proposed control method performs well following the required characteristics. Additionally, it ensures a safe environment for the patient without any risk of sudden movements.

After that, it is important to check the steady-state period and verify the correct maintenance of the fixed position, which is the most crucial part of the initial rehabilitation. In Figure 6.5, the results are reported for analysis. The position error (Figure 6.5b) is more evident in the second actuator, indicating that the patient is applying force with the forearm, the hypothetically uninjured part. The amplitude of the error is very contained; in fact, it oscillates in the range of $e_\theta \in [-0.02, 0.02]\,rad \simeq [-1.146, 1.146]°$, with two sporadic peaks outside this range: one at $e_\theta = 0.028\,rad \simeq 1.6°$ and one at $e_\theta = 0.047\,rad \simeq 2.69°$. The error related to the θ_1 coordinate is smaller than that of the second joint; specifically, it varies slowly within the range of $e_{\theta_1} \in [-0.005, 0.005]\,rad \simeq [-0.286, 0.286]°$. Thus, these can be defined as excellent results, and the error can be considered negligible.

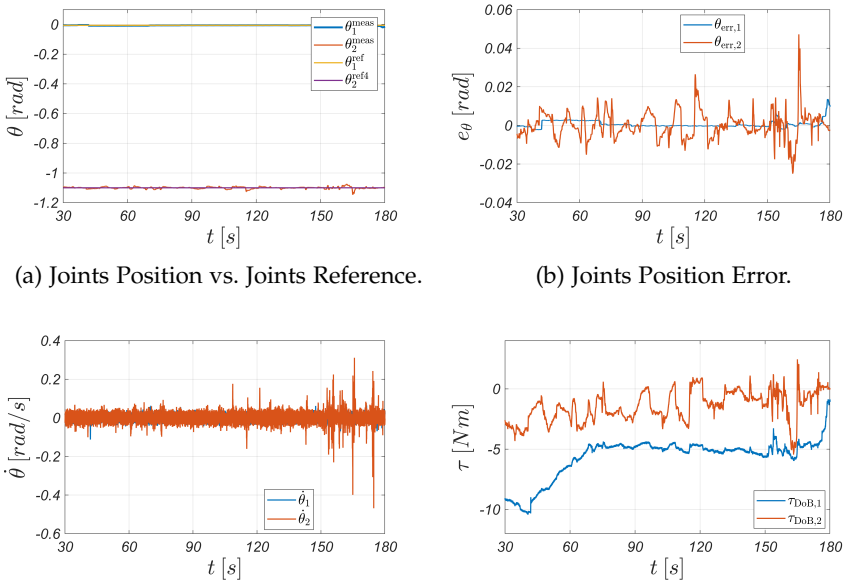

(a) Joints Position vs. Joints Reference.

(b) Joints Position Error.

(c) Velocity.

(d) DOB Torque Estimated.

Figure 6.5: Steady-State Results - Static Exercise.

Continuing and analyzing now the DOB control response, although the estimated total disturbance torque (Figure 6.5d) felt by the shoulder actuator is higher than the one applied to the elbow, the error is lower thanks to the higher g_{DOB} gain setting, which ensures a faster response and, consequently, a stiffer actuator response. It is possible to highlight the peak torque, relative to joint 1, at $t = 40.64s$ with a value of $\tau_1 = -10.37\,Nm$. Compared with the max available torque ($\tau_{peak} = 13\,Nm$) on the datasheet, it is less but it is outside the continuous operating range. However, the corresponding period of time is limited until $t = 51s$, and then the actuator operates only within the continuous range, with an average torque of $\bar{\tau}_1 = -4.9\,Nm$. This behavior is acceptable and does not compromise the actuator's performance or lead to potential overheating.
Regarding joint 2, the torque entity is lower, varying in the range of $\tau_2 \in [-4, 1]\,Nm$ with sporadic peaks due to a higher external force applied by the user; for example, $\tau_1 = -5.32\,Nm$ at $t = 163.2s$.
In light of these results and by comparing the potential critical points with the performance curve in Figure 3.4, each actuator operates within the continuous regime with a safe margin from the τ_{cont} value, except for the shoulder actuator in the initial part.

Turning now to the speed analysis, its results are very noisy, as shown in Figure 6.5c, particularly the speed related to the elbow joint. This can be attributed to the sudden changes in position due to the force applied by the patient to the exoskeleton. However, this does not affect the control performance, although it might be appropriate

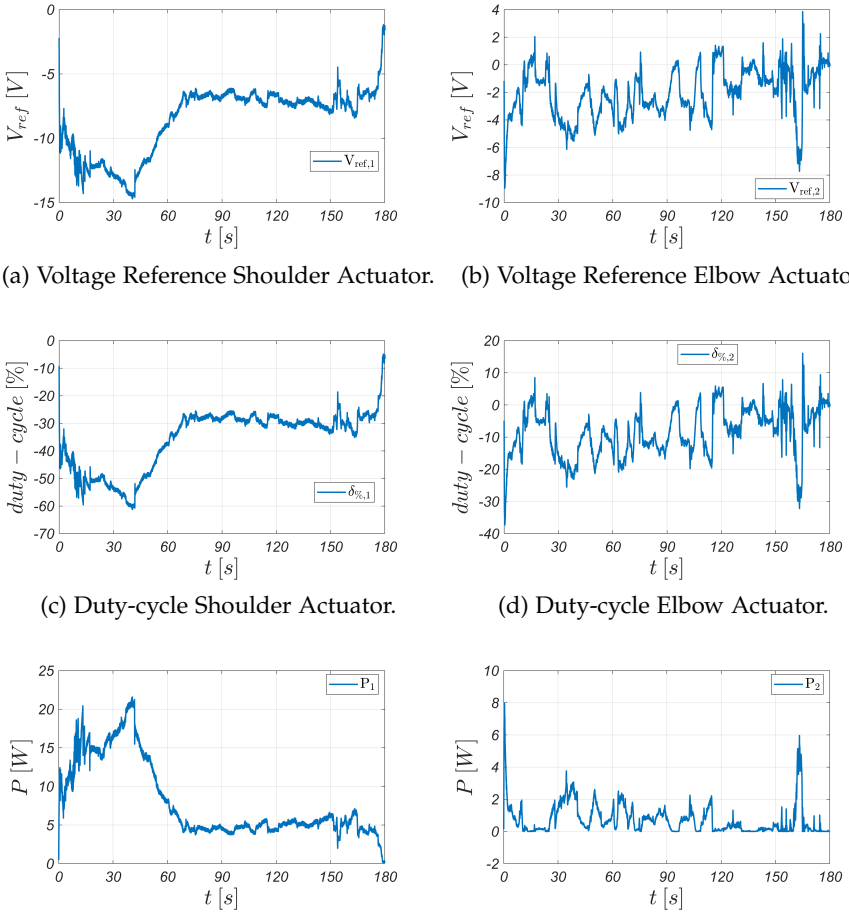

(a) Voltage Reference Shoulder Actuator.

(b) Voltage Reference Elbow Actuator.

(c) Duty-cycle Shoulder Actuator.

(d) Duty-cycle Elbow Actuator.

(e) Power Shoulder Actuator.

(f) Power Elbow Actuator.

Figure 6.6: Voltage Command & - Static ExerciseDuty-cycle.

to reduce the cut-off frequency g_{LPF} of the relative velocity low-pass filter.

Finally, it is also interesting to conduct an analysis from an energy perspective, focusing on variables reported Figure 6.6 with also the actuators currents of Figure 6.3e and Figure 6.3f.

In particular, from the current trends, we observe that, excluding the system's startup phase, most of the work is managed by the DOB. It estimates a significant current value primarily to compensate the gravity and the torque generated by the patient, especially in the first joint. This behavior is reflected in the voltage reference commands (Figure 6.6a-Figure 6.6b) and consequently in the duty cycle (Figure 6.6c-Figure 6.6d). Both parameters remain well within the limits, far from the maximum values of $V_{cc} = \pm 24V$ and $\delta_{\%} = \pm 100\%$, respectively. For reference[35], the following ranges were observed:

35 We do not consider sporadic peaks and we focus on average values, which are more relevant for an operational overview

- $V^1_{ref} \in [-14.47, -1.17]V$
- $V^2_{ref} \in [-7.65, 1.99]V$
- $\delta^1_{\%} \in [-61.2, 5.44]\%$
- $\delta^2_{\%} \in [-25.15, 5.55]\%$
- $P_1 \in [2.31, 21.43]W$
- $P_2 \in [0, 7.84]W$

As expected, the results for the shoulder actuator are higher than those for the elbow actuator. These ranges indicate that the actuators never operate in saturation or at maximum power, which is crucial for preserving component integrity and system reliability.

Beyond this experimental test, which provided the most interesting results, other tests were conducted on different types of patients. These are not reported here due to space constraints and to avoid redundancy in the results. However, the trends were similar, with different values that always remained within a reasonable operating range. Additionally, we collected feedback from individuals regarding their sensations during the exoskeleton's response while performing the exercises.

Thus, considering all the obtained results and feedback, we can confirm the correct operation of the proposed control system for static exercises. The system is capable of maintaining a fixed position with high accuracy, ensuring a high level of rehabilitation in term of its effectiveness. Furthermore, it guarantees a safe scenario at all times, minimizing any risks or issues for the patient.

6.3 DYNAMIC EXERCISES - RESULTS

Similarly, we tested the proposed control for dynamic rehabilitation, as presented in Chapter 4. This control is used in the second phase of the rehabilitation program, once the patient has regained enough muscle strength and started to achieve some autonomy in movement[36]. This part of the rehabilitation program can be organized as follows:

1. **Assistive Phase:** it is the first phase and the exoskeleton performs the exercise path while the patient's arm exerts no force. Through the guided movements carried out by the exoskeleton, the muscle begins to relearn basic movements;

2. **Corrective Phase:** it is the intermediate phase, when the patient's arm has acquired enough autonomy in exerting force and performing simple movements. The exoskeleton assists the movement and correcting the patient's arm when necessary, for instance by providing the missing force to reach a specific point in the exercise path;

3. **Autonomous and Resistive Phase:** it is the final phase, when the patient has sufficient strength to perform the exercises inde-

36 It can be also the only part of rehabilitation process if the ingury is not serious.

pendently. To further enhance muscle strength, the exoskeleton apply resistance against the patient's movements, stimulating him to exert more force.

To recreate the different phases, it is necessary to adjust the gains of the control part related to the impedance model. As explained in the theoretical part in Chapter 4, this part of the control allows us to manage the characteristics of the exoskeleton, such as stiffness.
The gains to be utilized are not standardized but should be tuned to the patient's feeling and muscle situation. In the following pages, we will analyze a case study for each phase listed to verify the effectiveness of the implemented control.

6.3.1 1^{st} *Phase - Assistive*

To obtain a very stiff exoskeleton that works as a guide, we tuned the system whit the gains reported in Table 7.

Gain	**Value**	
//	Shoulder X − 01122	Elbow X − 01157
K	75	75
D	0.5	0.5
K_f	10	10
g_{LPF}	$80Hz \approx 500rad/s$	$80Hz \approx 500rad/s$
g_{DOB}	$18Hz \approx 113.1rad/s$	$10Hz \approx 62.83rad/s$
g_{RTOB}	$8Hz \approx 50.27rad/s$	$5Hz \approx 31.42rad/s$

Table 7: Control Gains - Dynamic Exercise Assistive Phase.

The trajectory to be followed is composed by five points in the workspace coordinates (x, y), as reported in Table 8 and illustrated in Figure 6.7. The same table also provides the corresponding values in the joint space, i.e., the values of the joint angles θ_1 and θ_2. The

Points	**Coordinates**			
//	**WorkSpace**		**JointSpace**	
//	$x\,[m]$	$y\,[m]$	$\theta_1\,[°]$	$\theta_2\,[°]$
A	start	start	start	start
B	0.2	0.4	32.77	71.87
C	0.4	0.35	35.75	30.05
D	0.2	0.05	−43.59	86.61
E	0.24	−0.31	−90	90

Table 8: WorkSpace $\longleftrightarrow$ JointSpace Coordinates - Assistive Phase.

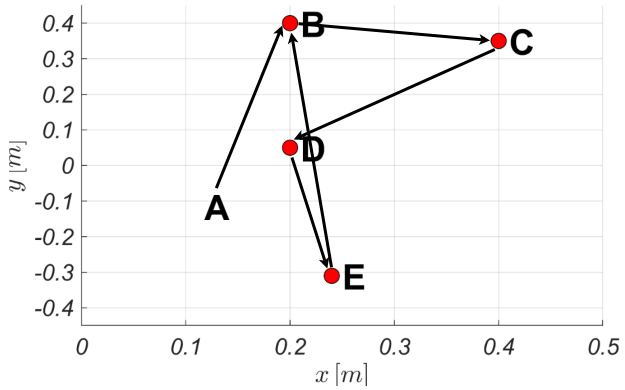

Figure 6.7: WorkSpace Coordinates - Assistive Phase.

starting point A is a generic initial point since the exercise can start from any point of the exoskeleton work area. At the intermediate points, we imposed zero velocity; for the start and end points, the velocity was set by the default settings of the Hebi® trajectory planning function.

The duration of one repetition of this exercise is 25 s, and the patient needs to repeat this sequence for a total of $15 - 20$ minutes. In the following figure, we will report and analyze only one repetition, which is sufficient to verify the control performance. Additionally, we asked the patient to apply force to the exoskeleton to verify the RTOB estimation and check if the stiffness corresponds to the set value.
The results are visible in Figure 6.8.

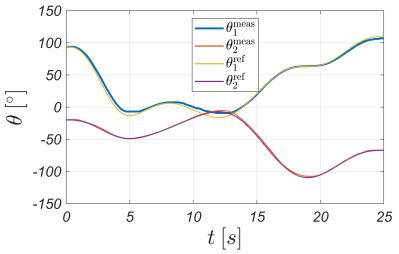

(a) Joints Position vs. Joints Reference.

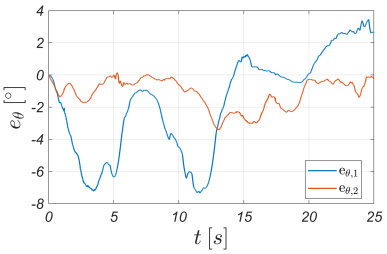

(b) Joints Position Error.

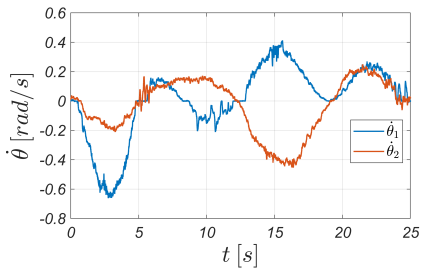

(c) Joints Velocity.

Figure 6.8: Results - Assistive Mode.

Starting from the position results (Figure 6.8a), it is evident that the exoskeleton follows the pre-calculated trajectory with high precision. In fact, by analyzing the position errors in Figure 6.8b, it is possible to identify the following ranges:

- $e_{\theta_1} \in [-0.15, 0.06]\,\text{rad} \simeq [-8.59, 3.44]^\circ$
- $e_{\theta_2} \in [-0.059, 0]\,\text{rad} \simeq [-3.38, 0]^\circ$

These errors are very contained and acceptable, further demonstrating the high precision of the control.

At the same time, the velocity is very low, as desired. The peak speeds registered are reported in Table 9, ensuring the smooth movements that were sought.

Joint	**Velocity** [rad/s]	**Velocity** [rpm]
$\dot{\theta}_1^+$	0.41	−3.92
$\dot{\theta}_1^-$	−0.64	6.11
$\dot{\theta}_2^+$	0.24	2.29
$\dot{\theta}_2^-$	−0.42	4.00

Table 9: Joints Peaks Velocities - Assistive Phase.

Now, we need to verify the stiffness of the exoskeleton through the RTOB estimation analysis. By representing the system as an equivalent spring-damper system, the estimated external torque by RTOB can be defined as follows:

$$\tau_{RTOB} = K \cdot (\theta_{ref} - \theta) + D \cdot (\dot{\theta}_{ref} - \dot{\theta}) = K \cdot e_\theta + D \cdot e_{\dot{\theta}}$$

The main component is K, and with good approximation, we can consider the damping D negligible. Thus, the stiffness can be approximated by:

$$\tau_{RTOB} = K \cdot e_\theta + \cancel{D \cdot e_{\dot{\theta}}} \implies K = \frac{\tau_{RTOB}}{e_\theta}$$

The collected data are illustrated in Figure 6.9, and the corresponding calculated values are reported in Table 10 and Table 11.

We chose two random points at different moments of the exercise. The results obtained are very satisfactory, and the stiffness K is very close to the set value. This means that the RTOB estimation can be considered reliable.

As shown in Figure 6.9, we also compared the RTOB trends with the torque sensor measurements. Due to the low accuracy[37] of 10 −

37 With further research, we discovered that the external torque measurement derived from an estimation of the spring deflection between the gearbox and the output, and in turn also the deflection is estimated. This method is not reliable due to the approximations introduced by each estimation.

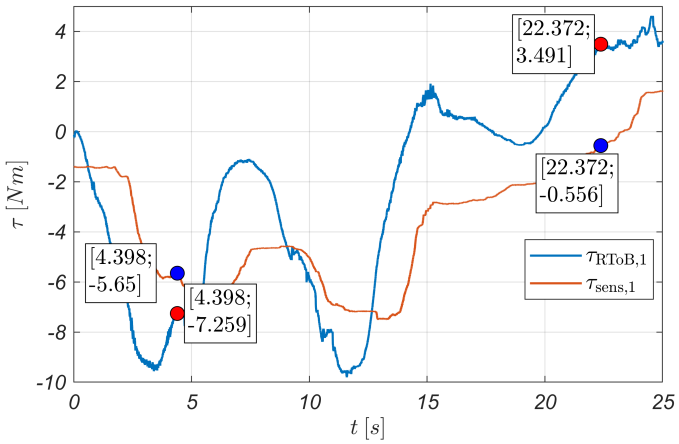

(a) Shoulder Actuator X – 01122.

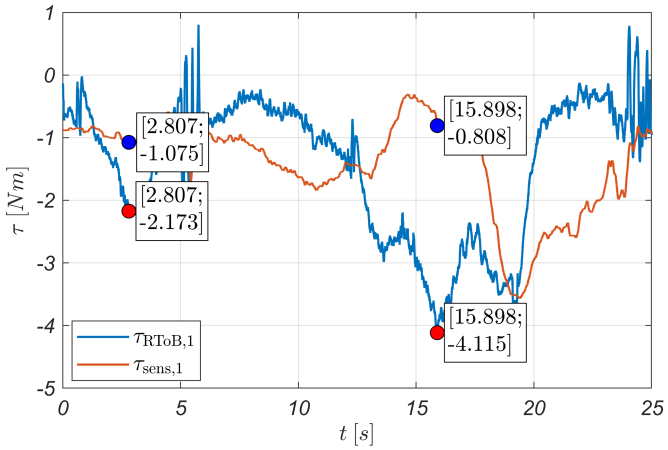

(b) Elbow Actuator X – 01157.

Figure 6.9: RTOB Estimation vs Hebi Torque Sensore - Assistive Mode.

Point	t[s]	τ_{RTOB}[Nm]	e_θ[rad]	K[Nm/rad]
p_1	4.398	−7.259	−0.096	75.726
p_2	22.372	3.491	0.045	78.232

Table 10: K values calculated - Shoulder Actuator - Assistive Phase.

Point	t[s]	τ_{RTOB}[Nm]	e_θ[rad]	K[Nm/rad]
p_1	2.807	−2.173	−0.03	78.153
p_2	15.898	−4.115	−0.05	79.378

Table 11: K values calculated - Elbow Actuator - Assistive Phase.

15% for the Hebi® torque sensor as declared by the company, the amplitude of the two signals cannot be directly compared. However, the behavior of the signals is similar, though there is a time offset, particularly in the shoulder actuator. This offset in torque measurement can be attributed to the methods used by the company for estimating the torque.

Thus, the Assistive Mode works well; the proposed control meets the defined characteristics. It correctly follows the exercise trajectory, ensuring efficient rehabilitation during this phase.

6.3.2 2^{nd} *Phase - Corrective*

In this phase, the support provided by the exoskeleton must be reduced. To achieve this, it is necessary to modify the impedance model, making it less rigid. The gains used in this phase are reported in Table 12.

Gain	**Value**	
//	Shoulder $X-01122$	Elbow $X-01157$
K	50	50
D	0.5	0.5
K_f	10	10
g_{LPF}	$80Hz \approx 500rad/s$	$80Hz \approx 500rad/s$
g_{DOB}	$18Hz \approx 113.1rad/s$	$10Hz \approx 62.83rad/s$
g_{RTOB}	$8Hz \approx 50.27rad/s$	$5Hz \approx 31.42rad/s$

Table 12: Control Gains - Dynamic Exercise Corrective Phase.

The trajectory is easier than the previous one and it is composed by two points in the workspace coordinates (x, y), as reported in Table 13 and illustrated in Figure 6.10. The same table also provides the corresponding values in the joint space, i.e., the values of the joint angles θ_1 and θ_2. The velocity conditions remain the same of the

Points	**Coordinates**			
//	**WorkSpace**		**JointSpace**	
//	$x\,[m]$	$y\,[m]$	$\theta_1\,[°]$	$\theta_2\,[°]$
A	start	start	start	start
B	0.338	0.12	-70	32
C	0.392	-0.02	10	15

Table 13: WorkSpace $\longleftrightarrow$ JointSpace Coordinates - Corrective Phase.

previuos phase.

The duration of one repetition of this exercise is 18 s, and the patient needs to repeat this sequence for a total of $15-20$ minutes. In

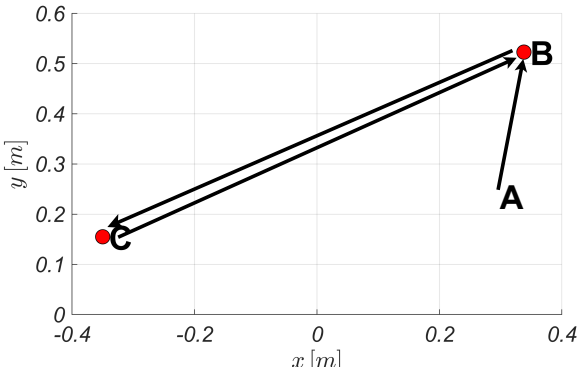

Figure 6.10: WorkSpace Coordinates - Corrective Phase.

the following figure, we will report and analyze two repetitions. During this exercise, the patient has to try to perform the movements independently, while the exoskeleton corrects any deviations from the intended path if necessary. The results obtained are shown in Figure 6.11.

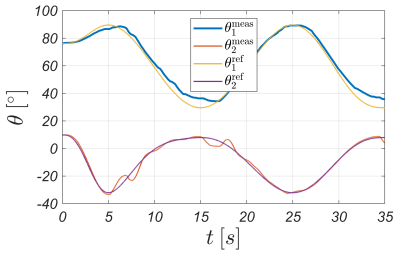

(a) Joints Position vs. Joints Reference.

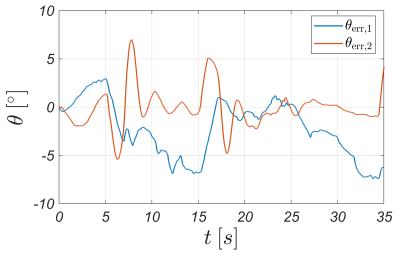

(b) Joints Position Error.

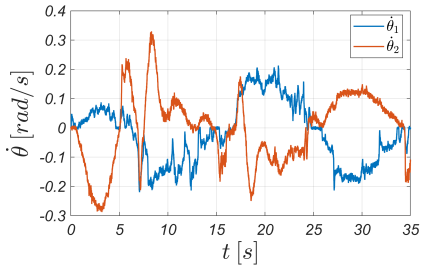

(c) Joints Velocity.

Figure 6.11: Results - Corrective Mode.

Analyzing the position trend, the exoskeleton brings the patient's arm back to the path when it deviates. This can be clearly observed, for example, at t = 15s for joint 1 and at t = 6s for joint 2. All the movements are executed at a low speed, as illustrated in Figure 6.11c, ensuring a smooth and safe situation. In particular the correction introduced by the exoskeleton is not sudden but gradual, as desired.

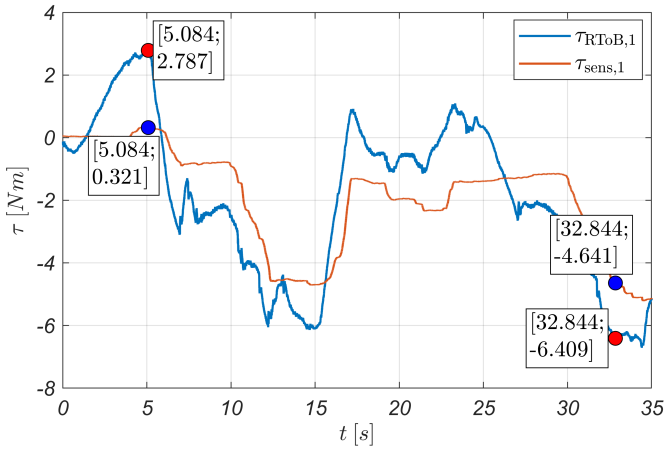

(a) Shoulder Actuator X – 01122.

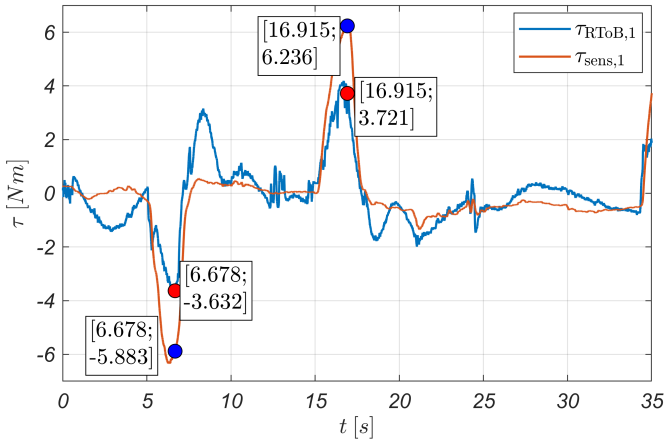

(b) Elbow Actuator X – 01157.

Figure 6.12: RTOB Estimation vs Hebi Torque Sensor - Corrective Mode.

Point	t[s]	τ_{RTOB}[Nm]	e_θ[rad]	K[Nm/rad]
p_1	5.084	2.787	0.321	54.865
p_2	32.844	−6.409	−0.126	50.69

Table 14: K values calculated - Shoulder Actuator - Corrective Phase.

Point	t[s]	τ_{RTOB}[Nm]	e_θ[rad]	K[Nm/rad]
p_1	16.915	3.721	0.071	52.615
p_2	6.678	−3.632	−0.077	47.435

Table 15: K values calculated - Elbow Actuator - Corrective Phase.

Afterward, we verified the correct stiff response through the RTOB estimation, as shown in Figure 6.12. The RTOB estimation can be considered good; its trend (in both actuators) is very similar to the sensor torque trend, though there is a significant difference in amplitude, particularly when the patient exerts force against the system to deviate from the path. During periods when the patient does not exert force, the two signals are more comparable[38]. Finally, we checked the exoskeleton stiffness, and it was consistent with the set value. Compared to the previous phase, the stiffness generated by the exoskeleton shows a non-negligible deviation, but it can be considered acceptable since the deviation is within the range of $e_K \in [-2.6, 4.9]$ Nm/rad.

In the end, we can say that the proposed control provides the correct support, and while the errors are acceptable, there is room for improvement, such as cleaning up the noisy RTOB estimation obtained.

6.3.3 3rd *Phase - Resistive*

In the last stage, the support provided by the exoskeleton needs to be further reduced since the exoskeleton has to work again the patient. The correspond gains to use can be the ones reported in Table 16.

Gain	**Value**	
//	Shoulder X − 01122	Elbow X − 01157
K	25	8
D	0.5	0.5
K_f	10	10
g_{LPF}	80Hz ≈ 500rad/s	80Hz ≈ 500rad/s
g_{DOB}	18Hz ≈ 113.1rad/s	10Hz ≈ 62.83rad/s
g_{RTOB}	8Hz ≈ 50.27rad/s	5Hz ≈ 31.42rad/s

Table 16: Control Gains - Dynamic Exercise Resistive Phase.

Also for this phase, we designed a trajectory composed of two points. The coordinates are reported in Table 17 and illustrated in Figure 6.13. The same table also provides the corresponding values in the joint space, i.e., the values of the joint angles θ_1 and θ_2.

The velocity conditions remain the same of the previous phase.

As can be seen from the position trend in Figure 6.14a, the patient can easily move against the exoskeleton. The exoskeleton attempts to bring the arm back, but according to the defined impedance model, it exerts less stiffness. This results in a resistive behavior where the patient can move the arm almost freely while the exoskeleton still exerts a resistive force that improve the muscle strength.
The velocity remains low as desired, which is also due to the high

38 That can be most attribute to the elbow actuator.

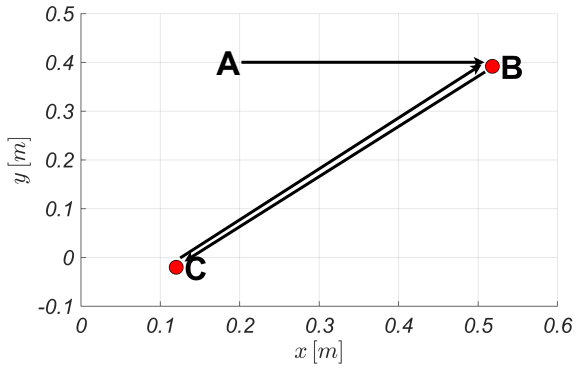

Figure 6.13: WorkSpace Coordinates - Resistive Phase.

Points	**Coordinates**			
//	**WorkSpace**		**JointSpace**	
//	x [m]	y [m]	θ_1 [°]	θ_2 [°]
A	start	start	start	start
B	0.518	0.12	0	30
C	0.392	−0.015	−40	90

Table 17: WorkSpace ⟷ JointSpace Coordinates - Resistive Phase.

gear ratio N. This is an advantage provided by the actuators, as smooth movements must also be ensured during this phase.

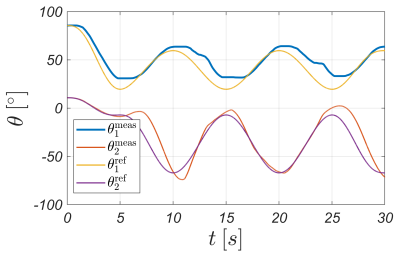

(a) Joints Position vs. Joints Reference.

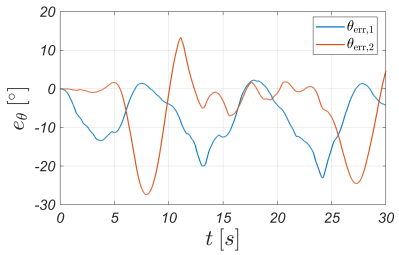

(b) Joints Position Error.

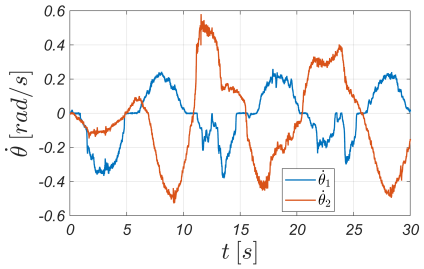

(c) Joints Velocity.

Figure 6.14: Results - Resistive Mode.

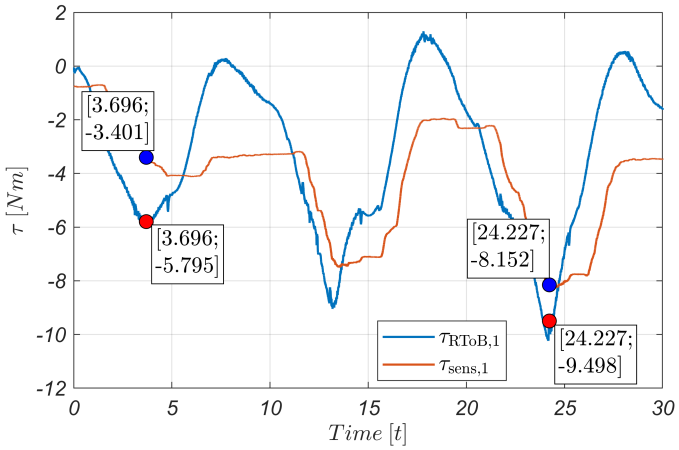

(a) Shoulder Actuator X – 01122.

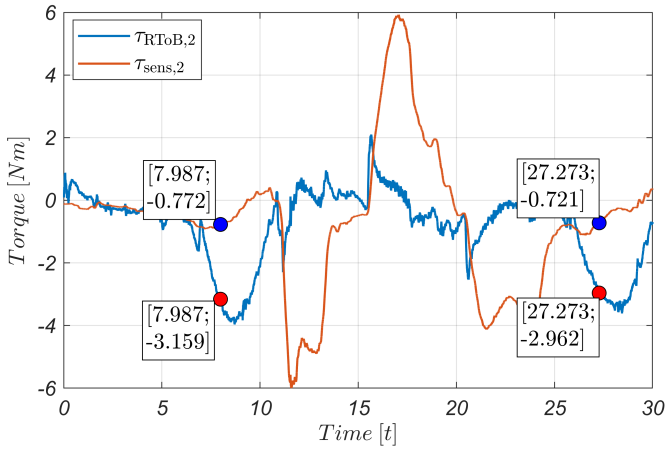

(b) Elbow Actuator X – 01157.

Figure 6.15: RTOB Estimation vs Hebi Torque Sensor - Resistive Mode.

Point	t[s]	τ_{RTOB}[Nm]	e_θ[rad]	K[Nm/rad]
p_1	3.696	−5.795	−0.234	23.738
p_2	24.227	−9.498	−0.401	23.713

Table 18: K values calculated - Shoulder Actuator - Resistive Phase.

Point	t[s]	τ_{RTOB}[Nm]	e_θ[rad]	K[Nm/rad]
p_1	7.987	−3.159	−0.478	6.611
p_2	27.273	−2.962	−0.429	6.916

Table 19: K values calculated - Elbow Actuator - Resistive Phase.

Due to the lower stiffness response, the tracking error (Figure 6.14b) is higher compared with the previous cases. The exoskeleton is not able to correct the patient's movements as effectively as in the previous phase and can only resist the patient's movements.

In this last case as well, the stiffness response is aligned with the parameters setted and the calculated results in Table 18 and Table 19 with the data extrapolated from the Figure 6.15 are proof of that. The comparison comments between the RTOB estimation and the torque sensor measurements previously written, remain valid.

To make this final rehabilitation phase more effective and accurate, the gains need to be adjusted and set higher to better stimulate the patient. Additionally, the control strategy may not be the most suitable and should be reconsidered, proposing a new and more appropriate one for this type of exercise. For example, it might be interesting to implement a pure force control, defining the force reference in workspace (x, y) coordinates that the patient should exert in each direction. Another approach could be to construct a control strategy that adapts the impedance model to the patient's strength: the more force the patient exerts, the stiffer the exoskeleton becomes. This could be an effective way to encourage the patient to improve their strength and regain full muscle autonomy.

These proposed suggestions are for future work due to the conclusion of the thesis period and the inability to implement and test them. They can be used as a starting point for the future development of the exoskeleton control system.

7 CONCLUSIONS

At the end of this project, we summarize the steps taken and the results obtained. Then, we will propose some future work that could improve the project, along with some ideas as a starting point.

In general, each step of the design and testing process can be considered satisfactory. Most of the goals set at the beginning of the project have been achieved. The final prototype has a lightweight structure, is portable, and uses sensorless control methods that allow for efficient rehabilitation. The Hebi® actuators have been confirmed to be a good choice based on experimental test results in both types of exercises. Despite their compactness and low weight, they provide high output torque, thanks to the high gear ratio N.

Regarding the proposed control methods, the experimental tests have shown high performance. In particular, the static exercise control achieved precision in maintaining a fixed position and good rejection of external disturbances, such as the force exerted by the patient in case of incorrect movements. The dynamic exercise control also performed well, and through the impedance model parameters, it is possible to adjust the response according to the patient's condition. The variation in the exoskeleton's response is very noticeable from the collected data and the patient's feedback during the training. Overall, the proposed controls guarantee tracking precision, low-velocity execution, and consequently smooth movements, and accurate torque estimation using RTOB methods, ensuring a safe, comfortable, and effective rehabilitation process. The control can be considered as reliable and robust.

On the other hand, as a first future work, the control can be improved. Firstly, it would be beneficial to compare the RTOB estimation with an external reliable sensor to obtain feedback on the estimation quality. Additionally, it would be worthwhile to try estimating the system's friction using a different method and comparing it with the current one. For example, one could be the one presented by Toshiyuki Murakami, Fangming Yu, and Kouhei Ohnishi in 1993 [13], exploiting DOB, which is already present in the control.

The control can also be improved in the dynamic exercises. One idea is to change the resistive phase approach, making it adjustable according to the force applied by the patient: more force implies more stiffness, and vice-versa. This can be achieved with a function that changes the impedance parameters according to pre-established ranges or using a force control. In addition, the trajectory can be eliminated.

After implementing these control upgrades, it is necessary to make the exoskeleton completely autonomous in terms of computer control and power supply. This was an important goal that had not yet been achieved. The idea is to install a *Raspberry PI4* as the brain controlling the exoskeleton, as it is compact, accessible, and flexible. Additionally, it can connect to Wi-Fi, which is useful for tele-rehabilitation. A remote connection can be created using TeamViewer® to adjust parameters in real-time. This needs to be tested and validated; in particular, a fast and stable connection is required, and the connection latency, a very important parameter, must be insignificant to avoid issues. Due to the Raspberry architecture (ARM architecture), MatLab® is not supported. Therefore, it is necessary to migrate to a different programming language such as `C/ C++/ Python`.

Regarding energy autonomy, it can be achieved by installing a 24V lithium rechargeable battery with sufficient capacity to carry out a single rehabilitation session without problems. An external plug can also be installed and used only in case of low-charge emergencies.

Another update that could be made is to change the exoskeleton structure, particularly the link material. Materials such as carbon fiber, titanium alloys, high-resistance plastic, or Kevlar-carbon hybrids, etc... can significantly reduce the system's weight while maintaining high stiffness.

Finally, another possible and important upgrade could be the addition of one Degree of Freedom (DoF). Adding an actuator near the shoulder joint, such as on the scapula, would increase the possible movements; for example, introducing the z axis would allow the arm to rotate frontally. This would increase the range of rehabilitation exercises and expand the exoskeleton's application area for various injuries, but at the same time, it would increase control complexity (due to 3DoF, rotating reference systems, etc...), costs, and overall weight.

This could be a very interesting challenge for the future and could result in a more complete product that can help many injured people.

APPENDIX

A

DOB - DISTURBANCE OBSERVER

In today's industrial landscape, a pervasive challenge across various sectors is the existence of different types of disturbances in systems. Effectively addressing these disturbances is a primary concern. When disturbances are measurable, a straightforward approach involves using sensors and implementing a feed-forward strategy for compensation, aiming to eliminate or mitigate their impact. However, relying on sensors can introduce errors or prove to be prohibitively expensive. Most of the time, disturbances are unknown and non-measurable; a good solution can be the estimation of them, using the measurable variables of the system (as position, velocity, current, voltage etc...) and generating a consequent signal for rejection. To accomplish this, the application of an observer mechanism, as illustrated in Fig.A.1, proves to be a simple yet effective approach [3]. Using this type of structure, we create an inner loop to reject the disturbances and the feedback loop.

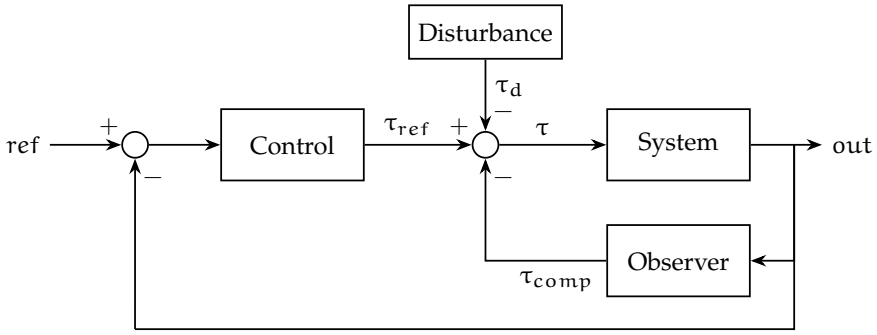

Figure A.1: System with the observer.

Disturbance Observer (DOB) is a distinct control approach used to estimate internal system uncertainties and external unknown disturbances, proposed by Professor Ohnishi in 1983 in Japan, in a velocity control of a DC-motor. It is a robust control method and is well-known in many Asian countries, where numerous engineers use it in their applications due to its simplicity, flexibility, stability, and efficacy. For its very simple structure, today is very applied in many control applications of robotics, automotive, mechatronics and power electronics.

In the beginning, the aim of *DOB* was to provide an alternative to the classical *PID* controller for counteracting the load torque (or in general, an external disturbance) by leveraging knowledge of all physical parameters of the system. Later, the concept changed, and the disturbance is now regarded as an external load (or external dis-

turbance), to which the effects of viscous friction and variations in system parameters are also added. This type of disturbance is called equivalent disturbance.
In this way, it is possible to construct the estimation using the nominal values that are well-known, as provided by the manufacturer of the used system. For example, in an application with a DC motor, nominal rotor inertia and nominal torque constant are needed and it is easy to find in the datasheet.
The operating principle is very easy: *DOB* compare the measure of the input and output signals with the dynamic model of the system and when a difference is detected, caused by disturbances, it generates a compensation signal to be added to the reference control signal.
To understand better, it is possible to consider a simple system as in Figure A.2, where $P(s)$ is the process (or real physical plant), $C(s)$ is the control (e.g. P, PD), $r(t)$ is the reference (or input), $u_r(t)$ is the control signal, $d(t)$ is the disturbance and $y(t)$ is the output.
If we implement the *DOB* in the generic system of Figure A.2, we ob-

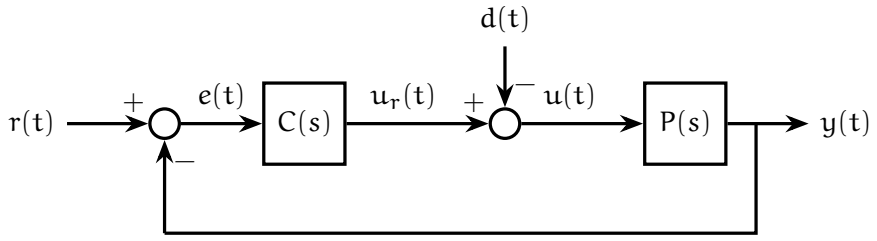

Figure A.2: Generic System Scheme.

tain the scheme of Figure A.3, where $P(s)$, $C(s)$, $r(t)$, $d(t)$, $u_r(t)$, $y(t)$ defined as previously and $u'_r(t)$ is the new control signal, $u_{comp}(t)$ is the compensated signal, $P_n^{-1}(s)$ in the inverse of the process with nominal values, $Q(s) = \dfrac{g_{DOB}}{s + g_{DOB}}$ is a low pass filter (LPF) to filter the compensation signal and g_{DOB} is called DOB gain.

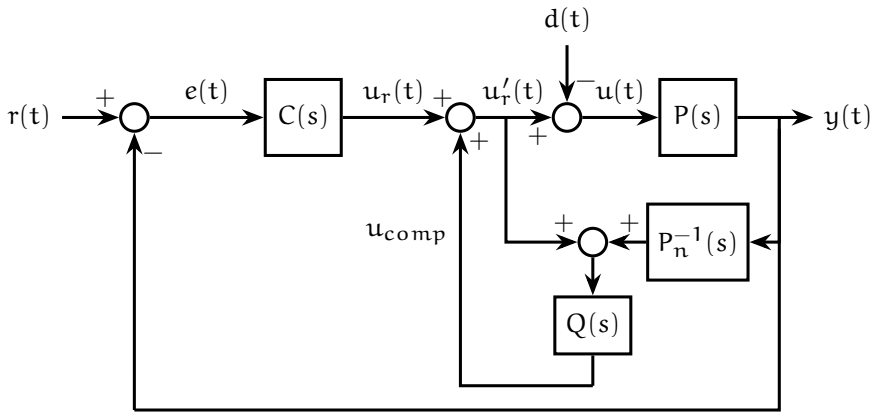

Figure A.3: Generic System with *DOB*.

By calculating the transfer function between $U(s)$ and $Y(s)$, results:

$$\frac{Y(s)}{U(s)} = \frac{\frac{1}{1-Q(s)}P(s)}{1+\frac{Q(s)}{P(s)}\frac{1}{1-Q(s)}P(s)} = P(s) \tag{23}$$

and it is easy to conclude that the *DOB* does not induce any changes within the system. If we compare its use with a pure control $C(s) = PID(s)$, we can also affirm that using *DOB* there are no variations in the system phase. In contrast, $PID(s)$ introduces a reduction in phase margin, leading to a consequent decrease in stability and robustness. To achieve a favorable response from *DOB*, it is necessary to adjust the gain g_{DOB}: higher value results in a faster system response, and vice versa. Optimal values for g_{DOB} are typically in the range of $800 \div 900, rad/s$, but it is important to fine-tune it according to the specific application. This tuning is independent of the control tuning $C(s)$, introducing another advantage to those described in the preceding lines. This is intuitive, as it is evident that an additional degree of freedom is now available. In particular, $C(s)$ have to be designed following the performance required while the *DOB* inner loop has to be tuned to reject the disturbances.

In conclusion, it can be stated that *DOB* is highly effective in rejecting unknown external disturbances and internal parameter variations, providing advantages in terms of system robustness, reliability, and stability. Additionally, it can be integrated with other types of observers such as the Reaction Torque Observer $(RTOB)$ or Reaction Force Observer $(RFOB)$ to estimate specifically contact torque or contact force, respectively. They have the same structure but input and output are different.

For this information, reference has been made to [14][20].

A.1 HOW DOB WORK IN A MOTOR CONTROL

We are supposed to have a DC motor and we don't know the variables like torque constant K_t, viscous friction B and inertia J_m with high accuracy but only with the nominal value from the datasheet. During operation, K_t can change due to the saturation of the magnetic circuit, J_m is very stable but it has the uncertainty of the instrumental measurement when the constructor defined it and B changes due to the temperature, motor age and component wear. After that, it is possible to define:

1. $K_t = K_{t,n} + \Delta K_t$
2. $J_m = J_{m,n} + \Delta J_m$

where $\bigcirc_{i,n}$ is the nominal value, $\bigcirc_i$ is the real value and $\Delta\bigcirc_i$ is the parameter variation, with $i = t, n$.

Now, it is possible to consider the motor with nominal inertia $J_{m,n}$ and affected by a disturbance $\tau_j = \Delta J_m$. Similarly, the same concept applies to the torque constant. We can see the equivalent model of the parameters as in Figure A.4a-Figure A.4b.

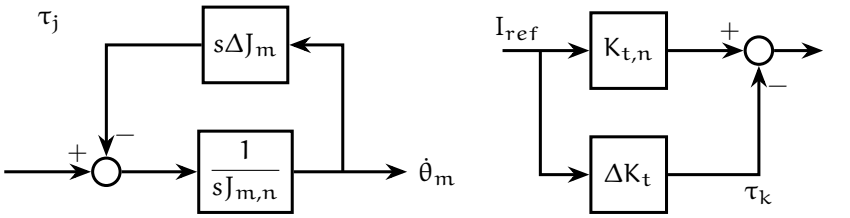

(a) Equivalent model with Inertia $J_{m,n}$. (b) Equivalent model with $K_{t,n}$.

Figure A.4: Equivalent Models.

At this point, we can also introduce viscous friction B as a disturbance to model a motor with nominal parameters, and every variation is considered as an external disturbance. With all these assumptions, as is stated in Appendix A, we do not have any variations in the transfer function and the final system results like in Figure A.5 where the

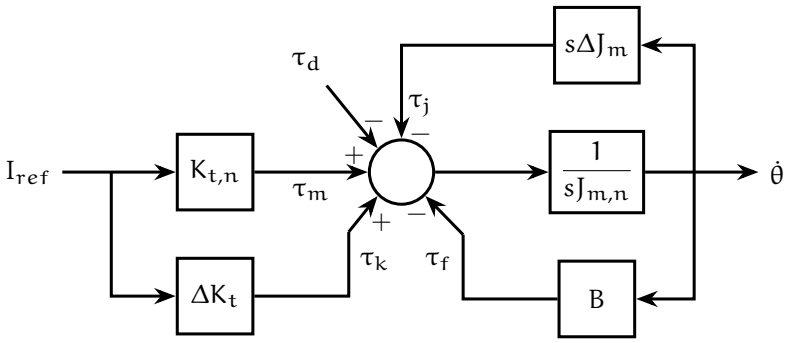

Figure A.5: Final Equivalent Model.

total disturbance τ_{dist} is:

$$\tau_{dist} = \tau_d + (s\Delta J_m + B)\dot{\theta}(s) - \Delta K_t I_{ref} = \tau_d + \tau_j + \tau_f + \tau_k \quad (24)$$

and the disturbances are associated as in Table 20.

Disturbance Type	Associated to	Notation	Equation
External Disturbance	/	τ_d	unknown
K_t variation	ΔK_t	τ_k	$\Delta K_t \cdot I_{ref}$
J_m variation	ΔJ_m	τ_j	$\Delta J_m \cdot \ddot{\theta}$
Viscous Friction	B	τ_f	$B \cdot \dot{\theta}$

Table 20: Disturbance Matching.

At this point, the challenge is to do a sensorless application and estimate the the total disturbance τ_{dist} (eq.24) from the information of the system as position, velocity, current etc... We insert in the system the estimator and we obtain the scheme of fig.A.6.

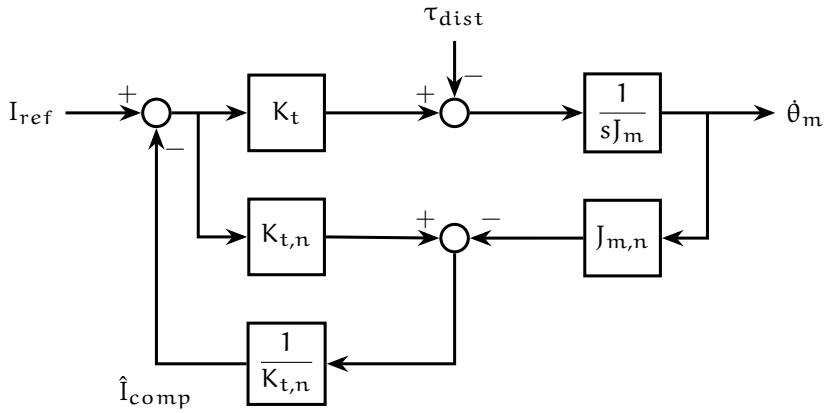

Figure A.6: Estimator of Disturbance.

Therefore, we implement an estimator that converts the estimation of the total disturbance applied to a system where we have a motor with real value and without friction and variation of torque constant and inertia. The latter are compensated through the current generated by the estimator, I_{comp}, and must be added to the reference current value I_{ref}. In this scenario, the motor produces a high torque. However, when we introduce the disturbance, the output aligns with the reference value.
The main problem of the scheme in Figure A.6 is in the right part, where we calculate $sJ_{m,n}$ and it presents a pure derivative that is impossible to be calculated. To solve this problem, we insert a low pass filter (LPF) with static gain and it generates an approximate version. The scheme of Figure A.6 becomes as described in Figure A.7.

Now, the challenge is the tuning of the LPF. There is a *trade-off* because a higher value of g_{DOB} results in increased disturbance rejection (and a higher response velocity), but it also leads to a noisier output from the filter. It is necessary to find the correct g_{DOB} value for a good system response and good rejection of the disturbance; we have to find the correct bandwidth where the system works well, is stable and is robust.

Starting from this theory, it is easy to apply this approach to eliminate the external disturbances to every possible plant.

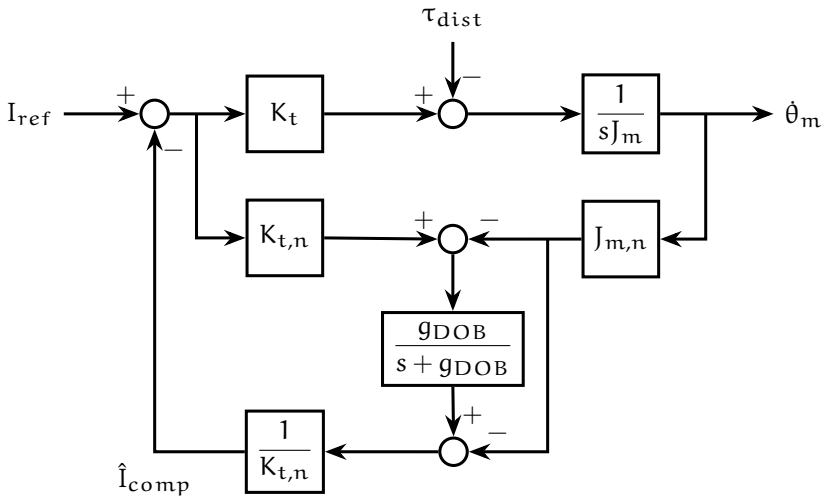

Figure A.7: Estimator with Filtered Derivative - *DOB*.

B

RTOB - REACTION TORQUE OBSERVER

Every day, a robot may work in an environment where it encounters obstacles, such as walls or humans. Additionally, robotic applications involving interaction with humans, such as collaborative robots, are common in the current industry. Similarly, in fields such as the medical sector, robots may interact with parts of the human body, or even the entire body, for medical surgery or rehabilitation. Thus, it is crucial to ensure that no harm is caused and that the workspace is safe.

For this reason, a control for environment or interaction force is required to be implemented in the robot. In Appendix A, it was discussed that the classical *DOB* can suppress external disturbances and variations in internal parameters, and its primary goal is not to estimate the interaction contacts with the surrounding environment or a person. To address this limitation, one option is to install one or more force/torque sensors in the system. However, this approach can be expensive and may not be entirely reliable at 100% due to the potential sensor problems such as signal noise, collocation in the physical system and errors or loss in accuracy. The challenge is to utilize an estimation of the contact force using a sensorless technique, known as *Reaction Torque/Force Observer (RTOB/RFOB)*[39]. The control scheme is the same as that of the DOB, but it is necessary to subtract all the compensated disturbances, allowing it to function as a force/torque sensor.
Thus, to do a force control, we need to combine:

- *DOB* in the inner loop to estimate the total external disturbances and define the equivalent current to compensate them;
- *RTOB* in the outer loop to estimate the contact force [19] and adjust the force/torque command;

In figB.1, we can find the generic corresponding scheme. After the estimation is performed using only the position (from the encoder), the velocity is consequently calculated, and the current command is defined. To ensure the estimation is reliable and accurate, the models of phenomena acting on the system, such as friction, parameter variation, and gravity components, must be precise mathematical models. Sometimes, this can be a difficult challenge due to the complexity of phenomena, such as friction, which can be non-linear.

By combining all these factors, the equivalent force/torque applied externally by the environment or a human can be well obtained. To confirm the effectiveness of the *RTOB*, it is recommended to compare

39 The name depends if we are estimating a torque or a force

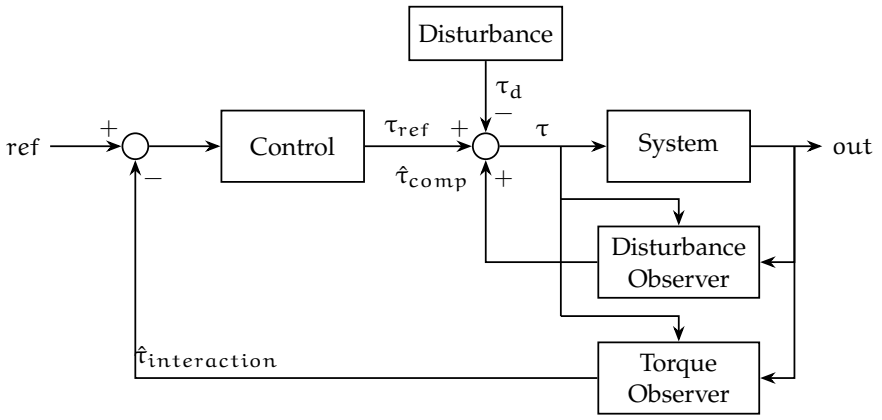

Figure B.1: Generic System with *DOB* and *RTOB*.

the RTOB output with that of a reliable external force/torque sensor. If necessary, the parameters, such as gain or mathematical models, should be adjusted to correct the estimation and make the estimation error negligible.

Thus, RTOB can be a good solution for eliminating the force sensor from the system and applying a sensorless control approach to a robotic application that involves environment-human interaction.

C

HEBI ROBOTICS® ACTUATOR

C.1 HEBI ROBOTICS® MOTOR - DIMENSIONS

The dimensions of the Hebi motor, as illustrate in Figure C.1 (sourced from the official Hebi Robotics® website [10]), emphasize its compactness, that minimize the encumbrance, fundamental element for the exoskeleton project.

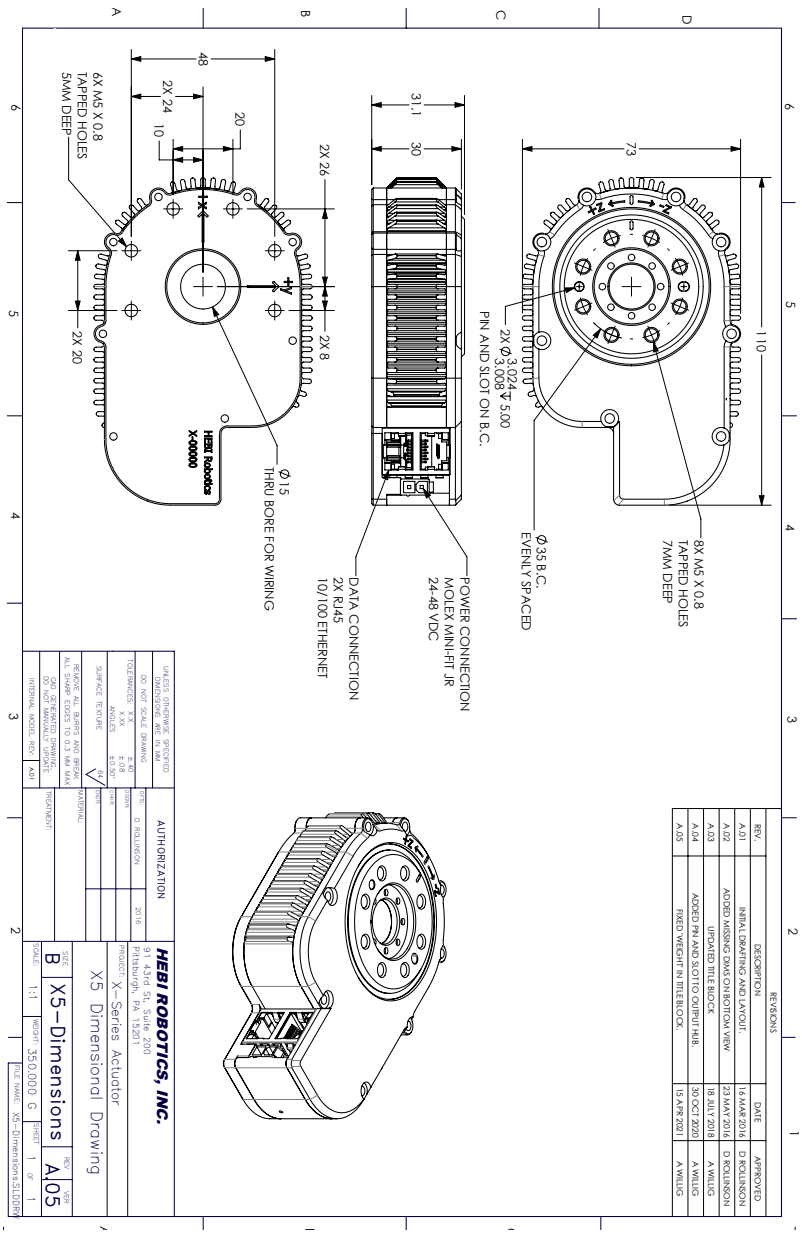

Figure C.1: Dimensions of the Hebi Robotics Actuator® X5 − 9 [10].

BIBLIOGRAPHY

[1] Buccelli, Stefano and Tessari, Federico and Fanin, Fausto and De Guglielmo, Luca and Capitta, Gianluca and Piezzo, Chiara and Bruschi, Agnese and Van Son, Frank and Scarpetta, Silvia and Succi, Antonio and others. A gravity-compensated upper-limb exoskeleton for functional rehabilitation of the shoulder complex. *Applied Sciences*, 12(7):3364, 2022. Accessed: 2024-08-17.

[2] Andrea Calanca, Riccardo Muradore, and Paolo Fiorini. A review of algorithms for compliant control of stiff and fixed-compliance robots. *IEEE/ASME Transactions on Mechatronics*, 21 (2):613–624, 2016. doi: 10.1109/TMECH.2015.2465849.

[3] Wen-Hua Chen, Jun Yang, Lei Guo, and Shihua Li. Disturbance-observer-based control and related methods—an overview. *IEEE Transactions on Industrial Electronics*, 63(2):1083–1095, 2016. doi: 10.1109/TIE.2015.2478397.

[4] S. Chiaverini and L. Sciavicco. The parallel approach to force/-position control of robotic manipulators. *IEEE Transactions on Robotics and Automation*, 9(4):361–373, 1993. doi: 10.1109/70.246048.

[5] Stefano Chiaverini, Bruno Siciliano, and Luigi Villani. Parallel force/position control schemes with experiments on an industrial robot manipulator. *IFAC Proceedings Volumes*, 29(1):25–30, 1996.

[6] J. De Schutter. A study of active compliant motion control methods for rigid manipulators based on a generic scheme. In *Proceedings. 1987 IEEE International Conference on Robotics and Automation*, volume 4, pages 1060–1065, 1987. doi: 10.1109/ROBOT.1987.1087856.

[7] Tong Heng Lee Wenyu Liang Clarence W. de Silva Kok Kiong Tan. *Force and Position Control in Mechatronics Systems - Design and Applications in Medical Devices*. Springer Nature Switzerland AG, 2021.

[8] William Haseltine. Revolutionizing rehabilitation: How exoskeletons are restoring mobility for neuromuscular patients, July 2023. URL https://www.forbes.com/sites/williamhaseltine/2023/07/31/revolutionizing-rehabilitation-how-exoskeletons-are-restoring-mobility-for-neuromuscular-patients/. Accessed: 2024-08-17.

[9] Hebi Robotics. X-series actuator — technical specifications. https://docs.hebi.us/hardware.html#x-series-mech-info, 2021. URL https://docs.hebi.us/resources/datasheets/X-SeriesDatasheet.pdf. Accessed: 05/08/2024.

[10] Hebi Robotics. X5 hebi robotics dimensions datasheet, 2021. URL https://docs.hebi.us/resources/datasheets/X5-Dimensions.pdf. Accessed: 05/08/2024.

[11] HEBI Robotics. Core concepts - hebi documentation - comunication and connection, 2023. URL https://docs.hebi.us/core_concepts.html,https://docs.hebi.us/. Accessed: 2024-08-18.

[12] Istituto Italiano di Tecnologia (IIT). Float: il nuovo esoscheletro per braccia di iit e inail, 2024. URL https://opentalk.iit.it/float-il-nuovo-esoscheletro-per-braccia-di-iit-e-inail/. Accessed: 2024-08-01.

[13] T. Murakami, F. Yu, and K. Ohnishi. Torque sensorless control in multidegree-of-freedom manipulator. *IEEE Transactions on Industrial Electronics*, 40(2):259–265, 1993. doi: 10.1109/41.222648. Accessed: 2024-08-18.

[14] Roberto Oboe. How disturbance observer changed my life. In *2018 IEEE 15th International Workshop on Advanced Motion Control (AMC)*, pages 13–20, 2018. doi: 10.1109/AMC.2019.8371055.

[15] Alex Owen-Hill. Robotics research 101: Getting started with force control. https://blog.robotiq.com/robotics-research-101-getting-started-with-force-control, 2016. Accesed: Dicember, 2023.

[16] Richter, Sebastian and Knoll, Alois. Efficient global optimization for markov random fields via graph cuts. In *IEEE International Symposium on Robotics and Automation*, pages 1658–1665, 2013. URL https://groups.csail.mit.edu/rrg/papers/Richter_ISRR13.pdf.

[17] D.W. Robinson, J.E. Pratt, D.J. Paluska, and G.A. Pratt. Series elastic actuator development for a biomimetic walking robot. In *1999 IEEE/ASME International Conference on Advanced Intelligent Mechatronics (Cat. No.99TH8399)*, pages 561–568, 1999. doi: 10.1109/AIM.1999.803231.

[18] Ruderman Michael. *Analysis and Compensation of Kinetic Friction in Robotic and Mechatronic Control Systems*. CRC Press, 2023.

[19] Emre Sariyildiz. A stability analysis for the reaction torque observer-based sensorless force control systems. In *2023 IEEE International Conference on Mechatronics (ICM)*, pages 1–5, 2023. doi: 10.1109/ICM54990.2023.10101940.

[20] Emre Sariyildiz, Roberto Oboe, and Kouhei Ohnishi. Disturbance observer-based robust control and its applications: 35th anniversary overview. *IEEE Transactions on Industrial Electronics*, 67(3):2042–2053, 2020. doi: 10.1109/TIE.2019.2903752.

[21] Arokia Pranesh Kanna Sorimuthu. How robotic applications are changing medical devices. https://www.mddionline.com/robotics/how-robotic-applications-are-changing-medical-devices. Accesed: October 2023.

[22] University of Auckland. Research | department of mechanical engineering, 2024. URL https://www.mdt.auckland.ac.nz/research/. Accessed: 2024-08-01.

[23] Yongkun Zhao, Haijun Wu, Mingquan Zhang, Juzheng Mao, and Masahiro Todoh. Design methodology of portable upper limb exoskeletons for people with strokes. *Frontiers in Neuroscience*, 17:1128332, 2023. Accessed: 2024-08-17.